Universidad Autónoma de Madrid
Departamento de Biología Molecular
Facultad de Ciencias

# Analysis of the assembly and maturation processes of the Infectious Bursal Disease Virus capsid

- TESIS DOCTORAL -

Nerea Irigoyen Vergara

Madrid, 2009

CENTRO NACIONAL DE BIOTECNOLOGIA

Universidad Autónoma de Madrid

# Universidad Autónoma de Madrid
## Departamento de Biología Molecular
## Facultad de Ciencias

Memoria presentada para optar al grado de Doctor
en Ciencias Biológicas por

**Nerea Irigoyen Vergara**
Universidad Autónoma de Madrid
Mayo 2009

**DIRECTORES DE TESIS:**

**Dr. José Francisco Rodríguez Aguirre**
C.N.B.-C.S.I.C.
**Dr. José Ruiz Castón**
C.N.B.-C.S.I.C.

CENTRO NACIONAL DE BIOTECNOLOGIA
CSIC

El trabajo recogido en esta memoria ha sido realizado en el Centro Nacional de Biotecnología (C.N.B.-C.S.I.C.) bajo la dirección conjunta de los Drs., José Francisco Rodríguez Aguirre y José Ruiz Castón. Su financiación corrió a cargo de una beca de Formación Personal Universitario del Ministerio de Educación y Ciencia y una beca para estudiantes de tercer grado de la "Residencia de Estudiantes" a cargo del Gobierno de Aragón. Para la realización de estancias breves en el extranjero se contó con ayudas del Ministerio de Educación y Ciencia y de la Universidad Autónoma de Madrid.

# Abbreviations:

**3D:** Three Dimensional
**3DR:** Three Dimensional Reconstrucción
**α–XX:** antibody anti-XX
**aa:** aminoacid
**AcPHV:** Autographa californica polyhedrosis Virus
**ATCC:** American Type Cell Collection
**BBV:** Black Beetle Virus
**BF**: Bursa of Fabricius
**bp**: base-pair
**BSA:** Bovine Serum Albumin
**BTV:** Bluetongue Virus
**$C_\alpha$:** α-carbon
**CEF:** Chicken Embryo Fibroblast
**CP**: coat protein
**crioEM:** electron cryomicroscopy
**C-terminal:** carboxi-terminal
**Da:**Dalton
**DNA:** Desoxiribonucleic acid
**dsRNA:** double stranded RNA
**DMEM:** Dulbecco Modified Eagle's Medium
**dNTP:** desoxiNucleotide TriPhosphate
**DTT :** ditiotreitol
**DXV:** *Drosophila* X Virus
**EDTA:** Ethylene Diamine Tetraacetic Acid
**EM:** electron microscopy
**FCS:** Fetal Calf Serum
**FHV:** Flock House Virus
**hp.i.:** postinfection hours
**HT/His-tag:** Histidine Tag
**IBD**: Infectious Bursal Disease
**IBDV:** Infectious Bursal Disease Virus
**IP**: immunoprecipitation
**IPNV:** Infectious Pancreatic Necrosis Virus
**IPTG**: isopropyl-β-D-thiogalactopyranoside
**kb:** kilobase
**kDa**: kilodalton
**MOI:** Multiplicity Of Infection
**mRNA:** messenger RiboNucleic Acid
**MW:** Molecular Weight
**MWM:** Molecular Weight Marker
**NωV:** Nudaurelia capensis ω virus
**N-terminal:** Amino-terminal
**ORF:** Open Reading Frame
**PBS:** Phosphate Buffered Saline
**PCR:** Polymerase Chain Reaction
**PDB:** Protein Data Bank
**PepN**: aminopeptidase N
**PFU:** Plaque Forming Unit
**PIPES:** piperazine-N,N-bis(2-ethanesulfonic acid)
**PSA**: Puromycin Sensitive Aminopeptidase
**RdRp:** RNA dependent RNA polymerase
**rmsd:** root square mean deviation
**RNA:** Ribonucleic Acid
**RNP:** RiboNucleoProtein
**r.p.m**.: revolutions per minute
**rBV:** recombinant BaculoVirus
**rVV:** recombinant Vaccinia Virus
**qRT-PCR**: Quantitative real time polymerase chain reaction
**T:** triangulation number
**TBE:** Tris-Borato-EDTA buffer
**Tris:** tri-(hidroximetil)-aminomethane
**SDS:** Sodium Dodecil Sulfate
**SDS-PAGE:** SDS Polyacrilamide Gel Electrophoresis
**sh**: Short hairpin
**ssRNA:** single stranded RNA
**(+) ssRNA:** positive single stranded RNA
**SVP:** Subviral Particle
**UTR:** UnTranslated Region
**VLP:** Virus Like Particle
**WB:** Western Blot

## Amino Acid Abbreviations

| | |
|---|---|
| **Alanine** | Ala, A |
| **Arginine** | Arg, R |
| **Aspartic Acid** | Asp, D |
| **Asparagine** | Asn, N |
| **Cysteine** | Cys, C |
| **Glutamic Acid** | Glu, E |
| **Glycine** | Gly, G |
| **Glutamine** | Gln, Q |
| **Histidine** | His, H |
| **Isoleucine** | Ile, I |
| **Leucine** | Leu, L |
| **Lysine** | Lys, K |
| **Methionine** | Met, M |
| **Phenylalanine** | Phe, F |
| **Proline** | Pro, P |
| **Serine** | Ser, S |
| **Tyrosine** | Tyr, Y |
| **Threonine** | Thr, T |
| **Tryptophan** | Trp, W |
| **Valine** | Val, V |

# INDEX

# ABSTRACT:

The IBDV virus is icosahedral, ~70 nm in diameter and contains two dsRNA segments and five encoded mature proteins (VP1 to VP5). IBDV capsid is based on a single T=13 levo lattice and formed by 260 VP2 trimers disposed in 12 pentamers and 120 hexamers.

VP2 is synthezided as part of a polyprotein that is cotranslationally self-cleaved, releasing three polypeptides, namely pVP2 (the VP2 precursor), VP4 (the protease), and VP3 (a polypeptide with scaffolding activity among others). pVP2 (512 residues) undergoes subsequent processing events mediated by VP4 at three secondary alanyldipeptide targets (positions 487, 494 and 501). The resulting intermediates are further cleaved twice between residues Arg-452 and Arg-453 and between residues Ala-441 and Phe-442 to yield VP2 and several C-terminal peptides (accountig for 71 residues). Here, we have dilucidated the executor of the last pVP2→VP2 proteolytic maturation events associated with the pVP2 assembly into a procapsid-like structure.

A cellular protease, a puromycin sensitive aminopeptidase (PSA) cleaves pVP2 in the 452-453 scissile bond, and an autoproteolytic activity based on the Asp-431 is responsible of the last processing event.

. The structural polymorphism of pVP2, is due to an amphipathic α-helix located at its C-terminal end which acts as a transient conformational switch. VP3, the other major protein, participates in capsid assembly by electrostatic interactions of its C-terminal region with the molecular switch, acting as a molecular triggering factor. Moreover, it will exist an electrostatic interaction between the autocatalaytic residue (Asp-431) and the basic region of VP3 C-terminal domain, that may block the VP2 cleavage by Asp-431 until the capsid has been correctly assembled.

Together, all these results provide a better understanding of the multistep maturation process for the IBDV capsid.

# INTRODUCTION

Los virus representan la vida reducida a su esencia. En realidad, no son poco más que material genético protegidos por una cubierta proteica o como Sir Peter Medawar una vez dijo, “un conjunto de malas noticias envueltas en proteína” (Medawar PB, 1983).

Su principal característica es una absoluta dependencia hacia un hospedador, siendo un parásito obligado y representando una plaga para el resto de organismos. En 1898, el científico holandés Beyerinck y los investigadores alemanes Loeffler y Frosch establecieron, basándose en experimentos de filtración, que los agentes causantes de ciertas enfermedades (de plantas y animales) eran más pequeños que todas las bacterias conocidas. Sólo dos años más tarde, la fiebre amarilla fue la primera enfermedad viral humana en ser determinada (Mayor Reed y asistentes, Armada Estadounidense, La Habana, 1900), y hasta la fecha más de 1938 especies virales pertenecientes a 287 géneros y 73 familias han sido identificados (Fauquet y Fargette, 2005). Probablemente, los virus son tan antiguos como la vida en la Tierra, pero para el público general saltaron a la palestra con la pandemia del SIDA, los brotes del síndrome respiratorio severo agudo (SARS) y la gripe aviar.

Las partículas virales compuestas por una cápsida proteica, envuelta o no por una membrana, y un ácido nucleico, están diseñadas para mover su genoma entre las células de un posible hospedador. Los genomas virales exhiben una gran diversidad, y pueden ser de cadena simple o doble de ADN, simple o doble de ARN, de polaridad negativa, positiva, o de ambos sentidos; con una topología circular o linear, y existir sólo un segmento o varios de ellos. La cubierta proteica proporciona una envuelta protectora para el ácido nucleico, y es la responsable de ciertas reacciones químicas necesarias para la maduración de la partícula viral y la entrada de la misma en la célula. Esta cápsida se forma por múltiples copias de productos génicos idénticos, lo cual minimiza la información génica que se requiere para su formación. Esta estrategia que reduce la cantidad de proteínas que se codifican, genera un problema en el ensamblaje de estos multímeros; con decenas, centenas o miles de subunidades, en un mismo marco biológico (Johnson y Speir, 1997). Las cápsidas virales representan un excelente marco de trabajo para el análisis de aspectos del ensamblaje de complejos macromoleculares así como del polimorfismo estructural y las conformaciones transitorias. Además, las

cápsidas complejas requieren a su vez, una o más proteínas auxiliares (de andamiaje, accesorias y proteolíticas).

Crick y Watson, propusieron en 1956 que las cápsidas esféricas debían poseer geometría icosaédrica; ya que era el modo más efectivo de conseguir el máximo volumen con una pequeña proteína. Una corroboración experimental de esta hipótesis fue proporcionada por D.L.D. Caspar, quien notificó que los intensos reflejos observados en fotografías de rayos X del virus del enanismo ramificado del tomate (Tomato Bushy Stunt Virus-TBSV) correspondían a una disposición icosaédrica de orden cinco (Caspar, 1956).

De los cuerpos platónicos (compuestos por subunidades idénticas), los icosaedros son los que poseen el mayor número de caras. Un icosaedro posee 20 caras formadas por triángulos equiláteros. Como cada cara posee una simetría de orden tres, el sólido resultante está formado por 60 unidades asimétricas idénticas. El icosaedro también se puede definir en términos de sus 532 puntos de simetría. Cada uno de los doce vértices icosaédricos coincide con un eje de simetría de orden cinco (5x12=60); los ejes de simetría van desde uno de orden cinco a través del centro del icosaedro y salen por la otra cara. Los ejes de orden tres pasan por el centro de las caras. Además, hay 30 ejes de orden dos (2x30=60) que se determinan a través de los contactos arista-arista entre las caras del icosaedro.

La ventaja de la geometría icosaédrica es que una secuencia relativamente corta de ARN/ADN puede codificar una proteína capaz de encapsidar el genoma completo. La teoría de la cuasiequivalencia describe como múltiplos de 60 proteínas se disponen en una simetría icosaédrica para poder crear volúmenes mayores (Caspar y Klug, 1962). El postulado fundamental de la cuasiequivalencia es que las proteínas de la cápsida viral pueden formar pentámeros y hexámeros usando los mismos contactos entre subunidades. El único requerimiento para formar la cara de un icosaedro es ser un triángulo equilátero con tres unidades asimétricas idénticas dispuestas con una simetría de orden tres. Usando una red hexagonal uno puede observar que hay una serie infinita de triángulos equiláteros que encierran un número integral de triángulos más pequeños denominado número de triangulación (T). El área de una unidad asimétrica para un triángulo con un vértice en el origen (0,0) y un segundo vértice en el punto (**h**, **k**) es:

**$T=h^2+hk+k^2$**. El tamaño del triángulo equilátero es proporcional al número de triangulación y cada partícula poseerá 60T subunidades, que se dispondrán como 12 pentámeros y 10 (T-1) hexámeros (**Fig. 1**).

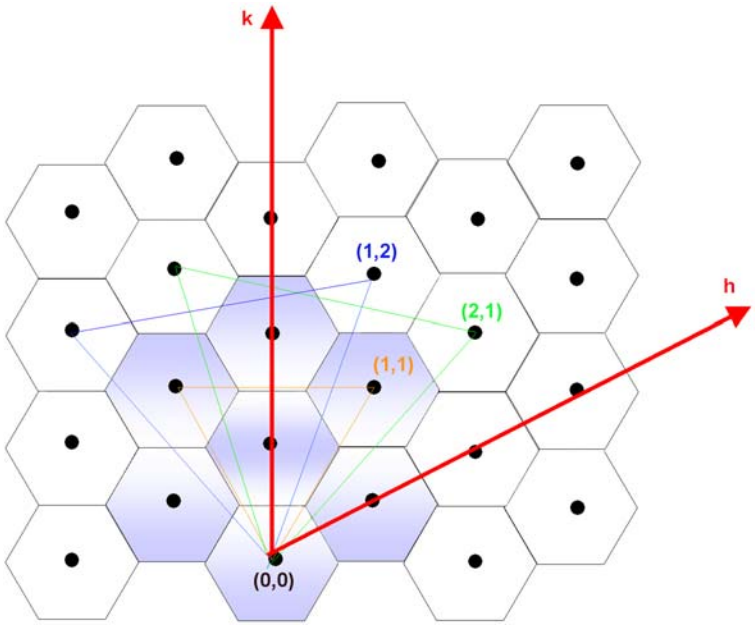


**Fig.1. Principios geométricos para la generación de superficies icosaédricas cuasi-equivalentes.** Los hexámeros se consideran inicialmente planos (un conjunto de formas hexaméricas forman una superficie plana como la que se muestra) y los pentámeros se consideran convexos, introduciendo una curvatura en la superficie de los hexámeros cuando se insertan. La cápsida icosaédrica cerrada, se genera por la inserción de 12 pentámeros en posiciones apropiadas de la red hexamérica. Para construir un modelo de superficie cuasi-equivalente, una cara de un icosaedro se genera en la red hexagonal. El origen se reemplaza con un pentámero y el hexámero (**h, k**) se reemplaza por otro pentámero. El tercer hexámero que se reemplaza se identifica con el orden se simetría de orden 3 (por ejemplo, para completar el triángulo equilátero de una cara). La cara icosaédrica de una superficie *T=3* se define por un triángulo de líneas naranjas (**h**=1, **k**=1). Existen dos posibles elecciones para una superficie *T=7* marcadas en verde y azul (**h**=2, **k**=1 o **h**=1, **k**=2, siendo imágenes especulares), y se requiere el conocimiento de la disposición de hexámeros, pentámeros y la estereoisomería de la cápsida para su completa definición (adaptado de Johnson y Speir, 1997).

La cuasisimetría surge debido a que las subunidades dentro de una unidad asimétrica no son equivalentes. En teoría, se pueden formar cápsidas cuasiequivalentes de cualquier tamaño y a veces distintos tipos de subunidades se utilizan para la formación de pentámeros y hexámeros, en cuyo caso se denomina pseudocuasiequivalencia y se define por un número P en lugar de T.

## 1.1. Diferentes mecanismos de control para el ensamblaje de la cápsida viral

En cápsidas con un número de triangulación mayor de uno, las subunidades proteicas deben adoptar distintas conformaciones dependiendo de su ambiente estructural dentro de la cápsida; lo que significa que las distintas uniones entre las subunidades no son idénticas existiendo distintas clases de confórmeros (Caspar y Klug, 1962). Estudios de estructurales de alta resolución han revelado algunas claves de cómo una proteína de la cápsida sabe la conformación que debe adoptar (Liddington y col., 1991; Rossmann y Johnson, 1989) aunque el mecanismo todavía se entiende poco (Johnson y Speir, 1997).

### 1.1.1. Control del cambio conformacional

La información del cambio conformacional que se requiere para el ensamblaje de una cápsida T>1 es intrínseca a las subunidades en sí mismas, lo que frecuentemente permite la formación de cápsidas correctas en la ausencia de otras proteínas y está determinado por factores como las regiones proteicas flexibles (lazos y dominios amino- y carboxi-terminales), interacciones con el ARN, iones metálicos, pH y distintas combinaciones de todos ellos (Johnson, 1996). En algunos casos, sin embargo, se forman una gran variedad de estructuras aberrantes relacionadas con la cápsida dependiendo de ciertas condiciones fisiológicas (Krol y col., 1999; Salunke y col., 1989; Savithri y Erickson, 1983; Schwartz y col., 2000). La restricción de esta flexibilidad inherente para que sólo las conformaciones apropiadas sean las que puedan ensamblarse, es algo muy importante en el proceso de ensamblaje casi tanto como la capacidad de generar variabilidad conformacional.

Hay una conexión muy estrecha entre el plegamiento de una proteína y su ensamblaje. Las proteínas estructurales virales son frecuentemente bastante flexibles en solución y cada subunidad elige su disposición en base al estado conformacional de sus vecinos (Berger y col., 1994).

### 1.1.2. Proteínas formadoras de "cores" y de andamiaje

Conforme la cápsida empieza a adquirir una mayor complejidad y el número de interacciones aumenta, la información adicional para constreñir las posibilidades conformacionales de la proteína de la cápsida y para asegurar la fidelidad en el proceso de ensamblaje también será mayor. Esta información, vendrá dada por una proteína que forma un "core" o que actúe como proteína de andamiaje.

Un "core" es lo suficientemente simple para poder autoensamblarse sin ninguna información adicional. Una vez que el tamaño de la cápsida es especificado por el "core", la simetría se determina por la disposición de los distintos multímeros de la proteína de la cápsida sobre este patrón (Berger y col., 1994), a pesar de que ciertas de estas interacciones sean relativamente no específicas (Grimes y col., 1998). Entre las proteínas mejor caracterizadas que cumplen esta función, se encuentra el precursor de la proteína VP22a de herpes simple tipo I, que interacciona con la proteína mayoritaria de la cápsida, VP5, a través de los últimos 25 residuos de su C-terminal. Esta interacción es esencial para el ensamblaje viral (Zhou y col., 1998).

El término de "proteína de andamiaje" se refiere usualmente a aquella que juega un papel estructural esencial en ciertos episodios del ensamblaje, y que posteriormente es retirada, de modo análogo al papel de las chaperonas moleculares en plegamiento de proteínas. Las proteínas de andamiaje suelen compartir una organización estructural similar, incluyendo su forma alargada, y un dominio específico de interacción con la cápsida en su C-terminal. La proteína de andamiaje por sí misma no forma una estructura simétrica pero aparentemente proporciona suficiente información para constreñir la simetría de la cápsida ya que define el tamaño global de la cápsida externa, (Dokland, 1999); por ejemplo, la proteína de andamiaje gp0 es necesaria para la formación de cápsidas viables de bacteriófagos P2 y P4 (Chang y col., 2009).

### 1.1.3. Cambios conformacionales mayores

Mientras los cambios conformacionales "menores" proporcionan el mecanismo necesario para la generación de diversidad estructural que se requiere en la formación de cápsidas grandes; algunos virus son capaces de llegar más allá y sufren una

reorganización a gran escala de su estructura. El ejemplo más típico se encuentra en los bacteriófagos de doble cadena de ADN, cuya cápsida sufre una expansión (Conway y col., 1995; Dokland y Murialdo, 1993). La resolución de la precabeza II, uno de los intermedios de ensamblaje del bacteriófago HK07, a 3.65Å de resolución ha revelado un mecanismo de expansión sin precedentes que describe esta transición (Gertsman y col., 2009).

### 1.1.4. Estructuras intermedias en el ensamblaje

Se ha asumido que los virus se ensamblan a través de estructuras intermedias, que representan un subconjunto de la estructura final de la cápsida; ya que el ensamblaje a través de estos intermedios reduce el número de errores de manera dramática (Berget, 1985). Ejemplos de virus que ensamblan a través de intermedios procápsidas son los herpesvirus (Newcomb y col., 2009) y bacteriófagos como T7 (Agirrezabala y col., 2007).

El proceso de ensamblaje se lleva a cabo a través de eventos separados de nucleación y crecimiento. De esta manera, el núcleo inicial que consiste en un subensamblaje específico va creciendo por la adición distintas subunidades y estructuras (Stehle y col., 1996).

### 1.1.5. Procesamiento proteolítico

Las proteasas pueden ser de origen celular o viral y juegan papeles esenciales en la replicación viral, incluyendo el ensamblaje coordinado y la maduración de los viriones (Hellen y Wimmer, 1992). La mayoría de estas enzimas pertenecen a una de estas tres clases (Ser, Cys o Asp) y están implicadas en dos funciones principales de la morfogénesis viral. La primera, es el corte proteolítico de grandes poliproteínas estructurales codificadas por retrovirus y virus de ARN, el cual es un prerrequisito para el ensamblaje de la partícula viral. La segunda función, es la maduración dependiente de ensamblaje de las partículas virales, que suele estar acompañada por la adquisición de la infectividad. Por ejemplo, en orthoretrovirus, la mayoría de las partículas que se liberan son inmaduras y una proteasa viral es la encargada de cortar la poliproteína Gag durante

o tras un tiempo corto tras el ensamblaje para permitir la maduración de las partículas (Adamson y Freed, 2007).

Por otro lado, las proteasas celulares procesan a los precursores de las proteínas virales de una manera convencional después que estos hayan sido transportados a compartimentos vesiculares, como en infecciones por el virus de la hepatitis A, en el que las procápsidas inmaduras llegan a lisosomas tempranos en los que la proteasa celular, catepsina L, elimina el péptido 2A madurándose así la partícula (Morace y col., 2008). Por el contrario, los cortes por proteasas virales son más complejos; y ocurren a través de una gran variedad de mecanismos facilitando el ensamblaje de estructuras virales complejas y la maduración post-ensamblaje del virión (Gallagher y Rueckert, 1998).

## 1.2. Familia *Birnaviridae*: el virus de la bursitis infecciosa

La familia *Birnaviridae* forma una familia distintiva de virus de ARN de doble cadena (dsRNA) que infectan a distintas especies animales tan diferentes como vertebrados, moluscos, insectos y rotíferos (Delmas, 2004). Posee tres géneros diferentes: *Aquabirnavirus, Entomobirnavirus* y *Avibirnavirus*. Los miembros representativos de cada uno de ellos son; el virus de la necrosis pancreática infecciosa (IPNV); el virus *Drosophila* X (DrXV); y el virus de la bursitis infecciosa (IBDV), respectivamente (Fauquet y Fargette, 2005). La mayoría de los esfuerzos realizados en investigación se han centrado en IBDV (Muller y col., 2003), con interesantes propiedades de virulencia y responsable de importantes pérdidas económicas en la industria avícola. Otro birnavirus económicamente importante es IPNV que se encuentra en salmónidos y produce grandes pérdidas económicas en piscifactorías (Delmas, 2004).

**IBDV** es el agente causal de la enfermedad de la bursitis infecciosa (IBD) que afecta a pollos jóvenes. Cuando IBD apareció en 1958, se designó como “enfermedad de Gumboro” ya que los primeros brotes se documentaron en Gumboro, Delaware, EEUU. Las infecciones con IBDV exacerban la infección con otros agentes etiológicos

y reduce la capacidad de respuesta a la vacunación; produciéndose un gran impacto económico a nivel mundial en la industria avícola (van den Berg y col., 2000).

Las células linfoides de la bolsa de Fabricio son las principales células diana de IBDV. Entre las tres y seis semanas tras la rotura del cascarón, la bolsa de Fabricio alcanza su máximo desarrollo, siendo en ese momento los pollos altamente susceptibles a la infección por el virus. La infección produce la depleción de linfocitos y la destrucción de la bolsa. En brotes clásicos, la mortalidad varía del 1 al 50%. También se ha observado una disminución en la producción de huevos con un deterioro en la calidad de los mismos, sobre todo de la cáscara y una inmunosupresión asociada a la infección con alta prevalencia de infecciones virales respiratorias y elevada mortalidad debida a airesaculitis y colisepticemia (Kaufer y Weiss, 1980).

IBDV es resistente a todos los procedimientos tradicionales de desinfección como la inactivación química o por calor. Por el momento, el único método disponible para controlar la expansión de la enfermedad son programas intensivos de vacunación (Negash y col., 2004), a pesar de que el uso indiscriminado de vacunas atenuadas permitió la rápida diseminación del virus alrededor del mundo (Yamaguchi y col., 1996). La búsqueda de nuevas estrategias para controlar y erradicar la enfermedad es nuestra prioridad, siendo especialmente importante en países en vía de desarrollo, donde la carne de pollo es la base proteica de la dieta.

### 1.2.1. Serotipos de IBDV

Hay dos tipos diferentes de serotipos de IBDV, I y II, que se distinguen por ensayos específicos de sero-neutralización (McFerran y col., 1980). El **serotipo I** incluye a aislados patogénicos en pollos domésticos, mientras que el **serotipo II**, presente en pavos no produce síntomas clínicos ni protección frente a los aislados de tipo I. Los aislados del serotipo I se subdividen en variantes clásica, antigénica y muy virulenta. IBDV de variante-antigénica sólo se ha documentado en Estados Unidos (desde 1985) y posee cambios simples de aminoácidos en una región específica de la proteína VP2 (región hipervariable), lo cual produce distintos fenotipos patológicos (Snyder, 1990). En Europa, desde 1988, se han descrito aislados de IBDV que han incrementado su virulencia (IBDV muy virulento [vvIBDV]) con la misma estructura antigénica que los aislados clásicos (Chettle y col., 1989). Diferencias en aminoácidos

entre las proteínas virales de aislados muy virulentos y clásicos se encontraron en todas las proteínas virales, aunque la mayoría de ellos se encontraban en la región hipervariable de VP2 (Brown y Skinner, 1996; Pitcovski y col., 1998).

### 1.2.2. Organización genómica de IBDV

El genoma de IBDV está formado por dos segmentos de ARN de doble cadena (dsRNA) de 3,2 kb (segmento A) y 2,8 kb (segmento B) (Muller y Nitschke, 1987a; Muller y col., 1979) con regiones no traducidas (UTR) en las regiones 5' y 3'. Estudios de síntesis de ssRNA *in vitro* muestran que la ARN polimerasa sintetiza ssRNA viral de manera semi-conservativa por un mecanismo de desplazamiento de la cadena parental por la cadena naciente (Spies y col., 1987) (**Fig. 2**).

El **segmento A** contiene dos marcos de lectura (open reading frame-ORF) parcialmente solapados. La ORF más pequeña codifica **VP5** (15 kDa), un polipéptido no esencial, que está involucrado en la diseminación viral (Lombardo y col., 2000) e inhibe la apoptosis en los estadios iniciales de la infección viral (Liu y Vakharia, 2006). La ORF más grande codifica una poliproteína de 110 kDa que sufre un procesamiento proteolítico cotraduccional por la proteasa viral VP4, dando lugar a **pVP2** (54.4 kDa), **VP3** (29 kDa), y **VP4** (26.7 kDa).

**Segmento B** codifica **VP1** (97.8 kDa), la polimerasa de RNA dependiente de RNA (RpRd) (Morgan y col., 1988; Muller y Nitschke, 1987b; von Einem y col., 2004) implicada en replicación viral. Como otras polimerasas dsRNA, **VP1** cataliza la replicación y transcripción viral (Pan y col., 2007; Spies y col., 1987; Xu y col., 2004). Aunque la polimerización de ARN y la iniciación ("priming") normalmente suponen diferentes componentes virales, en birnavirus la polimerasa es responsable de ambas actividades. VP1 se guanilida a sí misma actuando como "primer" para la síntesis de ARN (Dobos, 1993; Shwed y col., 2002; Spies y Muller, 1990; Xu y col., 2004).

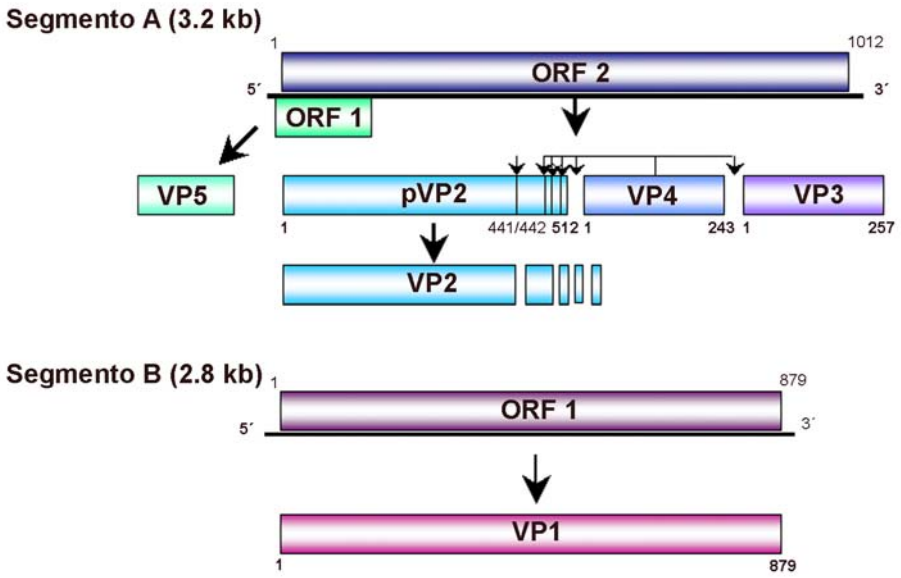


**Fig.2. Organización genómica de IBDV**. El segmento A posee dos marcos abiertos de lectura (ORFs) parcialmente solapados, que codifican la proteína VP5 y la poliproteína viral, respectivamente. La poliproteína sufre un autoprocesamiento por la proteasa viral VP4, dando lugar a pVP2, VP3 y VP4. El C-terminal de pVP2 es posteriormente procesada produciendo la VP2 madura. El segmento B codifica la VP1, la polimerasa RNA dependiente de RNA.

## 1.2.3. Estructura y morfogénesis de IBDV

### 1.2.3.1. Componentes estructurales del virión de IBDV

Las partículas infecciosas de IBDV, formadas por dos proteínas mayoritarias (VP2 y VP3) y dos minoritarias (VP1 y VP4), se ensamblan y se acumulan en el citoplasma (**Fig. 3B**).

Las purificaciones virales dan lugar a seis poblaciones diferentes que comparten una composición proteica idéntica pero con un coeficiente de sedimentación mayor conforme la densidad de la partícula se incrementa. Análisis estequiométricos de su genoma indica que estas diferencias biofísicas se correlacionan con el número de segmentos de dsRNA que encapsida la partícula viral. Las partículas de IBDV con un mayor número de copias del genoma poseen mayores ratios de infectividad (Luque y col., 2009a).

El virión posee una cápsida sencilla con un diámetro externo de 65-70nm formada por 260 subunidades triméricas cuasiequivalentes de **pVP2/VP2** organizadas

con una arquitectura T=13l (*levo*) (Bottcher y col., 1997; Caston y col., 2001; Coulibaly y col., 2005). Los trímeros de (p)VP2 se organizan en 12 pentámeros y 120 hexámeros, con cinco conformaciones distintas (a-e). VP2 representa el principal marcador de virulencia y patogénesis y también induce anticuerpos neutralizantes (Brandt y col., 2001) (**Fig. 3A**).

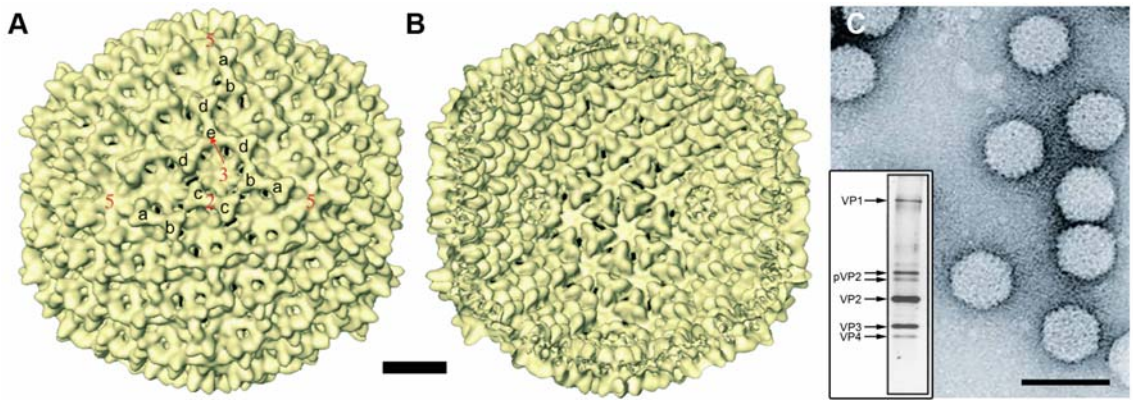


**Fig.3. Estructura de la cápsida**. (**A-B**). Representaciones de superficie a 10 Å (Luque y col., 2001) de la superficie externa (**A**) e interna (**B**) de la cápsida de IBDV vista desde un eje de simetría de orden tres. Los cinco tipos distintos de capsómeros triméricos se indican por las letras a-e. Barra=100 Å. Los ejes de simetría se indican con números rojos. (**C**). Viriones purificados de IBDV por tinción negativa con acetato de uranilo. Barra=100nm. En el recuadro se muestra el análisis electroforético y la tinción de plata viriones maduros de IBDV (Lombardo 1999). Las proteínas estructurales se indican por una flecha: VP1 (97.8 kDa), pVP2 (~54 kDa), VP2 (47 kDa), VP3 (29 kDa) y VP4 (26.7 kDa).

**pVP2** (512 residuos) es la forma precursora de la proteína de la cápsida VP2. Los 71 residuos finales del C-terminal de pVP2 son procesados proteolíticamente dando lugar al polipéptido maduro VP2 (47 kDa, 441 residuos). Se ha propuesto una maduración postraduccional en dos eventos distintos: procesamiento por VP4 en dianas secundarias de dipéptidos de alanina en las posiciones 487, 494 y 501 (generando como mínimo cuatro variantes distintas de pVP2) (Sanchez y Rodriguez, 1999), y el corte entre los residuos (441-442), que se discutirá más adelante. La maduración es necesaria para el correcto ensamblaje viral (Chevalier y col., 2002) y estos pequeños péptidos generados en este proceso permanecen asociados a las partículas virales (Da Costa y col., 2002), y poseen capacidad de desestabilización de membranas, con un posible papel en la internalización viral (Chevalier y col., 2005; Galloux y col., 2007). Además, una maduración post-ensamblaje similar de pVP2 se ha demostrado para IPNV (Villanueva y col., 2004).

**VP3** es una proteína con múltiples funciones que actúa a distintos niveles del ciclo viral. VP3 es una proteína de andamiaje durante el ensamblaje viral, probablemente por la interacción con VP2, este hecho se discutirá posteriormente. VP3 también interacciona con VP1 y dsRNA (Maraver y col., 2003a; Maraver y col., 2003b; Tacken y col., 2002). En realidad, la interacción de VP3 con VP1 es la responsable de la encapsidación de la polimerasa dentro de pseudopartículas virales (VLP) (Lombardo y col., 1999). La región de VP3 responsable de esta interacción se encuentra en un dominio de 16 aa con gran número de cargas eléctricas muy próximo al extremo C-terminal de la proteína (Maraver y col., 2003a). Recientemente se ha demostrado que esta interacción desbloquea el sitio activo de la RdRp, actuando así como un transactivador transcripcional (Garriga et al., 2007).

Por otro lado, el dominio de VP3 que interacciona con dsRNA se ha localizado por mutantes de deleción en 69 aa localizados muy cerca de la región N-terminal. Mediante ensayos *in vitro*, se demostró que la capacidad de unión a dsRNA era independiente de secuencia, consistente con una papel general de VP3 en estabilización del ARN viral (Kochan y col., 2003). VP1, VP3 y el genoma viral forman un complejo ribonucleoproteico (RNP) transcripcionalmente activo (Luque y col., 2009b).

**VP4** es una proteasa Lon Ser-Lys no canónica (Birghan y col., 2000), y su estructura atómica se ha determinado recientemente (Feldman y col., 2006; Lee y col., 2007). A VP4 le falta el dominio ATPasa de las proteasas Lon, aunque su sitio catalítico es la diada Ser-652-Lys-692. VP4 actúa de manera cotraduccional y autocatalítica (Birghan y col., 2000). VP4 es un componente estructural del virión aunque su encapsidación es variable (Granzow y col., 1997; Luque y col., 2009a). En células infectadas por IBDV, VP4 forma estructuras tubulares (túbulos tipo-II) con un diámetro de 25 nm.

### 1.2.3.2. Sistemas de expresión basados en virus para el análisis del ensamblaje de IBDV

Una de las aproximaciones más exitosas para el entender el papel de las distintas proteínas en el ensamblaje del virión, ha sido el uso de sistemas de expresión heterólogos capaces de mimetizar la formación de VLP.

La expresión de la poliproteína de IBDV en células de mamíferos usando un virus vaccinia recombinante (rVV) da lugar al correcto procesamiento de la poliproteína y a la acumulación de una gran cantidad de VLP de forma y tamaño similar a los viriones (Fernandez-Arias y col., 1998; Lombardo y col., 1999), mediante este sistema también se han recuperado cápsidas más pequeñas con un número de triangulación T=7, con tres conformaciones distintas.

La expresión de la poliproteína de IBDV en células de insecto mediante el sistema de expresión de baculovirus (rBV) también produce el procesamiento y la acumulación de pVP2, VP3 y VP4. Sin embargo, los ensamblados producidos son variables estructuralmente y la formación de VLP es bastante ineficiente. El uso de un vector de transferencia FastBac para generar un baculovirus que codifica la poliproteína produce estructuras tubulares rígidas (túbulos de tipo I), con diámetros de 50 nm (Martinez-Torrecuadrada y col., 2000). Estos túbulos, compuestos por pVP2, muestran una disposición hexagonal, similar a los observados en células infectadas por IBDV (Martinez-Torrecuadrada y col., 2000). Estos resultados indican que las células de insecto poseen algún factor(es) que interfieren negativamente con el ensamblaje de VLP (por ejemplo, proteínas celulares y/o el ambiente del hospedador), algunos de estos factores se discutirán más adelante.

### 1.2.3.3. Polimorfismo estructural de la proteína de la cápsida de IBDV

La expresión de formas maduras de VP2 usando distintos vectores basados en rBV resulta en la formación de partículas isométricas de 26 nm de diámetro (Caston y col., 2001; Coulibaly y col., 2005; Lee y col., 2003). Un examen de estas partículas subvirales (SVP) muestran que son estructuras dodecaméricas con un número de triangulación T=1, compuestas de 20 trímeros de VP2 (Caston y col., 2001) (**Fig. 4A**). Esto indica que los trímeros aislados de VP2, poseen la información intrínseca que se requiere para su ensamblaje en pentámeros pero no en hexámeros. Mientras la expresión de pVP2 produce estructuras tubulares poco ordenadas compuestas por hexámeros (**Fig. 4C and 4G**), pero no posee la suficiente información para producir el patrón de interacciones complejas que se requiere para construir una cápsida T=13 (Caston y col., 2001; Saugar y col., 2005).

Las diferencias de comportamiento en el ensamblaje de VP2 y pVP2 indican que la información que afecta a las interacciones entre subunidades está contenida dentro del dominio carboxi-terminal de pVP2 (pVP2CTD). Estos resultados sugieren que (i) pVP2CTD juega un papel importante en la determinación de las diferentes conformaciones de VP2, y (ii) la formación de la cápsida de IBDV requiere la interacción de VP2 con otros componentes virales.

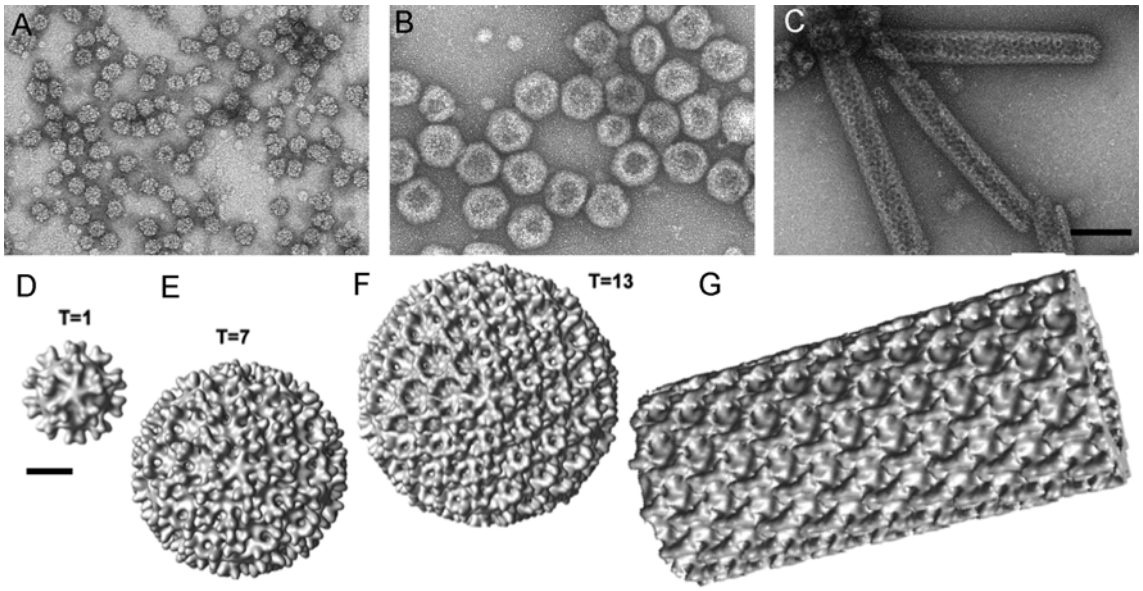


**Fig.4. Polimorfismo estructural de la proteína de la cápsida VP2 en células de insecto.** (**A**) SVPs T=1 (**B**) cápsidas T=13 y (**C**) tubos rígidos purificados de células de insecto infectadas con rBVs que expresan la proteína madura VP2, la proteína quimérica HT-VP2-466 y la poliproteína. Barra=100nm. Reconstrucción tridimensional de (**D**) una SVP, (**E**) cápsida T=7, (**F**) cápsida T=13 y (**G**) tubo pVP2 a 26 Å de resolución. Barra=10nm.

El péptido 443-GFKDIIRAIR-452 de pVP2CTD, ausente en la proteína madura de VP2, forma una hélice-α anfipática. VP2 con esta hélice-α es capaz de ensamblar en cápsidas T=13 (**Fig. 4B y 4F**), pero sólo cuando se expresa conjuntamente con una proteína quimérica que expresa en el N-terminal la extensión de un Tag de histidinas (His tag) (Saugar y col., 2005). Con esta configuración, la hélice-α anfipática actúa como un interruptor molecular temporal ("molecular switch"). El His tag emula parcialmente la región C-terminal de VP3, que actúa como un efector molecular ("triggering factor"). Los últimos cinco aminoácidos del C-terminal de VP3 son homólogos al segmento ácido del His tag. No se han encontrado segmentos similares en la secuencia VP3. Estudios indirectos confirman la importancia del domino C-terminal de VP3 (Chevalier y col., 2004; Gonzalez y col., 2005; Maraver y col., 2003b); cuya

función es aquella de las proteínas de andamiaje canónicas (Coulibaly y col., 2005; Saugar y col., 2005) y además se ha demostrado que VP3 participa en la capacidad inherente de pVP2 para adquirir las distintas conformaciones a través de pVP2CTD (Ona y col., 2004). Una posible interacción electrostática entre la hélice-α anfipática de VP2 y la región ácida del dominio C-terminal de VP3 se desarrollará más adelante.

### 1.2.3.4. Estructura atómica de VP2 y VP3:

La estructura atómica de T=1 SVP se ha resuelto por cristalografía de rayos-X [PDB 1WCD, (Coulibaly et al., 2005); PDB 2GSY, (Garriga et al., 2006); PDB 2DF7, (Lee et al., 2006)]. La subunidad de VP2 se pliega en tres dominios denominados proyección (P), carcasa o "shell" (S) y base (B) (**Fig. 5**). Los dominios S y P son barriles-β con una topología "jelly roll", orientada de tal manera que las láminas-β están orientadas tangencial y radialmente a la partícula esférica. El dominio B consiste en un conjunto de hélices-α que se forman de la extensión de los dominios amino- y carboxi-terminal de VP2, localizados en la superficie interna de la cápsida (**Fig. 5**). Más allá de las interacciones laterales entre los trímeros de VP2, las SVP están estabilizadas por iones $Ca^{2+}$ localizados en los ejes de simetría de orden tres e interaccionando con dos residuos ácidos Asp-31 y Asp-174, que agrega a las tres subunidades de cada trímero. Una mayor estabilización viene acompañada por una larga hélice C-terminal (α4) de la subunidad de VP2 que se proyecta más allá del "core" de la proteína, orientada a través del eje de simetría de orden tres a través del trímero vecino de VP2 (Garriga et al., 2006).

**VP3** posee un papel de andamiaje y su capacidad de autoensamblaje es similar a la de muchas otras proteínas de andamiaje en bacteriófagos (Tacken y col., 2000). La estructura atómica de la región central de la proteína VP3 (Casanas y col., 2008) (**Fig. 5B**) muestra dos dominios formados por hélices-α, cuya interacción forma aparentemente un dímero biológico. El uso de mutantes de deleción ha permitido señalar el dominio de oligomerización de VP3 entre los residuos 224 a 247, cerca del dominio C-terminal de la proteína (Maraver y col., 2003b)

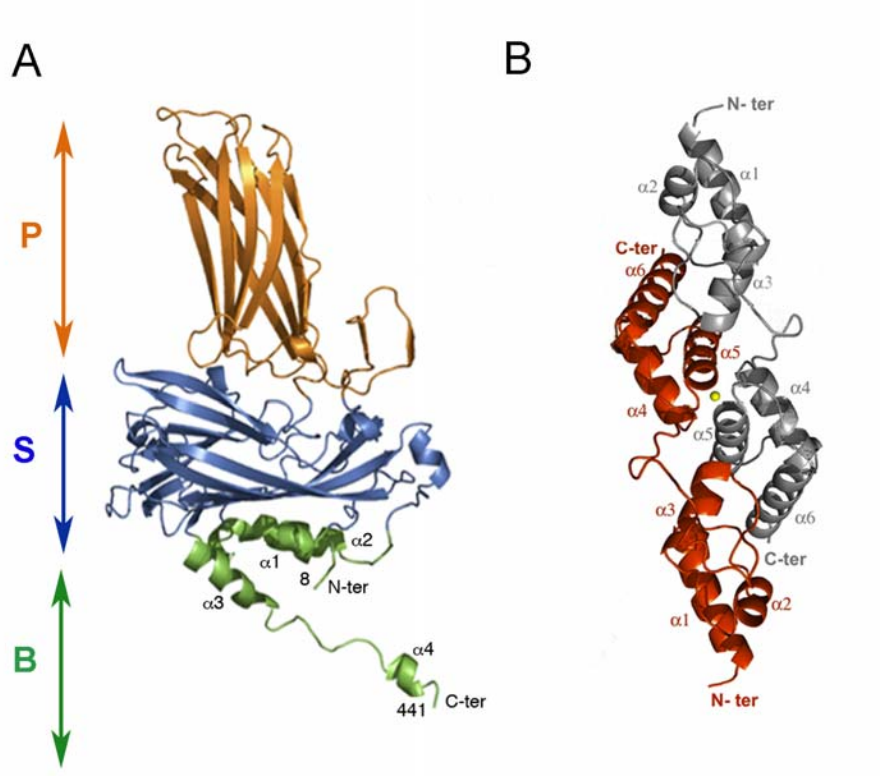


**Fig.5. Estructuras atómicas de VP2 y VP3.** (**A**) Modelo tridimensional de la estructura de VP2 ( entrada PDB 2GSY) resuelta por difracción de rayos-X a 2.6 Å (Garriga et al., 2006). Los dominios P, S y B están coloreados en naranja, azul y verde respectivamente. (**B**) Representación de un dímero de VP3, (entrada PDB 2Z7J) resuelto por difracción de rayos-X a 2.4 Å (Casanas et al., 2008), con un protómero marcado en rojo y el segundo en gris. Uno de los iones de oro (amarillo) ocupa el eje de orden dos y también participa en interacciones protómero-protómero.

## 1.3. Relaciones estructurales y funcionales de IBDV con virus ssRNA y dsRNA:

La arquitectura de la cápsida de IBDV es similar a las cápsidas externas de otros virus dsRNA, con los que comparte una organización T=13l. Sin embargo, a excepción de los birnavirus, todos los virus dsRNA poseen un "core" interno con una arquitectura característica T=1, constituida por 120 subunidades en el que la unidad fundamental es el dímero. Esta organización es una notable excepción a la teoría de cuasiequivalencia y se denomina cápsida "T=2" (el cual es un número "prohibido"). Hasta hace poco, el core T=2, como unidad funcional involucrada en la transcripción, replicación y protección del dsRNA frente a los mecanismos de defensa del hospedador (Gouet y col., 1999; Lawton y col., 1997; Prasad y Prevelige, 2003), se consideraba un componente

esencial de los virus dsRNA. Sin embargo, la existencia de los birnavirus claramente establece que el dsRNA puede replicarse sin la necesidad de esta estructura.

Los birnavirus deben compensar esta falta de nucleocápsida T=2, usando otras alternativas entre sus componentes estructurales. En este contexto, la interacción entre VP3, VP1 y el dsRNA posee un papel fundamental en la organización funcional de la cápsida de IBDV a nivel morfogenético, transcripcional y replicativo (Ahlquist, 2005; Garriga y col., 2007; Luque y col., 2009b).

También se han encontrado interesantes similitudes entre los birnavirus y los virus ssRNA, noda- y tetravirus. Estos dos grupos de virus poseen de igual manera, un genoma bisegmentado (Fauquet y Fargette, 2005), una permutación en sus RdRp (Gorbalenya y col., 2002), proteínas de la cápsida similares (Coulibaly y col., 2005) y una maduración proteolítica de la misma esencial para la adquisición de la infectividad viral (Gallagher y Rueckert, 1988; Schneemann y col., 1998; Zlotnick y col., 1994).

**Nudaurelia capensis ω virus (NωV)** es el prototipo de los **ω-tetraviruses**; virus ARN de cadena simple (ss) y polaridad positiva, sin envoltura y con un número de triangulación T=4 y genoma bisegmentado. Los dos segmentos de ARN empaquetados en cada cápsida viral se componen de, ARN1 de 5,3 kb, el cual codifica la polimerasa ARN dependiente de ARN (RdRp), y ARN2 de 2,4 kb codificante para el precursor de la proteína de la cápsida, proteína-α (70-kDa). Los tetravirus infectan exclusivamente a insectos del orden *Lepidopteran*. La expresión de proteína-α de NωV en el sistema recombinante de baculovirus, produce el ensamblaje espontáneo de un intermedio procápsida. Tras la acidificación del medio (pH 5.0) se produce un cambio conformacional a gran escala dando lugar a la cápsida madura (Canady y col., 2000), seguido del corte autoproteolítico de la proteína de la cápsida. Mutaciones puntuales en la Asn del sitio de corte (Asn-570-Phe-571) permite un cambio conformacional reversible procápsida-cápsida en función del pH (Taylor y col., 2002). Se ha propuesto como mecanismo de corte que el Glu-103 ejerce un ataque nucleofílico sobre Asn-570. Mutaciones en el residuo Glu-103 producen el corte de manera menos eficiente (Taylor y Johnson, 2005).

**Nodavirus** es una familia de pequeños virus icosaédricos que infectan insectos, mamíferos y peces, que incluye a las especies **Flock House Virus (FHV)** y **Black Beetle Virus (BBV)** (Hendry, 1991; Kaesberg, 1987; Mori y col., 1992). La partícula viral consiste en 180 copias de la proteína de la cápsida y un genoma bisegmentado. El genoma viral sólo codifica tres proteínas: la proteína-α (precursora de la proteína de la cápsida) en el ARN2; ARN1 codifica la replicasa y una pequeña proteína de 12-kDa denominada B2, que inhibe ARN de interferencia en células de *Drosophila* (Li y col., 2002). La cápsida de nodavirus posee una simetría icosaédrica con un número de triangulación T=3 que ensambla inicialmente en un provirión que madura por el corte autoproteolítico de la proteína-α, dando lugar a la proteína-β, que forma la cápsida viral, y el péptido-γ, que permanece asociado en el interior de la cápsida (Gallagher y Rueckert, 1988). La maduración proteolítica es necesaria para la adquisición de la infectividad (Schneemann y col., 1992) y estabilización del virión (Gallagher y Rueckert, 1988). La reacción proteolítica dependiente del residuo Asp-75 lanza un ataque nucleofílico sobre Asn-363 del sitio de corte (Zlotnick y col., 1994). En ambos casos, el péptido-γ**,** similar en FHV y NωV, parece estar involucrado en las translocación del ARN a través de membranas al principio de la infección (Cheng y col., 1994). También se ha demostrado el rescate de FHV defectivos en maduración y por tanto en infectividad con particulas similares a virus (VLP) maduras no infecciosas (Walukiewicz y col., 2008).

Por otro lado, un análisis de comparación de secuencias demuestra que las RdRp de los tetra- y birnavirus pertenecen a las polimerasas ARN no canónicas definidas por una permutación en el dominio de la palma con un motivo C-A-B en lugar del canónico A-B-C (Gorbalenya y col., 2002). Estos resultados sugieren que las polimerasas ARN primigenias podrían haber presentado una organización del dominio de la palma no canónico, a partir del cual las canónicas podrían haber evolucionado, siendo las RdRp de birna- y tetravirus trazas evolutivas de este proceso. La resolución cristalográfica por rayos X de VP1 (Garriga y col., 2007; Pan y col., 2007) demuestra que la permutación en el dominio C está asociado al mecanismo de regulación de la actividad catalítica por su interacción con el dominio C-terminal de VP3 (Garriga y col., 2007).

Adicionalmente, la proteína VP2 de los birnavirus es un híbrido estructural entre las proteínas de la cápsida de virus ssRNA de cadena positiva (noda- y tetravirus) y de

la cápsida T=13 de la familia *Reoviridae* (virus dsRNA) (Coulibaly y col., 2005). Mientras que el dominio S y B de VP2 posee una gran homología con sus equivalentes de la proteína de la cápsida de noda- y tetravirus, el dominio protuberante (P) de VP2 y de la proteína de la cápsida de reovirus T=13 son estructuralmente similares (**Fig. 6**). De hecho, en noda- y tetravirus así como en IBDV, las hélices-α que tapizan la superficie interna de la cápsida generan canales hidrofílicos en los ejes de simetría de orden cinco que podrían estar implicados en la translocación de las nuevas moléculas transcritas de ssRNA a través de la cápsida (Coulibaly y col., 2005; Garriga y col., 2006; Munshi y col., 1996); esta extrusión a través de los ejes pentaméricos es una estrategia que se ha demostrado para miembros de la familia *Reoviridae* (Diprose y col., 2001; Lawton y col,1997).

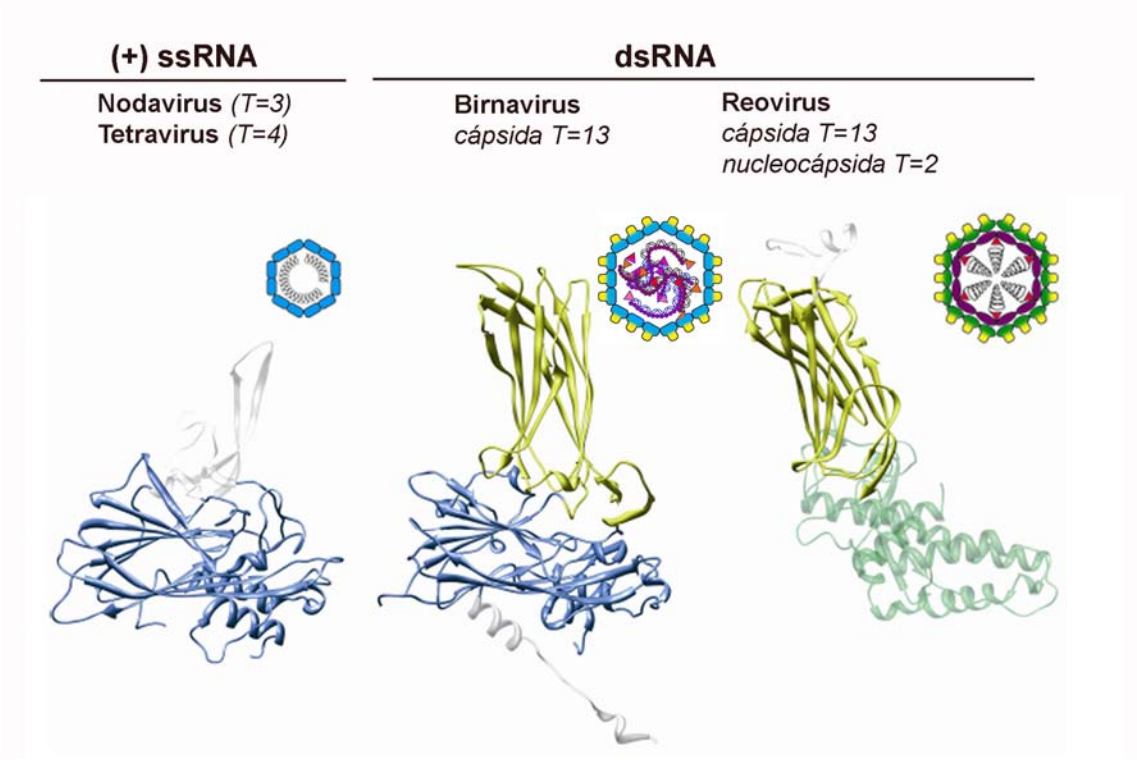


**Fig.6. Relación estructural entre las cápsidas proteicas de virus (+) ssRNA y dsRNA.** Comparación estructural de la estructura cristalográfica de la proteína β de FHV, un nodavirus (PDB 2Q26), con VP2 de IBDV (PDB 2GSY) y VP6 de rotavirus, un reovirus (PDB 1QHD). El código de color coincide con los aspectos estructurales similares entre las distintas familias *Nodaviridae/Tetraviridae*, *Birnaviridae* y *Reoviridae* representados en la parte superior. Las proteínas de la cápsida de nodavirus y birnavirus poseen una alta homología estructural (representada en azul) entre los dominios S y B. El dominio P de birnavius y reovirus es similar (en amarillo). Las cápsidas de nodavirus, birnavirus y reovirus contienen respectivamente, ssRNA desnudo, complejos filamentosos de dsRNA con VP3 (círculos naranjas) y VP1 (triángulos rojos); nucleocápsidas T=2 (púrpura) con dsRNA ordenado y complejos transcripcionales. Adaptado de Alquist 2005.

Viruses represent life stripped to the bare essentials. They are one of the smallest and simplest infectious agents identified to date. Indeed they are little more than a piece of genetic material protected by a protein coat or as Sir Peter Medawar said-“a piece of bad news wrapped up in protein” (Medawar PB, 1983).

The prime characteristic of viruses is their absolute dependence on a host for multiplication and, as such, they are obligate parasites and a plague to all living organisms. Back in 1898, the Dutch scientist Beyerinck and the German researchers Loeffler and Frosch established, based on filtration experiments, that the causative agents of certain plant and animal diseases were smaller than all known bacteria. Yellow fever was the first human viral disease to be recognized, two years later (Major Reed and assistants, US Army, Havanna, 1900). To date, more than 1938 virus species belonging to 287 genera of 73 families have been identified (Fauquet and Fargette, 2005). Probably, viruses are as old as life on Earth, but a broad public awareness is only emerging now, in view of the current AIDS pandemic and the recent outbreaks of severe acute respiratory syndrome and avian influenza.

Virus particles, composed of an enveloped or non-enveloped protein shell and nucleic acid, are designed to move its genome between cells of a susceptible host and between hosts. Viral genomes exhibit a great diversity; the different families have genomes formed by one double stranded DNA (dsDNA) or single-stranded DNA (ssDNA), dsRNA or ssRNA, with positive, negative or ambisense polarity, circular or linear topology and simple or multipartite genomes. The protein shell provides a protective coat for the nucleic acid, carries out required chemical reactions for particle maturation, and facilitates entry into the cell. Virus particles are always formed of multiples copies of identical gene products, minimizing the genetic information required for shell formation. This strategy reduces the burden of encoding a large protein but generates the new problem of assembling multimers, with tens, hundreds or thousands of subunits, in a biologically realistic time frame, being a paradigm in the optimization strategy of resources (Johnson and Speir, 1997). Viral capsids represent an excellent framework for the analysis of “built-in” features such as structural polymorphism and transient conformations. In addition, complex capsids may require one or more auxiliary proteins (scaffold, accessory, and proteolytic proteins) to trigger structural and functional changes.

Crick and Watson proposed icosahedral geometry for spherical capsids, reasoning that the most effective way of enclosing a large volume with a small protein is to arrange it in a regular geometric repeat, (Crick and Watson, 1956). An experimental corroboration for this hypothesis was provided by D.L.D. Caspar who noted that the arrangement of intense reflections in a X-ray photograph by bushy stunt virus corresponded to the arrangement of icosahedral five-folds (Caspar, 1956). Of the platonic solids (composed of identical faces), icosahedra have the largest number (20 equilateral triangles). Since each facet has a three-fold symmetry, the resulting solid is formed by 60 identical asymmetric units. Icosahedra can also be defined in terms of their 532-point symmetry. Each of the twelve icosahedral vertexes is coincident with a five-fold symmetry axis (5x12=60); five-fold symmetry axes run through one five-fold axis, through the centre of the icosahedron, and out the other side. Moreover, there are 30 two-fold axes (2x30=60) which run through the edge-edge contacts between facets.

Icosahedral geometry (with 60 identical copies) allows that a relatively short RNA/DNA sequence could code for a protein capable of encapsidating the complete genome. The theory of quasi-equivalence describes how multiples of 60 monomers can be arranged with quasi-icosahedral symmetry to enclose an even larger volume (Caspar and Klug, 1962). The underlying postulate of quasi-equivalence is that the viral coat protein can form pentamers and hexamers using the same subunits contacts, but with slight conformational changes between structural subunits. The only requirement for an icosahedral facet is being an equilateral triangle with three identical asymmetric units arranged with three-fold symmetry. Using a hexagonal grid one can see that there are series of equilateral triangles that enclose an integral number of smaller triangles (the so-called triangulation number, T). The area of an asymmetric unit for a triangle with one vertex on the origin (0, 0) and a second vertex at a point (**h**, **k**) is: $\mathbf{T=h^2+hk+k^2}$. The size of the equilateral triangle is proportional to the T number and each particle will contain 60T subunits. These will be arranged as 12 pentamers and 10 (T-1) hexamers (**Fig.1**).

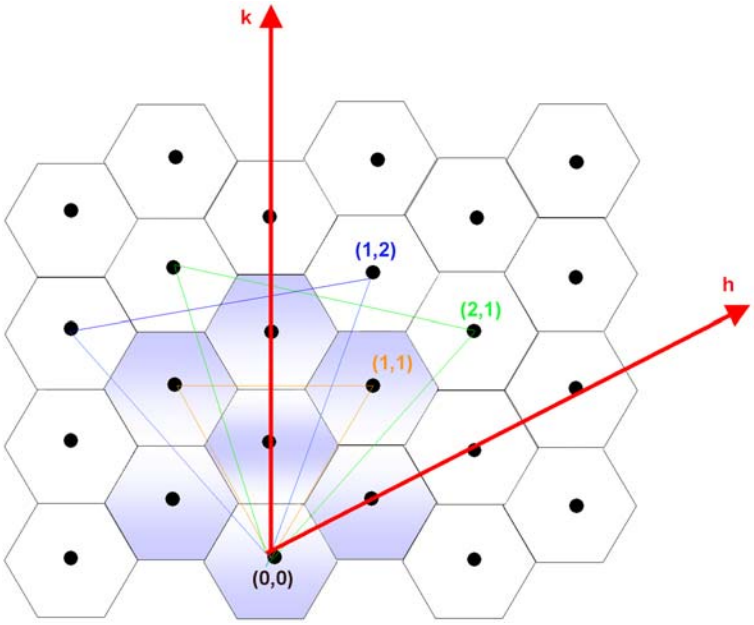


**Fig.1. Geometric principles for generating icosahedral quasi-equivalent surface lattices.** Hexamers are initially considered planar (an array of hexamers forms a flat sheet as shown) and pentamers are considered convex, introducing curvature in the sheet of hexamers when they are inserted. The closed icosahedral shell, composed of hexamers and pentamers, is generated when by inserting 12 pentamers at appropriate positions in the hexamer net. To construct a model of a particular quasi-equivalent lattice, one face of an icosahedron is generated in the hexagonal net. The origin is replaced with a pentamer and the (**h, k**) hexamer is replaced by a pentamer. The third replaced hexamer is identified by 3-fold symmetry (i.e. complete the equilateral triangle of the face). The icosahedral face for a *T=3* surface lattice is defined by the triangle in orange lines (**h**=1, **k**=1). Two possible *T=7* lattice choices are also marked in green and blue (**h**=2, **k**=1 or **h**=1, **k**=2, these being mirror images of each other), and require knowledge of the arrangement of hexamers and pentamers and the enantiomorph of the lattice for a complete lattice definition (adapted from Johnson J.E. and Speir J.A, 1997).

Quasi-equivalence arises because the subunits within an asymmetric unit are not fully equivalent. In theory, quasi-equivalent shells of any size can be formed. In other systems, different subunit polypeptides are also utilized for the formation of pentamers and hexamers; they are denominated as pseudoequivalent shell and defined and by a P number (pseudo-T number).

## 1.1. Different control mechanisms for viral capsid assembly

In capsids with T>1, the proteins subunits must adopt several different conformations depending on their different structural environments in the shell; that is, the bonding properties of subunits are not identical, and several classes of conformers

exist (Caspar and Klug, 1962). High-resolution structural studies have revealed some clues about how a capsid protein is able to know the conformation that must adopt (Liddington et al., 1991; Rossmann and Johnson, 1989) although the mechanism is still poorly understood (Johnson and Speir, 1997).

### 1.1.1. Control of conformational switching

The information for the conformational switching required for the assembly of a T>1 shell is intrinsic to the subunits themselves, which are often able to form morphologically correct shells in the absence of other proteins and are determined by factors like flexible protein regions (loops and N- and C-terminal domains), RNA interactions, metallic ions, pH and different combinations between all of them (Johnson, 1996). In many cases, however, they form a variety of aberrant shell-related structures depending on the physiological conditions in a way (Krol et al., 1999; Salunke et al., 1989; Savithri and Erickson, 1983; Schwartz et al., 2000). Restrict the inherent flexibility, in which only the appropriate conformations are formed, is as important to the assembly process as the generation of conformational variability.

There is a close connection between protein folding and assembly. Viral structural proteins are often quite flexible in solution and each subunit chooses its conformation on the basis of the conformational state of its neighbours (Berger et al., 1994).

### 1.1.2. Cores and scaffolds

As the size of the shell gets larger and interactions become numerous, additional information may be required to constrain the conformational possibilities of the capsid protein and to ensure the fidelity of the assembly process. This information might come from a scaffold or core proteins.

The core itself is presumably simple enough to assemble without any additional information. Once the shell size is specified by the core, the symmetry may be governed by simple pattern formation (Berger et al., 1994), while core-shell interactions are relatively non-specific (Grimes et al., 1998). Among the best characterized of such

proteins is the precursor of the herpes simplex virus type I VP22a protein (Zhou et al., 1998). PreVP22a interacts with the major capsid protein, VP5, through its C-terminal 25 residues, and this interaction is essential for capsid assembly.

The term “scaffolding protein” usually refers to a protein playing an essential structural role during assembly but is subsequently removed, analogous to the role of molecular chaperones in protein folding. Scaffolding proteins share a similar structural organization, including an elongated shape, and a specific capsid interaction domain at the C-terminus. The scaffolding protein itself does not form a symmetric structure, but apparently provides sufficient information to constrain the shell symmetry by defining the overall size of the outer shell, (Dokland, 1999), i.e. P2 internal scaffolding protein gp0 required for the formation of viable capsids of both P2 and P4 bacteriophages (Chang et al., 2009).

### 1.1.3. Major conformational changes

While conformational switching provides the mechanism for generating the structural diversity required to make large capsids, some virus capsids go further and undergo a large-scale reorganization of their entire structure. The typical example is found in the dsDNA phages which undergo capsid expansion, (Conway et al., 1995; Dokland and Murialdo, 1993). The resolution of prohead II, one of the intermediate assembly capsid of the lambda-like bacteriophage HK97, at 3.65Å resolution has unveiled an unprecedent expansion mechanism that describes the transition (Gertsman et al., 2009).

### 1.1.4. Assembly intermediates and pathways

It is assumed that viruses assemble via a pathway of intermediates, particularly for large and complex viruses, each consisting of a subset of the final capsid structure, forming a precursor particle- the provirion or procapsid. Assembly through intermediates reduces the errors dramatically (Berget, 1985). Examples of viruses that assemble through procapsids intermediates are herpesvirus (Newcomb et al., 2000) and bacteriophages, like T7 (Agirrezabala et al., 2007).

The assembly process proceeds through separate nucleation and growth events. Thus, the initial nucleus may consist of a specific subassembly whereas subsequent growth proceeds from other structures (Stehle et al., 1996).

### 1.1.5. Proteolytic processing

Proteases can be cellular and viral origin and play essential roles in viral replication, including the coordinated assembly and maturation of virions (Hellen and Wimmer, 1992). Most of these enzymes belong to one of three classes, Ser-, Cys- or Asp-proteases, and can play two general roles in viral morphogenesis. The first one is that of structural proteins encoded by retroviruses and many RNA viruses as part of large polyproteins. Their proteolytic release is a prerequisite for particle assembly. The second role is in assembly-dependent maturation, which is accompanied by the acquisition of infectivity. For instance, in orthoretroviruses, most of the newly released particles are “immature”; virus-encoded protease cleaves the Gag polyprotein during or soon after assembly to allow the transformation from immature to mature particles (Adamson and Freed, 2007).

Host-encoded proteases cleave viral protein precursors in a conventional manner after the precursor polypeptides have been transported to vesicular compartments; i.e. during the course of Hepatitis A virus particle assembly, immature procapsids might be targeted to early lysosomes where they encounter cellular proteases including cathepsin L that remove 2A peptide and thereby fully mature the particles (Morace et al., 2008). In contrast, cleavage by viral proteases is more complex. It occurs by a variety of mechanisms facilitating the assembly of complex viral structures and the post-assembly maturation of the virion (Gallagher and Rueckert, 1988).

## 1.2. *Birnaviridae* family: Infectious bursal disease virus

The *Birnaviridae* family forms a distinct family of dsRNA viruses infecting animal species as different as vertebrates, molluscs, insects, and rotifers (Delmas, 2004). It groups three different genera: *Aquabirnavirus, Entomobirnavirus* and *Avibirnavirus*; and the representative members are: Infectious pancreatic necrosis virus (IPNV);

*Drosophila* X virus (DXV); and Infectious bursal disease virus (IBDV), respectively (Fauquet and Fargette, 2005). Most of the research efforts on birnaviruses have focused on IBDV (Muller et al., 2003), which shows interesting virulence properties and is responsible for important losses in the poultry industry. Another economically relevant birnavirus is IPNV, of salmonids that affects a wide variety of farmed fish species (Delmas, 2004).

**IBDV** is the causative agent of the infectious bursal disease (IBD) that affects young chickens. When IBD appeared in chickens in 1959, the disease was designated as "Gumboro disease" after the geographic location of the first recorded outbreaks (Gumboro, Delaware, USA). Infections caused by IBDV may exacerbate the susceptibility to other pathogens, and reduce the chicken's ability to respond to vaccination. This causes a severe economical impact on poultry industry worldwide (van den Berg et al., 2000).

Lymphoid cells in the bursa of Fabricius (BF) are the main target cells of IBDV. Between 3 and 6 weeks after hatching, when the BF reaches maximum development, chickens are highly susceptible to the virus. Infection results in lymphoid depletion and the final destruction of the bursa as the predominant feature of the IBD pathogenesis. In the classical form of the outbreaks, the mortality rate may range from 1 to 50%. Depression in egg production and deterioration in eggshell and internal quality of eggs in commercial laying strain flocks are also observed. In addition to mortality, IBDV is immunosuppressive. Immunosuppression is denoted by a high prevalence of viral respiratory infections and elevated mortality due to airsacculitis and colisepticemia during the terminal third of the 6-8 week growing cycle (Kaufer and Weiss, 1980).

IBDV has been described to be resistant to all the conventional disinfection procedures like chemical or heat inactivation. At the moment, the only available method to control the disease is the implementation of intensive vaccine programs (Negash et al., 2004). The indiscriminate use of attenuated vaccines has led to the rapid virus dissemination around the world (Yamaguchi et al., 1996). The search of new strategies to control and erradicate the disease is a flock farming priority. This is especially important in developing countries, in which chicken meat is the main protein source of the diet.

### 1.2.1. IBDV serotypes

There are two different serotypes for IBDV, I and II that are distinguished by sero-neutralization assays (McFerran et al., 1980). **Serotype I** includes all the pathogenic isolates for domestic chickens, whereas **serotype II** isolates, mostly from turkeys, do not produce clinical symptoms or protection against type I isolates. Pathogenic serotype I isolates are subdivided into classical, antigenic-variant, and very virulent isolates. Antigenic-variant IBDV have only been reported in the United States (since 1985) and were found to have single amino acid changes in a specific region of the VP2 protein (the hyper variable region), leading to a different pathologic phenotype (Snyder, 1990). Since 1988 in Europe, (Chattel et al., 1989), there were reports describing IBDV isolates that had an enhanced virulence (very virulent IBDV [vivid]) while having the same antigenic structure as classical isolates. Amino acid differences between viral proteins of vivid and classical IBDV isolates were found scattered throughout all viral proteins, although most of them were found in the hyper variable region of VP2 (Brown and Skinner, 1996; Pitcovski et al., 1998).

### 1.2.2. IBDV genomic organization

The IBDV genome is formed by two segments of dsRNA of 3,2 kb (segment A) and 2,8 kb (segment B) (Muller and Nitschke, 1987a; Muller et al., 1979) with untranslated regions (UTR) at the 5' and 3' ends. In vitro ssRNA synthesis studies show that the RNA polymerase synthesizes viral ssRNA by a semi-conservative strand displacement mechanism, whereby the nascent strand displaces one of the parental strands (Spies et al., 1987) (**Fig.2**).

**Segment A** contains two partially overlapping open reading frames (ORFs). The smaller ORF codes for **VP5** (15 kDa), a non-essential polypeptide that is involved in virus dissemination (Lombardo et al., 2000), and inhibits apoptosis at the very early stage of virus infection (Liu and Vakharia, 2006). The larger ORF encodes a 110 kDa polyprotein that undergoes an auto-cleavage by the viral protease VP4, yielding the **pVP2** (54.4 kDa), **VP3** (29 kDa), and **VP4** (26.7 kDa) polypeptides.

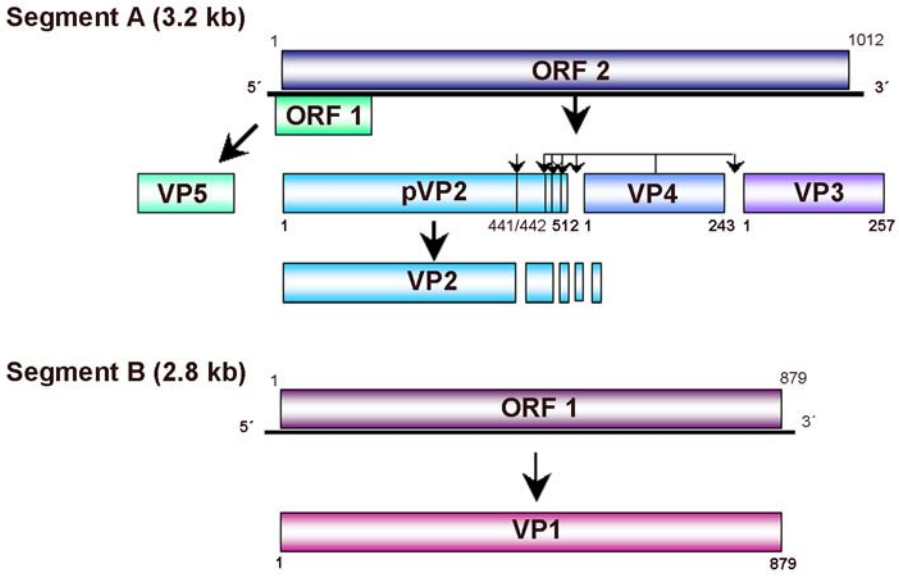


**Fig.2. IBDV genomic organization**. Segment A possesses two open reading frames (ORFs) partially overlapped, which codes for protein VP5 and viral polyprotein, respectively. The polyprotein undergoes an auto-cleavage by the viral protease VP4, yielding pVP2, VP3 and VP4. pVP2 C-terminal domain is removed during further processing, rendering the mature VP2. Segment B encodes for VP1, the viral RNA-dependent RNA polymerase.

**Segment B** encodes **VP1** (97.8 kDa), the viral RNA-dependent RNA polymerase (RpRd) (Morgan et al., 1988; Muller and Nitschke, 1987b; von Einem et al., 2004) with different functions related to viral replication. Like other viral dsRNA polymerases, **VP1** catalyzes transcription and viral genome replication (Garriga et al., 2007; Pan et al., 2007; Spies et al., 1987; Xu et al., 2004). Although RNA polymerization and priming usually involve different viral components, in birnaviruses the polymerase is responsible for both activities. VP1 guanylylates itself acting as a primer for the RNA synthesis (Dobos, 1993; Shwed et al., 2002; Spies and Muller, 1990; Xu et al., 2004).

## 1.2.3. IBDV structure and morphogenesis

### 1.2.3.1. Structural components of IBDV virion

IBDV infectious particles assemble and accumulate in the cell cytoplasm, and consists of two major (VP2 and VP3) and two minor proteins (VP1 and VP4) (**Fig.3B**).

Virus purification renders six different populations sharing an identical protein composition but showing higher sedimentation coefficients as particle density increases. Biochemical analyses showed that these biophysical differences correlate with the number of dsRNA segments present within the viral capsid. IBDV particles with greater genome copy number (i.e. polyploid viruses) have higher infectivity rates (Luque et al., 2009a).

The virion has a single-shelled capsid with an external diameter of 65-70 nm formed of 260 quasi-equivalent **pVP2/VP2** trimeric subunits, arranged with a T=13l (*levo*) architecture (Bottcher et al., 1997; Caston et al., 2001; Coulibaly et al., 2005). The (p) VP2 trimers are organized in 12 pentamers and 120 hexamers, and from a geometrical perspective, exist in five distinct conformations (a-e). VP2 represents the main marker for virulence and pathogenesis, and also induces neutralizing antibodies (Brandt et al., 2001) (**Fig.3A**).

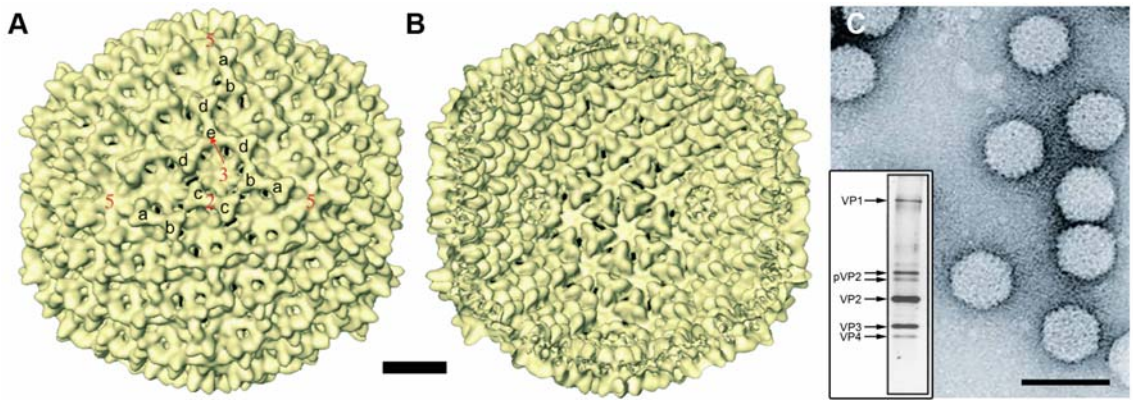


**Fig.3. Capsid structure**. (**A-B**). Surface-shaded representations at 10 Å (Luque et al., 2007) of the outer (**A**) and inner (**B**) surfaces of IBDV capsids viewed along a three-fold axis of icosahedral symmetry. The five different types of trimeric capsomers are indicated by letters a to e. Bar=100 Å. Icosahedral symmetry axes are indicated in red numbers. (**C**) IBDV purified virions negative stained with uranyle acetate. Bar=100nm. In the square, the electrophoretic analysis and silver staining of mature IBDV virions is shown (Lombardo 1999). Structural proteins are indicated by an arrow: VP1 (97.8 kDa), pVP2 (~54 kDa), VP2 (47 kDa), VP3 (29 kDa) and VP4 (26.7 kDa).

**pVP2** (512 residues) is the precursor form of the capsid protein VP2; the C-terminal 71 residues (pVP2 C-terminal domain, pVP2CTD), are removed, rendering the mature VP2 polypeptide (47 kDa, 441 residues). It has been proposed that the

postranslational maturation of pVP2 occurs by two different proteolytic events: processing by VP4 in secondary alanyldipeptide targets in position 487, 494 and 501 (generating at least four different variants of pVP2) (Sanchez and Rodriguez, 1999), and a processing event between residues (441-442), as discussed below. The maturation is required for correct viral capsid assembly (Chevalier et al., 2002). The small pVP2-based peptides generated remain associated to the viral particle (Da Costa et al., 2002), and possess membrane desestabilization capacity, which suggests their implication during viral internalization (Chevalier et al., 2005; Galloux et al., 2007). A similar post-assembly pVP2 maturation pathway has also been demonstrated for IPNV (Villanueva et al., 2004).

**VP3** is a multi-tasking protein involved in numerous processes during viral cycle. VP3 acts as a scaffolding protein during virus assembly, probably interacting with VP2, as discussed below. In addition to its interaction with pVP2, VP3 interacts with VP1 and the dsRNA genome (Kochan et al., 2003; Maraver et al., 2003a; Maraver et al., 2003b; Tacken et al., 2002). Actually, the interaction of VP3 with VP1 is responsible for the encapsidation of the viral polymerase into VLP (Lombardo et al., 1999). The region of VP3 responsible has been mapped within the highly charged 16 amino-acid domain located near its C-terminus (Maraver et al., 2003a). Recently, it has been demonstrated that this interaction releases the inherent blockade of the active site of the viral RNA RdRP, thus acting as a transcriptional transactivator (Garriga et al., 2007).

Finally, the domain of VP3 that directs the dsRNA binding activity of the protein has been mapped by deletion mutagenesis to a 69 amino-acid region located near the N-terminus. Based on in vitro assays, it has been shown that the dsRNA binding activity is sequence independent, consistent with a general role for VP3 in stabilizing the viral RNA (Kochan et al., 2003), and protecting it from cellular RNases. VP1, VP3 and the virus genome form a transcriptionally active ribonucleoprotein complex (RNP) (Luque et al., 2009b).

**VP4** is a non-canonical Ser-Lys Lon protease (Birghan et al., 2000), and its atomic structure has been recently determined (Feldman et al., 2006; Lee et al., 2007). VP4 lacks the ATPase domain of the Lon proteases, although its catalytic site is the Ser-

652-Lys-692 dyad. Moreover, VP4 acts in a cotranslational and autocatalytically manner (Birghan et al., 2000). VP4 protein is a true structural component of the virion although its encapsidation is highly variable (Granzow et al., 1997; Luque et al., 2009a). In IBDV-infected cells, VP4 forms tubular structures (so called, type II tubules) with a diameter of about 25 nm.

#### 1.2.3.2. Virus based expression systems to analyze IBDV capsid assembly

One of the most successful approaches to understanding the role of IBDV proteins in particle assembly has been the use of heterologous expression systems capable of supporting VLP formation.

Expression of the IBDV polyprotein in mammalian cells using inducible recombinant vaccinia virus vectors results in the correct processing of the polyprotein and the accumulation of abundant levels of VLP. The size and shape of these VLP are similar to those of authentic IBDV particles (Fernandez-Arias et al., 1998; Lombardo et al., 1999), thus, demonstrating the reliability of this expression system. Smaller capsids are also observed, representing a T=7 (**Fig. 4E**) arrangement of equivalent trimeric capsomers. Unlike the T=13 capsid, with its five classes of trimeric capsomers, the T=7 icosahedron displays only three trimer classes.

The expression of the IBDV polyprotein in insect cells using a baculovirus expression system also results in the processing and accumulation of pVP2, VP3 and VP4. However, the assemblies produced with this expression system are structurally varied and, in general, the formation of VLP is rather inefficient. The use of a FastBac transfer vector to generate a baculovirus encoding the polyprotein yields rigid tubular structures (type I tubules), with diameters of 50 nm (Martinez-Torrecuadrada et al., 2000). These tubular structures, made up of pVP2, exhibit an equivalent hexagonal arrangement, similar to the type I tubules observed in IBDV-infected cells (Martinez-Torrecuadrada et al., 2000). A comparable result has been obtained with other baculovirus-based constructs (Chevalier et al., 2002). Overexpression from other baculovirus systems leads to the assembly of VLP, flexible tubules, and intermediate assembly products formed by icosahedral caps elongated in tubules. All these structures consist of pVP2 and variable amounts of VP2 and VP3 (Martinez-Torrecuadrada et al.,

2000). These results with the baculovirus expression system support the idea that insect cells have important cellular factor(s) interfering negatively with VLP assembly (e.g. cellular proteins and/or host environment); some of these factors will be further discussed in the present report.

### 1.2.3.3. Structural polymorphism of IBDV coat protein

Expression of the mature form of VP2 using different baculovirus-based vectors results spontaneously in the formation of isometric particles of 26 nm diameter (Caston et al., 2001; Coulibaly et al., 2005; Lee et al., 2003). Analysis of these subviral particles (SVP) shows that they are dodecameric T=1 structures, composed of 20 trimers of VP2 (Caston et al., 2001) (**Fig. 4A and 4D**). VP2 trimers alone posses the intrinsic information required for their assembly into pentameric, but not hexameric units. Whereas pVP2 expression leads to poorly ordered tubular structures with a hexagonal lattice (**Fig. 4C and 4G**), but lacks sufficient information to produce the complex interaction pattern required for building a T=13 capsid (Caston et al., 2001; Saugar et al., 2005).

Differences in the assembly behaviour of VP2 and pVP2 suggest that information affecting inter-subunit interactions is contained within the pVP2 CTD or is induced by the interaction of pVP2 CTD with additional viral components. These results suggest that (i) the pVP2CTD plays an important role in determining different VP2 conformations, and (ii) IBDV capsid formation requires the interaction of VP2 with other viral components.

The pVP2CTD peptide 443-GFKDIIRAIR-452, absent in the mature protein VP2, forms an amphiphatic α-helix (Galloux et al., 2007; Saugar et al., 2005). pVP2 intermediates containing this α-helix are able to assemble into the T=13 VLP (**Fig. 4B and 4F**), but only when expressed as a chimeric protein containing an N-terminal His tag extension (Saugar et al., 2005). In the context of this construct, the amphiphatic α-helix acts as a temporal molecular switch, and the His tag acts as a molecular triggering factor, partially emulating the VP3 C-terminal region. The last five residues in the VP3 C-terminal end are homologous to the acidic segment of the His tag. Indirect studies confirmed the importance and uniqueness of the VP3 C-terminal end (Chevalier et al.,

2004; Gonzalez et al., 2005; Maraver et al., 2003b). The VP3 role is akin to those of canonical scaffolding proteins rather than an intrinsic component of the capsid (Coulibaly et al., 2005; Saugar et al., 2005). Effectively, VP3 participates in the inherent ability of pVP2 to acquire different conformations through the pVP2 C-terminal end (Ona et al., 2004) by a putative electrostatic interaction between the VP2 C-terminal domain and the VP3 Ct acidic region, will be discussed below.

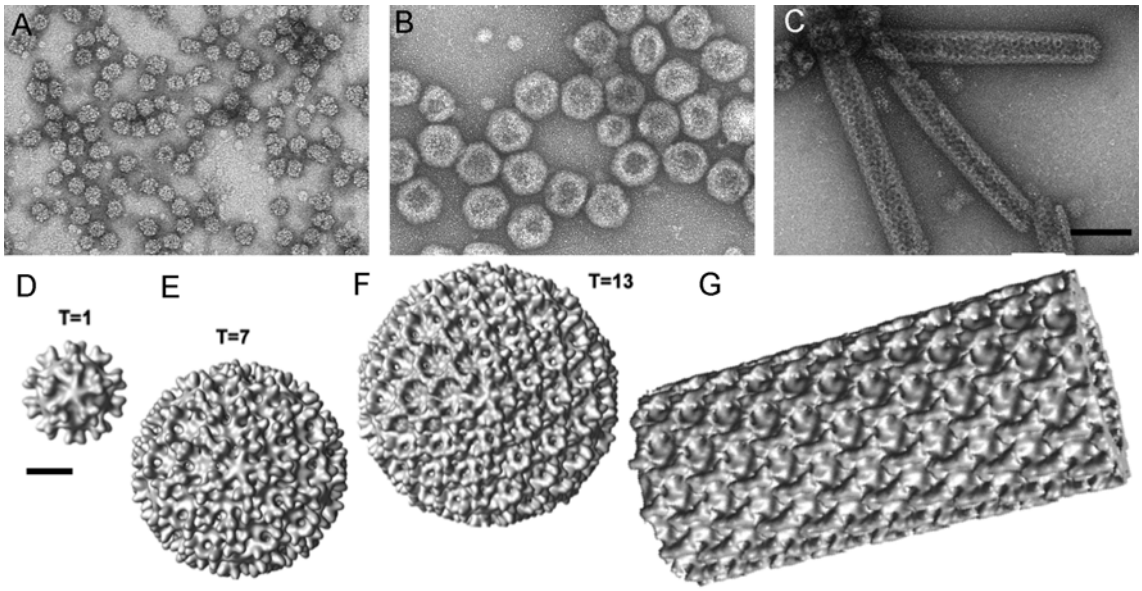


**Fig.4. Structural polymorphism of VP2 coat protein in insect cells.** (**A**) SVPs T=1 (**B**) T=13 capsids and (**C**) rigid tubes purified from insect cells infected by rBVs that express the mature protein VP2, the HT-VP2-466 chimeric protein and the polyprotein.Bar=100nm. 3DR of (**D**) a SVP, (**E**) T=7 capsid, (**F**) T=13 capsid and (**G**) pVP2 tube at 26 Å resolution. Bar=10nm.

### 1.2.3.4. Atomic structures of VP2 and VP3:

The atomic structure of the T=1 SVP has been solved by X-ray crystallography [PDB 1WCD, (Coulibaly et al., 2005); 2GSY, (Garriga et al., 2006); 2DF7, (Lee et al., 2006)]. The VP2 subunit is folded into three domains named projection (P), shell (S), and base (B) (**Fig.5A**). Domains S and P are β-barrels with a jelly roll topology, oriented such that their β-strands are oriented tangentially and radially, respectively, to the spherical particle. The B domain consists of α-helices, formed from extensions of the N- and C-termini of VP2, facing the inner surface of the capsid (**Fig.5B**). Besides lateral interactions between the VP2 trimers, SVPs are stabilized by $Ca^{2+}$ ions located at the three-fold icosahedral axes that interact with the two acidic Asp-31 and Asp-174

residues, linking together the three subunits of each trimer. Further stabilization is accomplished by the long C-terminal helix (α4) of the VP2 subunit that is projected away from the core of the protein, oriented towards the three-fold axis of the neighbouring VP2 trimer (Garriga et al., 2006).

**VP3** has a scaffold role, consistent with the finding that VP3 is able to self-assemble, as many bacteriophage scaffolding proteins do (Tacken et al., 2000). The atomic structure of the central region of the protein VP3 shows two domains formed by α-helices, whose interaction can form an apparently biological dimer (Casanas et al., 2008) (**Fig. 5B**). The use of deletion mutants has allowed mapping of the VP3 oligomerization domain between residues 224 to 247, near the C-terminal end of the protein (Maraver et al., 2003b).

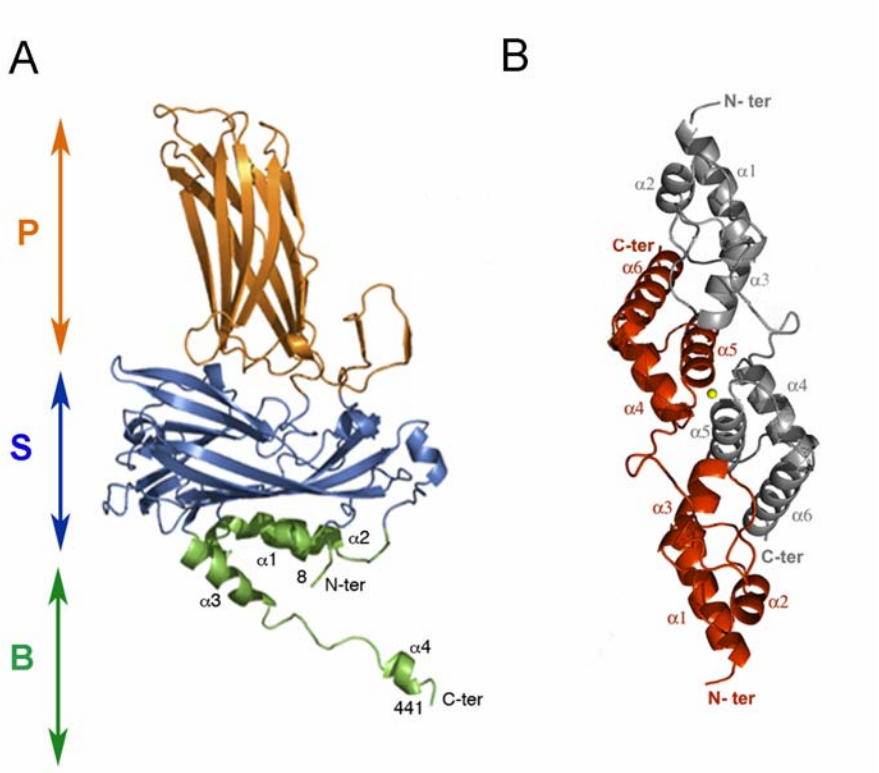


**Fig.5. VP2 and VP3 atomic structures.** (**A**) 3D model of VP2 structure (PDB entry 2GSY) resolved by X ray diffraction at 2.6 Å (Garriga et al., 2006). Domains P, S, and B are coloured orange, blue, and green, respectively. (**B**) Ribon plot of a VP3 dimer, (PDB entry 2Z7J) resolved by X-ray diffraction at 2.4 Å (Casanas et al., 2008), with one protomer shown in red and the second one in grey. One of the gold ions (yellow) occupies the two-fold axis and also participates in protomer-protomer interactions.

## 1.3. IBDV structural and functional relationships with ssRNA and dsRNA viruses

The IBDV capsid architecture is very similar to the outer capsids of many other dsRNA viruses sharing a T=13l organization. However, with the exception of birnaviruses, all dsRNA viruses posses an internal core with a characteristic T=1 architecture, constituted by 120 subunits in which the fundamental unit is a dimer. This organization, a notable exception in the quasi-equivalence theory, is denominated "T=2" capsid (which is a "forbidden" number). Until recently, the T=2 core, was considered to be an essential component of all dsRNA viruses, as a functional unit involved in transcription, replication and protecting the dsRNA genome from host defence mechanism (Gouet et al., 1999; Lawton et al., 1997; Prasad and Prevelige, 2003). However, the existence of birnaviruses clearly establishes a mechanism in which a segmented dsRNA genome can fully be accomplished in the absence of this T=2 shell.

Birnaviruses should compensate the lack of the T=2 capsid by using some alternative structural components. In this context, the ribonucleoprotein complex formed by VP3, VP1 and viral dsRNA appears to exert a fundamental role in the functional organization of IBDV capsid in a morphogenetic level as well as in the transcriptional and replication mechanisms (Ahlquist, 2005; Garriga et al., 2007; Hjalmarsson et al., 1999; Luque et al., 2009b).

Interesting structural and functional similarities between birnaviruses and positive ssRNA virus such as noda- and tetraviruses have been found. These two virus groups posses a bisegmented genome (Fauquet and Fargette, 2005), a permutation in their RdRps (Gorbalenya et al., 2002), similar coat proteins (Coulibaly et al., 2005) and an autoproteolytic maturation step of the capsid protein essential for virus infectivity (Gallagher and Rueckert, 1988; Schneemann et al., 1998; Zlotnick et al., 1994).

**Nudaurelia capensis ω virus (NωV)** is the prototype of the **ω-tetraviruses**; nonenveloped, positive sense ssRNA viruses with T=4 icosahedral symmetry and bipartite genomes. Both RNA segments are packaged in each viral capsid. RNA1 is 5.3 kb and encodes the RNA-dependent RNA polymerase, while RNA2 is 2.4 kb and codes

for the 70-kDa coat protein precursor called α–protein. Tetraviruses exclusively infect insects of the *Lepidopteran* order. The expression of NωV RNA2 in a recombinant baculovirus system, yields a porous procapsid intermediate composed by 240 chemically identical copies of protein-α. After acidification (pH 5.0) this intermediate undergoes a large-scale conformational change into the mature capsid (Canady et al., 2000).

The conformational change is followed by an autoproteolytic cleavage that requires an acidic environment (pH 5.0). The asparagine residue at the scissile bond (Asn-570-Phe-571) is required for cleavage and a point mutation allows the particles to undergo the conformational change from procapsid to capsid reversibly as a function of pH (Taylor et al., 2002). As a cleavage mechanism, it has been proposed that Glu-103 participates in this reaction enabling to perform a nucleophilic attack on Asn-570 (Taylor and Johnson, 2005). Intermediates formed by a protein containing mutations in the Glu-103 residue cleave significantly less efficient than the wild-type capsid (Taylor and Johnson, 2005).

**Nodavirus** is a family of small icosahedral viruses infecting insects, mammals and fish, which include **Flock House Virus (FHV)** and **Black Beetle Virus (BBV)** (Hendry, 1991; Kaesberg, 1987; Mori et al., 1992). The nodavirus particle consists of 180 copies of the coat protein, which encapsidates a bipartite genome. RNA1 encodes protein A, a 112-kDa RdRp. A subgenomic RNA3 is produced from RNA1 in infected cells and encodes the 12-kDa B2 protein, which has been shown to inhibit RNAi in a drosophila cell line (Li et al., 2002). Finally, RNA2 encodes the 43-kDa capsid protein-α (Hendry, 1991; Kaesberg, 1987). Nodavirus capsids (T=3 icosahedral symmetry) are initially assembled as provirions of α-protein, which undergoes a post-assembly cleavage leading the β-protein, that forms the virus capsid protein, and the γ-peptide that remains associated at the interior of the capsid, (Gallagher and Rueckert, 1988). This proteolytic maturation is required for the acquisition of infectivity (Schneemann et al., 1992) and increases the virion stability (Gallagher and Rueckert, 1988). The proteolysis reaction occurs near the interior surface of the protein shell and is dependent on the Asp-75 residue, that triggers Asn-363 residue of the cleavage site by a nucleophilic attack (Zlotnick et al., 1994). In both cases the γ-peptide, which is similar in FHV and

NωV, seems to be involved in the RNA membrane translocation at the beginning of the infection (Cheng et al., 1994). It has been also demonstrated the rescue of maturation-defective FHV infectivity with non-infectious mature virus-like particles (VLP) (Walukiewicz et al., 2008).

On the other hand, sequence comparison analysis demonstrates that tetra- and birnaviruses polymerases belongs to the non-canonical RNA polymerases defined by a permutation in the palm domain with a C-A-B motif instead of the A-B-C canonical one (Gorbalenya et al., 2002). These results suggest that primigenic RdRp had a non-canonical palm domain organization from which canonical RdRp could have evolved; being birna- and tetravirus RdRp evolutive traces of this process. Recently, the X-ray crystallographic resolution of VP1 (Garriga et al., 2007; Pan et al., 2007) demonstrated that the C motif permutation is associated to a catalytic activity regulation mechanism by its interaction with the VP3 C-terminal domain (Garriga et al., 2007).

Birnaviruses VP2 protein is a structural hybrid between the capsid protein of positive ssRNA viruses (noda- and tetravirus) and the capsid protein T=13 of *Reoviridae* family (dsRNA viruses) (Coulibaly et al., 2005). Whereas the shell (S) and the base (B) domains of VP2 have a high structural homology with the capsid proteins of noda- and tetraviruses, its projection domain (P) is structurally homologous to that of reovirus T=13 capsid protein (**Fig.6**). α-helices surrounding the inner surface of the capsid in noda- and tetraviruses as well as in IBDV, generate hydrophilic channels in the five-fold symmetry axes that might be involved in the translocation of newly transcribed ssRNA (Coulibaly et al., 2005; Garriga et al., 2006; Munshi et al., 1996); the extrusion through the pentameric axes has been demonstrated for the *Reoviridae* family members (Diprose et al., 2001; Lawton et al., 1997).

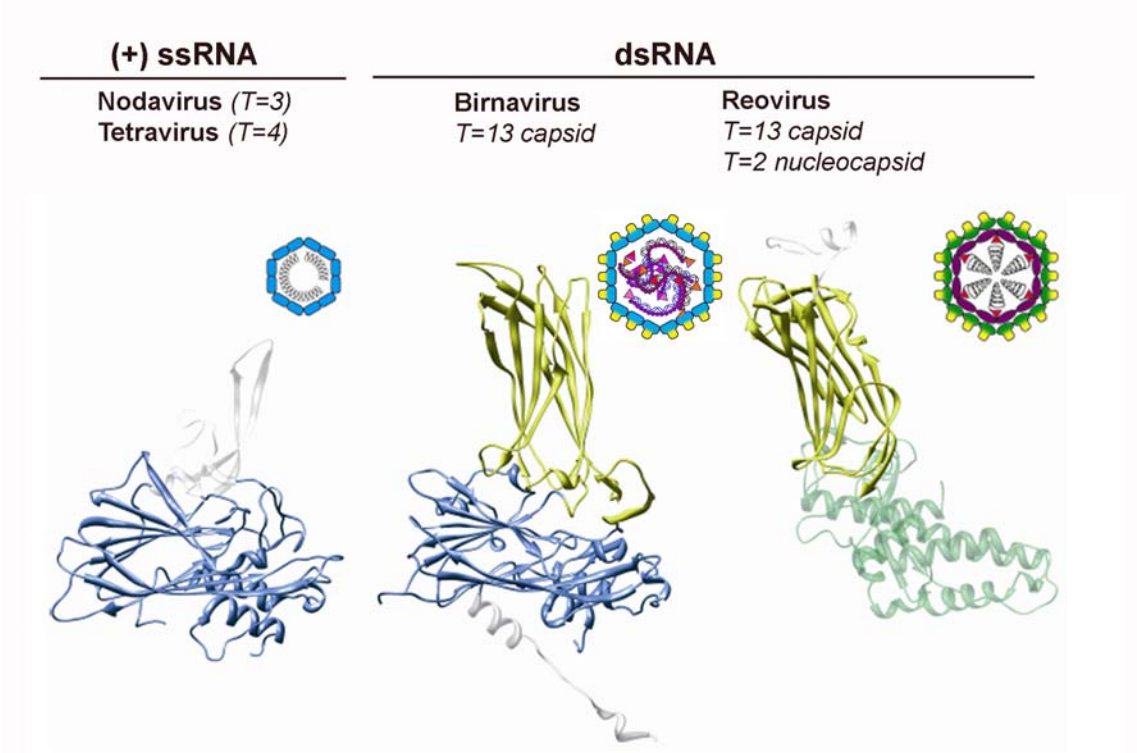


**Fig.6. Structural relationships between capsid proteins of (+) ssRNA and dsRNA viruses.** Structural comparison of the crystallographic structure of protein β of FHV, a nodavirus (PDB 2Q26), with VP2 of IBDV (PDB 2GSY) and VP6 of rotavirus, a reovirus (PDB 1QHD). Colour code is coincident with comparative diagrams of main structural features of virions of families *Nodaviridae/Tetraviridae*, *Birnaviridae* and *Reoviridae* represented in the upper part. Capsid proteins of nodavirus and birnavirus posses a high structural homology (coloured in blue) between S and B domains. P domains of birnavirus and reovirus are similar (in yellow). Nodavirus, birnavirus and reovirus capsids contain, respectively, naked ssRNA; filamentous complexes of dsRNA with VP3 (orange circles) and VP1 (red triangles); T=2 nucleocapsids (purple) with ordered dsRNA and transcriptional complexes. Adapted from Alquist 2005.

**AIMS**

The general aim of this thesis is the characterization of the maturation process of IBDV capsid. In this context, the following topics were proposed:

1. Analysis of the putative interaction between the pVP2 and VP3 C-terminal ends involved in the structural polymorphism of the IBDV capsid protein.

2. Characterization of the post-translational processing events for the precursor of the capsid protein and its implication in viral assembly.

# EXPERIMENTAL PROCEDURES

## 3.1 Biological Material

### 3.1.1 Prokaryotic cells

*E. coli* DH5α (Raleigh E.A., 2003) was used for the amplification of recombinant plasmids. *E. coli* DH10-Bac (Luckow et al., 1993) has been utilized for the generation of baculovirus infective bacmids.

### 3.1.2 Eukaryotic cells

Expression experiments were carried out with BSC-40 mammalian cells, kidney epithelial cells from *Cercopithecus aethiops* (Brockman and Nathans, 1974) (ATCC, CRL-2761) or QM7 quail muscle cells (Antin and Ordahl, 1991) (ATCC, CRL-1962) for vaccinia recombinants (rVV) and IBDV infections, and Trichoplusia ni (H5) insect cells (*Invitrogen*), adapted for monolayer growth from the cellular line Sf9 of *Spodoptera frugiperda* (Vaughn et al., 1977) (ATCC, CRL-1711) for baculovirus recombinants (rBV) infections. For silencing assays, 293T cells, human epithelial kidney cells (DuBridge et al., 1987) (ATCC CRL-11268); and DF-1 cellular line, derived from *Gallus gallus* fibroblasts (Himly et al., 1998) (ATCC, CRL-12203) were used.

BSC-40, QM7 and 293T cells were grown in Dulbecco's modified Eagle's medium (DMEM) (Dulbecco and Freeman, 1959) containing 10% fetal calf serum, penicillin (100 U/ml), streptomycin (100 µg/ml), gentamycin (50 µg/ml), fungizone (1 µg/ml) and non-essential aminoacids at 37ºC. DF-1 cells were grown in the same medium but at 39ºC; silenced DF-1 cells are also maintained with puromycin 2µg/ml not to lose the retroviral gene. H5 cells were grown in TC-100 medium (*Gibco-BRL*) containing 10% fetal calf serum, penicillin (100 U/ml), streptomycin (100 µg/ml), gentamycin (50 µg/ml) and fungizone (1 µg/ml) at 28ºC.

### 3.1.3 Plasmids

pFastBac1 and pFastBacHT plasmids from *Invitrogen* company were utilized to generate rBVs. Both plasmids, heterologous genes are under control of the polyhedrin

promoter and have specific sites for the recombinant gene transposition in the bacmid. pFastBacHT plasmid also possesses a Histidine tag (His tag) and a spacer region in the amino terminal extreme of the recombinant protein.

pVOTE.2 plasmid (Ward et al., 1995) was kindly provided by Bernard Moss (NIH, Bethesda, Md.) and used for the generation of rVVs.

The pRETROSUPER vector is derived from the Murine Embryonic Stem Cell virus (pMSCV). The pRETROSUPER vector contains the pSUPER short hairpin RNA (shRNA) expression cassette (Netherlands Cancer Institute, NKI/AvL).

### 3.1.4 Viruses

IBDV infections have been carried out with the *Soroa* isolate (Lombardo et al., 1999), which was isolated from an infected chicken in the Soroa region (Cuba) and adapted to grow in chicken embrionary fibroblasts (CEF) primary cultures. Afterwards, it has been adapted to grow in different mammalian cells.

Generation of rBVs has been made from a baculovirus (BV) FastBac (*Invitrogen*). This virus was generated by genetic manipulation from a field isolate of the polyhedrosis virus *Autographa californica* (AcPHV).

To construct rVVs, genes of interest are inserted into pVOTE.2 transfer vectors. The latter are then transfected into BSC-40 cells infected with a vaccinia virus that encodes the T7 RNA polymerase and lac repressor, VT7lacIO. Recombinant virus isolation is facilitated by mycophenolic acid selection. The expression of our protein is induced by the addition of upon addition of isopropyl-β-D-thiogalactopyranoside (IPTG) (Ward et al., 1995).

rVV VT7LacOI/POLY, and rBV FB/VP2-452, FB/VP2-501 and FB/HTVP2-466 were previously described (Caston et al., 2001; Lombardo et al., 1999; Saugar et al., 2005).

### 3.1.5 Antibodies

During this study, rabbit anti-VP2 and VP3 sera, previously described (Lombardo et al. 1999; Sánchez and Rodríguez 1999), have been used. Commercial antibody against His tag (*Sigma*) has been also applied.

## 3.2 Manipulation and generation of recombinant vectors

### 3.2.1 PCR

Reactions were carried out in a final volume of 50 µl with 0.2 mM dNTPs, 200 ng of each primer, 2 ng of DNA template, 20 mM Tris-HCl pH 8.8, 10 nM KCl, 2 mM $MgSO_4$, 10 mM $(NH)_4SO_2$, 0.1% Triton X-100 y 2 U of DNA polymerase *Vent* (*New England Biolabs*). As amplification protocol the current method was used: 1 min at 94ºC; 30 cycles of 40 sec at 92ºC, 40 sec at 60ºC and 1 min 30 sec at 75ºC; 5 min at 75ºC.

### 3.2.2 DNA fragments ligation reactions

Reactions were carried out in a final volume of 15 µl en a buffer composed by 50 mM Tris-HCl pH 7.8, 10 mM MgCl2, 10 mM DTT, 1mM ATP, 25 µg/ml BSA; using 200 ng/ml of each DNA fragment and 200 U of T4 DNA ligase *(New England Biolabs)* during 16 hours at 16ºC.

### 3.2.3 Enzymatic restriction reactions

*New England Biolabs*, *Roche* and *Fermentas* enzymes were used following the manufacturer's guidelines.

## 3.2.4 Generation of recombinant plasmids

### 3.2.4.1. Plasticity domain of the C-terminal of pVP2

pFB/HTVP2-466 (Saugar et al., 2005) and pFB/POLY (Ona et al., 2004) plasmids were used as a template for PCR synthesis to generate rBV/Δ2-10HTVP2-466 and rBV/Δ11-25HTVP2-466. PCR was performed with 5' (5'-GCGCAGATCTATGGATTACG ATATCCCAACGACC for rBV/Δ2-10HTVP2-466 and 5'-CGCAGATCTATGTCNTAYTAYCAYCAYCAYCAYCAYCAYATGGGATC TATGACAAACCTGTCAGATCAA for rBV/Δ11-25HTVP2-466) and common 3'end primer (5'-GCGCAAGCTTAGGCAGGTGGGAACAATGTGG). *Bgl*II-*Hind*III-digested PCR fragments were cloned into FastBac *BamH*1-*Hind*III polylinker sites for protein expression.

pFB/CtVP3-VP2466 fusion was constructed by generation of two overlapping PCR fragments. The first one using pVOTE.2/VP3 (Kochan et al., 2003) as a template in combination with primers 5'-GCGCCGGTCCGAAACCATGGGTCGGCTGGGCC GCTGGATCAGG and 5'-GTCTCTGATGAGGACCTTGAGATCCCAACGACCGAA AACCTG. The second fragment was generated using primers 5'-CAGGTTTTCGGT CGTTGGGATCTCAAGGTCCTCATCAGAGACGG and 5'-AAGACAATTAGCCC TG, and pFB/HTVP2-466 (Saugar et al., 2005) as a template. PCR overlap extension was carried out with primers 5'-GCGCCGGTCCGAAACCATGGGTCGGCTGGGCC GCTGGATCAGG and 5'-AAGACAATTAGCCCTG. The resulting DNA fragment was digested with *Rsr*II and used to replace the original *Rsr*II fragment of the pFB/HTVP2-466 plasmid.

Using PCR overlap extension four different mutants for pFB/HTVP2-466 were generated containing the following single mutations: D11R and D13R in the His tag, K445D and R449D in VP2. PCR reactions were carried out using the pFB/HTVP2-466 plasmid as template, and the set of mutator primers **(Table 1)** in combination with primers 5'-GTATTTTACTGTTTTCGTAACAG and 5'-AAGACAATTAGCCCTG for the His tag mutations and 5'-GGCCGCAAACAATGGGCTGACG and 5'-GCGCAAGCTTAGGCAGGTGGGAACAATGTGG for the α-helix of pVP2

mutations. The resulting DNA fragments were digested with *Rsr*II for the His tag, and *BamH*1 and *Hind*III for the α-helix of pVP2, and replaced the original sequences of the pFB/HTVP2-466 plasmid. Double mutants, D11R/K445D, D11R/R449D, D13R/K445D and D13R/R449D, were generated by ligation of the corresponding mutated *Bam*H1/*Hind*III α-helix fragment into the single mutant His tag plasmid.

In a similar way, four different mutants for pFB/CtVP3-VP2466 were generated containing the following single mutations: D13R (Asp-252) and D15R (Asp-254) of VP3 C-terminal domain; K445D and R449D for VP2. PCR reactions were carried out using the pFB/CtVP3-VP2466 plasmid as template, and the set of mutator primers **(Table 1)** in combination with primers previously described for the His tag mutations and the α-helix of pVP2 mutations. The resulting DNA fragments were digested with *Rsr*II for the CtVP3, and *BamH*1 and *Hind*III for the α-helix of pVP2, and replaced the original sequences of the pFB/CtVP3-VP2466 plasmid. Double mutants, D13R/K445D, D13R/R449D, D15R/K445D and D15R/R449D, were generated similarly to the double mutations in pFB/HTVP2-466 previously described.

**Table 1**. Synthetic oligonucleotides used to generate constructs used in "Plasticity domain of the C terminal of pVP2".

| **Name** | **Sequence (5'-3')** |
|---|---|
| **pFB/HTVP2-466D11R** | CACCATCACCATCACCGTTACGATATCCCAACG |
| **pFB/HTVP2-466D11Rc** | CGTTGGGATATCGTAACGGTGATGGTGATGG |
| **pFB/HTVP2-466D13R** | CACCATCACGATTACCGTATCCCAACGACCG |
| **pFB/HTVP2-466D13Rc** | CGGTCGTTGGGATACGGTAATCGTG ATG G |
| **pFB/HTVP2-466K445D** | GGAGCATTCGGCTTCGACGACATAATCCGG G |
| **pFB/CtVP3-VP2466-K445D** | |
| **pFB/HTVP2-466K445Dc** | CCCGGATTATGTCGTCGAAGCCGAATG TCC |
| **pFB/CtVP3-VP2466-K445Dc** | |
| **pFB/HTVP2-466R449D** | CAAAGACATAATCGACGCCATAAGGAGGATAGC |
| **pFB/CtVP3-VP2466-R449D** | |
| **pFB/HTVP2-466R449Dc** | TCCTCCTTATGGCGTCGATTATGTCTTTGAAGC |
| **pFB/CtVP3-VP2466-R449Dc** | |
| **pFB/CtVP3-VP2466-D13R** | ATCAGGACCGTCTCTCGTGAGGACCTTGAGATCCC |
| **pFB/CtVP3-VP2466-D13Rc** | GATCTCAAGGTCCTCACGAGAGACGGTCCTGATCC |
| **pFB/CtVP3-VP2466-D15R** | ACCGTCTCTGATGAGCGCCTTGAGATCCCAACG |
| **pFB/CtVP3-VP2466-D15Rc** | CGTTGGGATCTCAAGGCGCTCATCAGAGACGG |

Using PCR overlap extension three mutant polyprotein genes were constructed containing the following single mutations in the VP3 C-terminal domain: R248D, R245D and R242D. PCR reactions were carried out using the polyprotein gene, cloned in the pVOTE.2/POLY plasmid as template, and the set of mutator primers (**Table 2**) in combination with primers 5'-GCGCGCATGCAGAGAAGAGCCGGTTGGCA and 5'-GCGCGCTCAGCGGTGGCAGCAGCCA for VP3 C-terminal domain. Primers 5'-GATGCCATCACAAGCCTCAGC and 5'-CGCAGTCGAGGTTGTGTGCAC were used for D431R. The resulting DNA fragments were digested with *Nde*I and *Sph*I for D431N or *Sph*I and *Blp*I for VP3 mutants, and used to replace the original *Nde*I-*Sph*I or *Sph*I-*Blp*I fragment in the pVOTE.2/POLY plasmid. For double or triple mutants in D431 and VP3 C-terminal, *Sph*I-*Blp*I resulting DNA containing mutations in VP3 was used to replace the original fragment in pVOTE.2/D431R.

**Table 2**. Synthetic oligonucleotides used to generate constructs used in "Implication of the catalytic residue in viral assembly".

| Name | Sequence (5'-3') |
|---|---|
| **pVOTE.POLYR248D** | TGGTGATCTGGGCCGCTGGATC |
| **pVOTE.POLYR248D c** | GATCCAGCGGCCCAGATCACC |
| **pVOTE.POLYR245D** | TGGGCGATTGGATCAGGACC |
| **pVOTE.POLYR245D c** | GGTCCTGATCCAATCGCC |
| **pVOTE.POLYR242D** | GGATCGATACCGTCTCTGATG |
| **pVOTE.POLYR242D c** | CATCAGAGACGGTATCGATCC |

### 3.2.4.2. Maturation of pVP2

Using PCR overlap extension five mutant pVP2 genes were constructed containing the following single and double mutations: A441G, F442G, A441G/F442G, D431N and D391N. PCR reactions were carried out using the pVP2 gene, cloned in the pFB/POLY plasmid as template, and the set of mutator primers (**Table 3**) in combination with primers 5'-GCCATCACAAGCCTCAGCGTTGG and 5'-GTGCAC CGCGGAGTACCCCAG for A441G, F442G and A441G/F442G. Primers 5'-GATGC CATCACAAGCCTCAGC and 5'-CGCAGTCGAGGTTGTGTGCAC were used for D431N and D391N. The resulting DNA fragments were digested with *Nde*I and *Sph*I and used to replace the original *Nde*I-*Sph*I fragment of the pVOTE.2/POLY plasmid.

**Table 3**. Synthetic oligonucleotides used to generate constructs used in "Maturation of pVP2".

| Name | Sequence (5'-3') |
|---|---|
| **pVOTE.POLYA441G** | GAAGATTGCAGGAGGATTCGGCTTC |
| **pVOTE.POLYA441G c** | GAAGCCGAATCCTCCTGCAATCTTC |
| **pVOTE.POLYF442G** | GAAGATTGCAGGAGCAGGCGGCTTCAAAGAC |
| **pVOTE.POLYF442G c** | GTCTTTGAAGCCGCCTGCTCCTGCAATCTTC |
| **pVOTE.POLYA441G/F442G** | CCTGAAGATTGCAGGAGGAGGCGGCTTCAAAGACATAATCC |
| **pVOTE.POLYA441G/F442G c** | GGATTATGTCTTTGAAGCCGCCTCCTCCTGCAATCTTCAGG |
| **pVOTE.POLYD391N** | GTTACAGAATACGGCCGATTTAATCCAGGAGCCATGAACTACAC |
| **pVOTE.POLYD391N c** | GTGTAGTTCATGGCTCCTGGATTAAATCGGCCGTATTCTGTAAC |
| **pVOTE.POLYD431N** | GTGAATACTTCATGGAGGTGGCCAATCTCAACTCTCCCCTGAAGATTG |
| **pVOTE.POLYD431N c** | CAATCTTCAGGGGAGAGTTGAGATTGGCCACCTCCATGAAGTATTCAC |

### 3.2.4.3. Implication of the catalytic residue in the viral assembly

FB/VP2-452 and FB/VP2-501 were previously described (Caston et al., 2001; Saugar et al., 2005). The pVOTE.2/D431N and pVOTE.2/D391N plasmids were used as a template for PCR synthesis to generate rBV/VP2-452D431N, rBV/VP2-452D391N and rBV/VP2-501D431N. PCR was performed with common 5' and 3'end primer (5'-GCGCAGATCTATGACAAACCTGTCAGATCAAACCC and 5'-GCGCAAGCTTA CCTTATGGCCCGGATTATGTCTTTGAAGC). *Bgl*II-*Hind*III-digested PCR fragments were cloned into FastBac *BamH*1-*Hind*III polylinker sites for protein expression.

### 3.2.4.4. The role of a cellular protease

From cDNA of DT40 cells, cytosol alanylaminopeptidase or puromycin sensitive aminopeptidase (PSA) cellular protease was amplified using primers 5'-GCGCAGATCTCCGGCCAAGC and 5'-GCGCAAGCTTTCAGTTACCTGTGGC. *Bgl*II-*Hind*III-digested PCR fragments were cloned into pFastBac HTb *BamH*1- *Hind*III polylinker sites for protein expression.

Using PCR overlap extension two mutant pVP2 genes were constructed containing the following single mutations: R452A and R453A. PCR reactions were carried out using the polyprotein gene, cloned in the pVOTE.2/POLY plasmid as

template, and the set of mutator primers (**Table 4**) in combination with primers 5'-GATGCCATCACAAGCCTCAGC and 5'-CGCAGTCGAGGTTGTGTGCAC. The resulting DNA fragments were digested with *Sac*I and *Sal*I and used to replace the original *Sac*I-*Sal*I fragment in the pFastBac/POLY plasmid.

**Table 4**. Synthetic oligonucleotides used to generate constructs used in "The role of a cellular protease".

| Name | Sequence (5'-3') |
|---|---|
| **pFastBac/POLY R452A** | GACATAATCCGG GCCATAGCG AGG ATAGCTGTG CCG GTG |
| **pFastBac/POLY R452A c** | CACCGG CACAGCTATCCTCGCTATGGCCCG GATTATGTC |
| **pFastBac/POLY R453A** | CATAATCCG GGCCATAAG GGCGATAGCTGTGCCGGTGGTC |
| **pFastBac/POLY R453A c** | GACCACCGG CACAGCTATCGCCCTTATGGCCCG GATTATG |

### 3.2.5 Generation of recombinant baculoviruses

rBVs have been generated by the Bac-to-Bac (*Invitrogen*) system following the manufacturer's protocols. This method is based in the recombinant genes transposition into a vector (bacmid) that is propagated in *E.coli* DH10-Bac (Luckow et al., 1993).

First, our interest sequence is cloned in a donator plasmid (pFastBac), which is used to transform DH10-Bac bacteria, where the recombinant gen transposition is going to occur. Once recombinant bacmids have been selected, they are used to generate rBVs by H5 cells transfection. Finally, rBVs are amplified by the infection of H5 cells, with the supernatant of cells previously transfected.

### 3.2.6. Generation of recombinant vaccinia viruses

To generate rVVs, BSC-40 cells are infected with the VT7LacOI virus at a 0,05 multiplicity of infection (MOI). After an hour, these cells are transfected with pVOTE plasmids with our gene of interest, using lipofectamine (*Gibco BRL*). Plasmids can recombine with the wt vaccinia virus by haemaglutinin (HA) sequences. After 72hp.i recombinant viruses are selected three times by the addition of mycophenolic acid. Mycophenolic acid inhibits the inosine-monophophatedehydrogenase enzyme provoking purine nucleotides depletion. Only viruses that have been recombined with the transfection vector will include in their genome the *E. coli* gpt

(phosphoribosyltransferase) gen, which in xanthine and hypoxanthine presence can produce puric nucleotides. rVVs are amplified in BSC-40 cells.

### 3.2.7. Generation of DF1 silenced cells

The PSA short hairpin (sh) oligonucleotides were first cloned in pRETRO-SUPER. pRETRO-SUPER vector was digested with *Bgl*II and *Hin*dIII, and the annealed oligonucleotides targeting the cellular protease, 5'-GATCCCC**GGCAACTTTTGATATTTCA**TTCAAGAGA**TGAAATATCAAAAGTTGCC**TTTTTGGAAA and 5'-AGCTTTTCCAAAAA**GGCAACTTTTGATATTTCA**TCTCTTGAA**TGAAATATCAAAAGTTGCC**GGG for **sh1**; 5'-GATCCCC**AACCTGGTGGAAGTCAAGT**TTCAAGAGA**ACTTGACTTCCACCAGGTT**TTTTTGGAAA and 5'-AGCTTTTCCAAAAA**ACCTGGTGGAAGTCAAGT**TCTCTTGAA**ACTTGACTTCCACCAGGTT**GGG for **sh2**; 5'-GATCCCC**GGAAAGTTTGCATTAGAGG**TTCAAGAGA**CCTCTAATGCAAACTTTCC**TTTTTGGAAA and 5'-AGCTTTTCCAAAAA**GGAAAGTTTGCATTAGAGG**TCTCTTGAA**CCTCTAATGCAAACTTTCC**GGG for **sh3**; were ligated with the vector, yielding **pRETRO-SUPER-sh1**, **pRETRO-SUPER-sh2** and **pRETRO-SUPER-sh3**. The 19-mer PSA targeting sequence in the oligonucleotide is indicated in bold. The hairpin oligonucleotides for the SUPER RNAi™ library are cloned downstream of the polymerase III Histone H1-RNA promoter (H1).

Upon transfection using lipofectamine *(Gibco BRL)* of pRETRO-SUPER-sh1, sh2, sh3 and an empty plasmid as positive control for non-silencing of the protein, into packaging cell line 293T with pCL-anfo as a helper plasmid, pRETROSUPER expresses a transcript containing the viral packaging signal, the H1-shRNA cassette and the puromycin resistance gene. At 48 hours post transfection, we collect the supernatant, which should be filter through a 0.45 μm filter, and then is added to DF1 recipient cells. The infection of DF1 cells with the retrovirus-containing supernatant is made three times in 24 hours with the addition of polybrene at 4μg/ml or 8μg/ml. Then the selection of silenced cells starts with the addition of 2μg/ml of puromycin. Selection will take between two and three days.

### 3.2.8. Reverse genetic analysis

DNA fragments containing cDNA versions corresponding to the complete positive strand RNAs of to the IBDV Soroa strain segments A and B, fused to the T7 bacteriophage promoter (in 5' position with respect of the IBDV cDNAs) and a cDNA corresponding to the hepatitis delta virus ribozyme (in 3' position with respect of the IBDV cDNAs) sequences were generated by in vitro gene synthesis (*Genescript Co*.), and inserted into the multiple cloning site of the pUC57 cloning plasmid (*GenBank/EMBL*). These plasmids were named pT7-SA-Rz and pT7-SB-Rz, containing the cDNA corresponding to segment A and B, respectively.

Plasmid pVOTE/D431N, described above, was digested with *Sph*I and *Nde*I, and ligated to pT7-SA-Rz previously digested with the same enzymes. The resulting plasmid, pT7-SA (D431N)-Rz, was sequenced to determine the correctness of its sequence.

QM7 cells were transfected with a combination of either pT7-SA-Rz and pT7-SB-Rz or pT7-SA (D431N)-Rz and pT7-SB-Rz, respectively, using lipofectamine (*Gibco BRL*). At 6 h after transfection, cultures were infected with 1 PFU/cell of VT7LacOI, an rVV inducible expressing the T7 RNA polymerase. After infection, cultures were maintained at 37ºC in DMEM containing 10% FCS supplemented with 1mM IPTG. At 72 h pi, cultures were harvested, and subjected to three freeze-thawing cycles. After removing cell debris by low speed centrifugation, supernatants were recovered and passed through 0.1 μm filters (*Millipore*) to eliminate contaminant rVV particles, and used to infect fresh QM7 cell monolayers. Infections were performed in triplicate with undiluted and $10^{-1}$ to $10^{-5}$ serial dilutions of the initial stocks. A set of infected cells was used to determine the IBDV titre at 72 hp.i. Another set was harvested at 72 hp.i., and the corresponding extracts analyzed for the presence of VP1 and VP2 proteins. The absence of contaminant infecting rVV particles was also monitored by Western blot, using the mAbC3. The third set was also harvested at 72 hp.i., and used to collect cells originally infected with the undiluted stocks. These samples were subjected to three freeze-thawing cycles, and the procedure described above was repeated; thus allowing the analysis of the initial virus stock and two subsequent virus amplification rounds.

## 3.3 Infections and protein expression

### 3.3.1 rBV infection

H5 cells confluent cultures were infected with a MOI of 1 to 5 plaque forming units per cell (pfu/cell) of the corresponding rBV in minimal volume. After an hour of adsorption, the inocule was released and TC-100 medium supplemented with 2% FCS was added.

### 3.3.2 rVV infection

BSC-40 and QM7 cells confluent cultures were infected with a MOI of 2 pfu/cell of the corresponding rVV in minimal volume. After an hour of adsorption, the inocule was released and DMEM medium supplemented with 2% FCS, and IPTG 1M to a final concentration of 2mM was added.

### 3.3.3 IBDV infection

For IBDV virions purification, QM7 cell cultures were infected at a 70-80% confluence with a MOI of 1-2 pfu/cell in a minimal volume. After an hour of adsorption, the inocule was released and DMEM medium supplemented with 2% FCS was added. Culture supernatant was collected at 48-72 hp.i. depending on the cytopathic effect (CPE) observed.

For IBDV stock production, the same procedure was followed using a MOI of 0.02-0.05 pfu/cell and collecting supernatants at 72-96 hp.i.depending on the CPE.

### 3.3.4 IBDV Titration

Viral titres were determined by immunostaining assays against the capsid protein VP2. QM7 cell monolayers were infected at a 50-60% cell confluence with higher virus dilutions. After the adsorption hour, the inocule was released and DMEM supplemented with 2%FCS was added. At 72 hp.i cells were fixed by a methanol-

acetone solution (1:1) during 2 minutes at room temperature. Cells were incubated with an anti-VP2 antibody during 1hour and 30 minutes and a posterior incubation with a secondary antibody conjuged with peroxidase (*GE Healthcare*). Lysis plaques were developed when the substrate $H_2O_2$/3, 3'-diaminobenzidine (*Sigma*) in the presence of $NiSO_4$ was added. Titres were determined by lysis plaques counting.

### 3.3.5 rVV Titration

Viral titres were determined by lysis plaques assays. BSC-40 confluent cell monolayers were infected with higher virus dilutions. After the adsorption hour, the inocule was released and DMEM supplemented with 2%FCS was added. At 48 hp.i cells were fixed by a 10% formaldehyde solution during 2 minutes at room temperature and stained with a 2% violet crystal solution. Titres were determined by lysis plaques counting.

## 3.4 Purification of IBDV polyprotein-derived structures

QM7 and H5 cells (2-5x$10^8$ cells) were infected with appropriate rVV or rBV (MOI 1-5pfu/cell). At 72 hp.i. in rVV assays and at 48 hp.i. in rBV assays, cells were harvested, lysed in PES buffer (25 mM piperazine-N, N'-bis (2-ethanesulfonic acid), pH 6.2, 150 mM NaCl, and 20 mM CaCl2) plus 1% IGEPAL CA-630 (*Sigma*) and 1% of proteases inhibitor (*Complete Mini, Roche*) on ice during 30 min. The lysate was clarified by centrifugation at 3,000 r.p.m. (1,000xg) during 10 min in a swing 5624 rotor (*Hettich Zentrifugen*). The supernatant was processed on a 25% sucrose cushion at 37,000 r.p.m. (170,000xg) during 2h 30 min in a SW41 rotor (*Beckman-Coulter Inc*). The pellet was resuspended in PES buffer and centrifuged in a microfuge at 13,000 r.p.m. (16,000xg) during 1 min and the supernatant processed in a linear 20-50% sucrose gradient at 40,000 r.p.m. (200,000xg) during 45 min in a SW41 rotor (*Beckman-Coulter Inc*). The particulate material containing polyprotein-derived structures was fractionated in 12 and concentrated 20-fold by ultracentrifugation at 50,000 r.p.m. (240,000xg) during 2 hours in a SW55 rotor (*Beckman-Coulter Inc*). All purification steps were made at 4ºC.

## 3.5 Biochemical analysis

### 3.5.1 Electrophoretic analysis in denaturing polyacrylamide gels

Infected cell extracts (25 μl) or concentrated sucrose gradient fractions (10 μl) were added to Laemmli's sample buffer (62.5 mM Tris-HCl pH 6.8, 1% SDS, 0.06% bromophenol blue, 25% glycerol and 10 mM DTT) to a 1x final concentration and heated at 100ºC for 3 min. Electrophoresis was performed in 11% polyacrylamide gels (37.5:1).

Afterwards, gels were electrotransferred to nytrocellulose membranes or stained with a 2% Coomassie blue solution in 10% methanol and 10% acetic acid.

### 3.5.2 Electrotransference and immunodetection (*Western Blot*)

Following PAGE, gels were blotted at 200 mA for 90 min onto nitrocellulose membranes (*Protan*) using a semi-dry blotter (*Bio-Rad*). Before the transference gels and membranes were incubated during 10 min in Tris 48 mM, glycine 39 mM, SDS 0.0375 % (p/v), methanol 20 % (v/v) buffer. Membranes were saturated in a blocking solution (5% powder skimmed milk in phosphate saline buffer (PBS)) during 30 min at room temperature. And then incubated with a diluted primary antibody (α-VP2 1:1000; α-VP3 1:1000; α-His 1:1000) in blocking solution during 2 hours at room temperature. After washing membranes three times with PBS, were incubated with a goat secondary antibody conjugated with peroxidase (*GE Healthcare*) diluted 1:5000 in blocking solution. Membranes were washed three times with PBS during 10 min and developed by the commercial chemiluminescent method ECL (*GE Healthcare*) or by the addition of 4-chloro-1-naphtol with 0,025% of $H_2O_2$.

### 3.5.3 Immunoprecipitation (IP) of VP2

QM7 cell monolayers were infected with the corresponding rVV at a MOI of 2 pfu/cell and maintained in the presence of IPTG. At 18 hp.i., cells were washed twice and metabolically labeled with methionine-free DMEM containing 125 μCi/ml of [$^{35}$S]Met and IPTG for 1h. After this period, cells were washed three times with DMEM

containing a 10 fold concentration of cold methionine and then maintained in DMEM supplemented with IPTG and 2% FCS. At 0, 24, 48, 72 h post-labelling, cells were harvested, washed twice with PBS, and resuspended in lysis buffer (50 mM Tris [pH 7.5], 100 mM NaCl, 5 mM EDTA, 0.5% IGEPAL CA-630). IPs were carried out with protein A-Sepharose CL-4B (*Pharmacia Biotech AB, Uppsala, Sweden*) after incubation of the extracts with specific rabbit anti-VP2 antisera. Immunoprecipitated samples were resuspended in Laemmli sample buffer to a 1x final concentration, subjected to 11% SDS-PAGE followed by autoradiography.

## 3.6. Microscopy

### 3.6.1. Electron microscopy

2-5 µl samples of concentrated sucrose gradient fractions were applied to glow-discharged (K100X, *Emitech*) carbon-coated grids for 2 min and negatively stained with 2% aqueous uranyl acetate. Micrographs (*Kodak* SO-163) were recorded with a JEOL 1200 EXII electron microscope operating at 100kV at a nominal magnification of 40,000x.

### 3.6.2. Immunofluorescence and confocal laser scanning microscopy analysis

DF1 silenced cells and H5 cells seeded onto glass coverlips were infected with IBDV and rBVs, respectively, at a MOI of 1 PFU/cell. Cells were washed twice with phosphate-buffered saline at 30 hp.i for DF1 cells and at 48hp.i for H5 cells and then fixed in methanol-acetone (1:1) for 5min. After fixation, coverlips were airdried, blocked in phosphate-buffered saline containing 20% fetal calf serum for 1h and incubated with rabbit anti-VP2 and mouse anti-His tag specific sera, followed by incubation with goat anti-rabbit Ig coupled to Alexa 488 (green) and goat anti-mouse Ig coupled to Alexa 594 (red) for H5 cells; for DF1 cells only a rabbit anti-VP2 followed by a goat anti-rabbit Ig coupled to Alexa 488 (green) were used. Cell nuclei were stained with ToPro-3. Fluorescent signals detected by CLSM were recorded separately by using appropriate filters. Samples were visualized by epifluorescence using a Zeiss Axiovert 200 microscope equipped with a Bio-Rad Radiance 2100 confocal system. Images were captured using the Laser Sharp software package (*Bio-Rad*).

## 3.7 Crystallization and data collection

Cubic crystals belonging to space group P213 (a=b=c=326.72 Å) were obtained by the vapour diffusion method in hanging drops at room temperature by mixing 2 volumes of VP2-452D431N derived SVP (1.6 mg/ml) and 1 volume of the reservoir solution, containing 14 to 17% PEG 4K, 0.1 M TRIS pH 9.0 and 5% isopropanol. Crystals were transferred to a cryoprotecting solution containing 20% glycerol in the crystallization buffer and incubated 1 minute before they were flash frozen by immersion in liquid nitrogen. X-ray data were collected from a single crystal using synchrotron radiation at the ESRF, Grenoble, France (beamline ID14-2), to 3.1 Å resolution. Diffraction images were processed using MOSFLM (Leslie, 1991) and internally scaled with SCALA (Evans, 1994).

### 3.7.1 Structure refinement

Crystals of D431N-mutated SVP were isomorphous to the previously obtained of native VP2 SVPs [PDB code 2GSY, (Garriga et al., 2006)]. The initial maps for D431N-mutant were obtained after a rigid body fitting of the coordinates of native SVPs (PDB code 2GSY) to the new unit cell. The D431N mutation and other subtle changes were manually rebuilt using Coot (Emsley, 2004) and the structure was then refined with CNS (Brünger, 1998), using the twentyfold non crystallographic symmetry as a restraint.

The final refinement statistics are summarized in **Table 5.**

**Table 5.** Data collection and refinement statistics**.**

| **Data collection** | **D431N** |
|---|---|
| Space group | $P2_13$ |
| Cell dimensions | |
| a=b=c (Å) | 326.72 |
| Wavelength | 0.933 |
| Resolution (Å) | 50-3.1 |
| $R_{sym}$ | 0.12 |
| I/σI | 9.3 |
| Completeness (%) | 99.0 |
| Redundancy | 5.3 |
| **Refinement** | |
| Resolution (Å) | 20.0-3.1 |
| No. Reflections | 187110 |
| Cutoff | 3σF |
| $R_{work}/R_{free}$ | 0.28/0.28 |
| No. Residues | |
| Protein | 428 |
| Ligand/ion | 1 |
| Water | - |
| Averaged B-factors | 26.7 |
| R.m.s. deviations | |
| Bond lengths (Å) | 0.006 |
| Bond angles (º) | 0.803 |

## 3.7.2. Protein structure accession number

The coordinates and structure factors have been deposited into the Protein Data Bank (accession no. **3FBM**).

## 3.8. Quantitative real time polymerase chain reaction (qRT-PCR)

### 3.8.1. Total cellular RNA extraction

In the determination of the presence or not of the PSA in different cell lines, as well as in the qRT-PCR to check the quantity of the cellular protease in the silenced cells, cells were lysed directly in a culture dish by adding 1ml of TRIzol LS Reagent (*Invitrogen*). The homogenized samples were incubated for 5 min at room temperature to permit the complete dissociation of nucleoprotein complexes and 0.2 ml of chloroform was added. Samples were centrifuged at 12,000x g for 15 min at 4ºC and the upper aqueous phase was recovered, where RNA remained. RNA was precipitated by mixing with isopropyl alcohol for 10 minutes and centrifuged at 12,000x g for 10 min at 4ºC. The RNA pellet was washed once with 75% ethanol and then resuspended in 100µl of DEPC water. The RNA concentration and the relation 260/280 nm were determined by a spectrophotometer Nano-Drop ND-1000 *(NanoDrop Technologies, Wilmingon, DE; USA)*. RNA integrity was checked in a 1% agarose gel.

### 3.8.2. RNA Purification and cDNA synthesis

Total RNA was treated with DNase I RNases-free (*Qiagen*) for 10 min at room temperature to eliminate contaminant genomic DNA. Afterwards, the RNA was purified by RNeasy Mini Kit (*Qiagen*) following manufacturers' guidelines.

cDNA synthesis was made from 1µg of total RNA in a reaction total volume of 20µl with 1X PCR Buffer II (*Applied Biosystems*), 5mM $MgCl_2$, 1mM dNTP, 1U/µl RNase inhibitor (RNasin, Promega), 2.5 U/µl of MuLV reverse transcriptase (*Applied Biosystems*), 5mM of random primers (*Gibco*) and DEPC water.

### 3.8.3. Oligonucleotides design

To detect PSA transcripts levels, a pair of oligonucleotides were used which originated an amplification product of 143pb.(**Table 6**) As a control, a pair of oligonucleotides which generates an amplification product of 154 pb of the

glyceraldehide-3-phosphate dehidrogenase (GAPDH) enzyme *Gallus gallus* gen was used **(Table 6)**. In all cases, oligonucleotides were designed using "Primer Express 2.0" program (*Applied Biosystems, Foster City, CA, USA*).

**Table 6**. Primers used in qRT-PCR reactions.

| **Name** | **Sequence (5'-3')** |
|---|---|
| **GAPDH (*Gallus gallus*)** | ATGGTGAAAGTCGGAGTCAACG |
| **GAPDH (*Gallus gallus*) c** | GACAGTGCCCTTGAAGTGTC |
| **PSA (*Gallus gallus*)** | TGCCTTAGACAACAGTCATCC |
| **PSA(*Gallus gallus*) c** | TCCGAAAGTCCTCATCACCA |

### 3.8.4. Conditions and analysis of qRT-PCR

PCR reactions were carried out in 96-multiwell (*Applied Biosystems*). Transcript levels were determined by qRT-PCR using the real time 7300 PCR system (*Applied Biosystems*) and SYBRGreen (*Applied Biosystems*) as a detector. Reactions were made in a final volume of 20µl in which 10µl was PCR master mix "Power SYBR Green PCR" 2x (where "AmpliTaq Gold", dNTPs and "SYBR Green" are included), 250nM of the 5' and 3' specific oligonucleotide, 1µL of the 1:10 cDNA dilution and water. After the enzyme activation at 95ºC for 10 min, amplification was carried out during 40 2- steps cycles: i) 95ºC for 15 sec for the denaturalization of the dhDNA, and ii) 60ºC for 1 min for the hybridization and product extension. Negative controls were included and reactions were made by triplicate.

Data were analyzed by qBase Plus (BioGazelle) program. Expression levels were calculated using the standard curve method and normalized using GAPDH gen as a reference control.

## 3.9. Computer programs

### 3.9.1. Sequence alignment

For the alignment of different IBDV isolates and different cytosol alanylaminopeptidases from several organisms, the Clustal W 2.0 program was used.

# RESULTS

## 4.1. Plasticity domain of the pVP2 C-terminal end

VP2 is synthesized as a 512 residue precursor, pVP2, which undergoes a variety of defined C-terminal processing events to render the mature VP2 (441 residues). The molecular switch controlling VP2 polymorphism resides within the C-terminal 71 residues, which are removed when its function has been completed. Previous results obtained in our laboratory (Saugar et al., 2005) indicated that the VP2 molecular switch is located in the temporally bound 443-GFKDIIRAIR-452 segment that is organized as an amphipathic α-helix (**Fig.7**). The hydrophilic side of this α-helix is built of three basic and an acidic residues and an interaction with other proteins is possible.

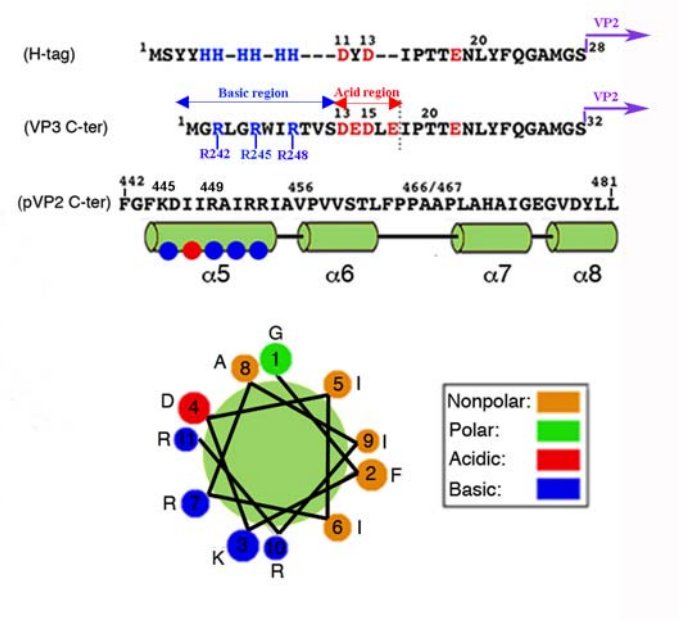


**Fig.7**.**VP3 and VP2 polypeptide segments involved in structural polymorphism of VP2.** In the upper panel, VP3 C-terminal and His tag sequences are aligned based on their polarity. Basic residues are represented in blue and acid ones in red. The His tag is composed of six canonical His and a spacer arm corresponding to residues Asp-11 until Ser-28, from which the VP2 sequence would start. VP3-Ct end is shown in the opposite direction, from C-terminal to N-terminal domain respect to the polyprotein sequence and the last residue (Glu-17) is indicated by a line, after that, part of the spacer arm of the His tag has been introduced .The C-terminal VP2 sequence is shown in the middle. The amphiphatic α-helix (443-453 residues) is shown as helix-α5; helices-α6, α7 and α8 were determined by NMR analysis (Galloux et al., 2007). A helical wheel representation of the amphiphatic α-helix is shown at the bottom. Group colour key is indicated. All residues that are going to be mutated are marked by a number.

Previous results from our laboratory showed that, in the absence of VP3, efficient T=13 capsid-like assembly is dependent upon the presence of a His tag located at the VP2 N-terminus, indicating that the His tag mimics the VP3 function, acting as a

triggering factor, during virion assembly (Saugar et al., 2005). We compared the His tag and VP3 sequences to search for an explanation to this observation. The acid character of the last five residues in the VP3 C-terminus align well with an equivalent region of the His tag (**Fig.7**). A charge complementarity with the proposed α–helix is evident, tempting us to suggest that electrostatic interactions may be the initial event in the adoption of different pVP2 conformational states. Both acid segments in the His tag and the VP3 C-terminal residues are preceded by a basic segment that might also have an additional function. This electrostatic interaction has been postulated to be transmitted to the rest of VP2, inducing the correct conformational change (Saugar et al., 2005).

### 4.1.1. The role of the basic and acid segments of the His tag in T=13 VLP assembly

To analyze whether the basic region of the His tag is necessary for the correct assembly of the T=13 VLP, different deletion mutants were made in the HT-VP2-466 recombinant polypeptide. HT-VP2-466 in the baculovirus system, which banded at the middle of a sucrose gradient, is able to assemble into structures morphologically similar to T=13 infectious particles with minor differences in the outermost and the inner surface of the capsid (**Fig.8A**). This chimeric VP2 polypeptide possesses two elements required for a correct T=13 assembly, the VP2 amphiphatic α-helix and the His tag emulating VP3 C-terminus. Different experiments were carried out to determine the implication of the basic and the acid regions. Two different deletion mutants were generated in the baculovirus system. The rBV/HT-VP2-466Δ2-10 expresses the chimeric VP2 protein lacking residues 2-10; this region includes six basic residues of the His tag (**Fig.7 and Fig.8B**); in HT-VP2466Δ11-25, the deletion removed the acid region, residues 11-25, which mimic VP3 Ct acid region (**Fig.7 and Fig.8C**). Cell extracts infected with these rBVs were analyzed by sucrose gradient and ultracentrifugation, and EM analysis by negative staining. As shown in **Fig. 8B and 8C**, expression of the HT-VP2-466Δ2-10 gene results in the assembly of large tubular structures, whereas the HT-VP2-466Δ11-25 construct assembles as T=1 SVP were recovered. The formation of T=13 capsid assemblies is prevented for both deletion mutants, suggesting that basic and acid residues are required for the proper T=13 VLP assembly.

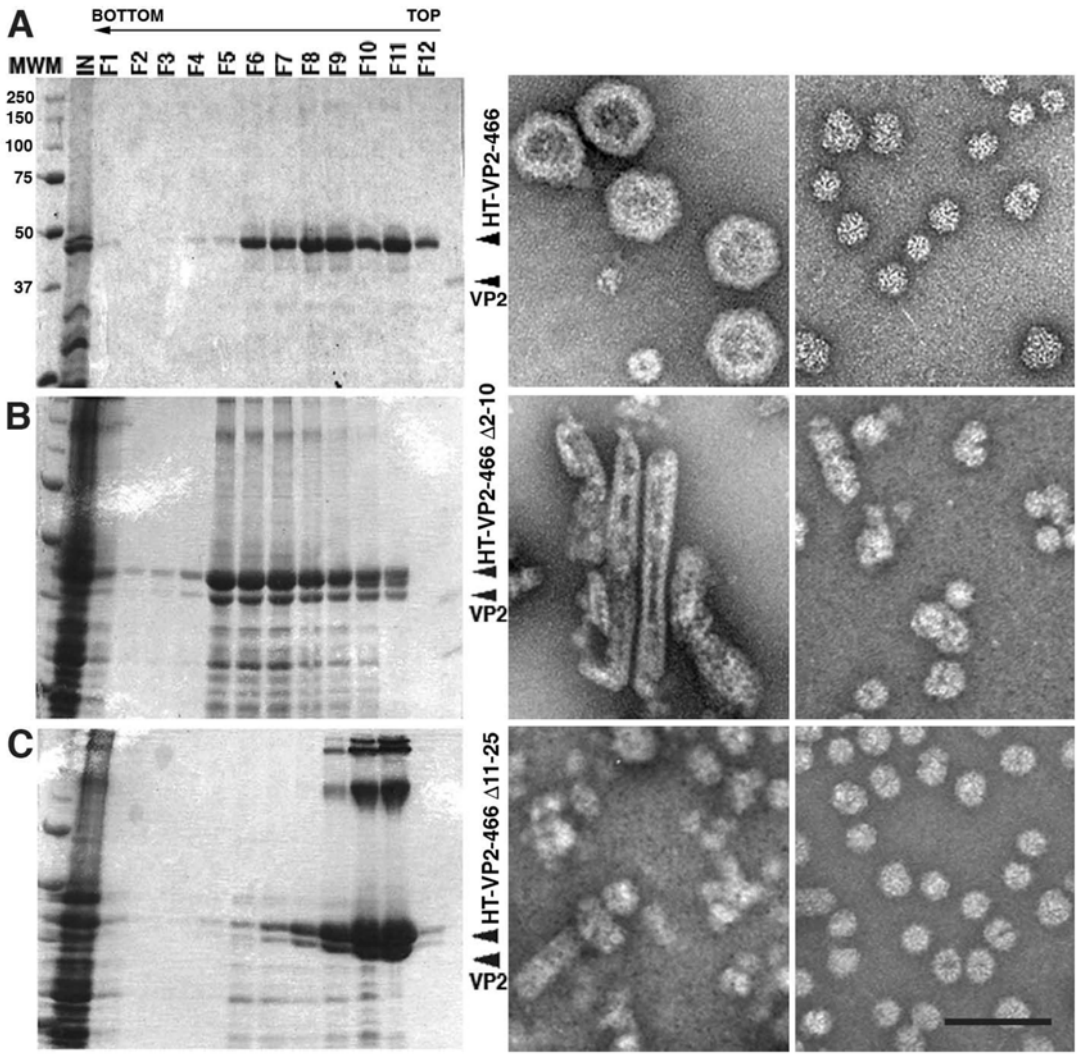


**Fig.8**. **The role of the basic segment of the His tag in capsid assembly**. (**A**) Wild type HTVP2-466 assemblies were purified by ultracentrifugation on sucrose gradients. Gradients were collected into 12 fractions, concentrated by ultracentrifugation, and analyzed by SDS-PAGE and Coomassie staining. The direction of sedimentation was right to left, with fraction 12 representing the gradient top. The image shown on the right corresponds to a representative electron microscopy micrograph (negative staining) of wild-type HTVP2-466 capsids, present at the middle and the top gradient fractions. (**B**) Mutant HTVP2-466-Δ2-10 and (**C**) HTVP2-466-Δ11-25 assemblies were analyzed as described above. The image shown on the right corresponds to a representative electron microscopy micrograph (negative staining) of the middle and upper fractions. Bars = 100 nm.

## 4.1.2. The emulation of VP3 C-terminal domain by the His tag

To definitely confirm whether the His tag functionally emulate the VP3, the His tag was exchanged by VP3 C-terminal region, including basic residues domain. This was generated in rBVs expressing VP2-456 and VP2-466, as their homologues BV/HT-VP2-466 and BV/HT-VP2-456, were previously determined to be able to assemble in T=13 capsids indistinguishable of IBDV virions by electron microscopy.

BV/Ct-VP3-VP2-456 and BV/Ct-VP3-VP2-466 were harvested and at 48h.pi. analyzed by sucrose gradient and ultracentrifugation. As it can be observed in **Fig. 9A and B**, this change permits the correct assembly of T=13 VLP in both cases, indicating that the His tag is clearly emulating VP3 C-terminal domain.

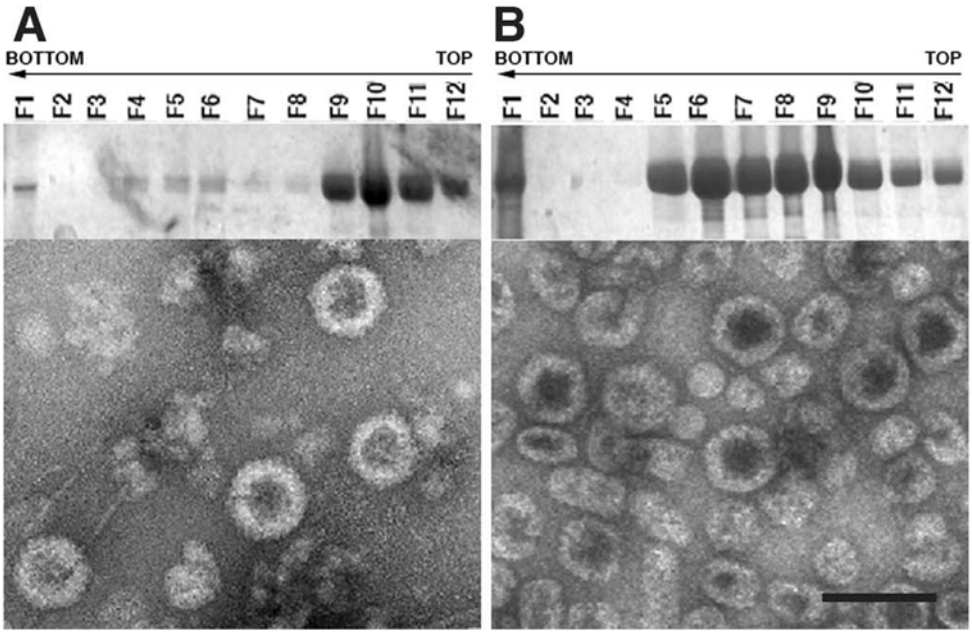


**Fig. 9**. **The emulation of VP3 C-terminal domain by the His tag**. (**A**) CtVP3-VP2-456 and (**B**) CtVP3-VP2-466 assemblies were purified by ultracentrifugation on sucrose gradients. Gradients were collected into 12 fractions, concentrated by ultracentrifugation, and analyzed by SDS-PAGE and Coomassie staining. The direction of sedimentation was right to left, with fraction 12 representing the gradient top. Images shown correspond to a representative electron microscopy micrograph (negative staining) of structure recovered at the middle gradient fractions. Bars=100 nm.

To further test these results; different point mutants were generated in the rVV polyprotein system (Lombardo et al., 1999) which allows the efficient assembly and

accumulation of VLPs. In comparison with the basic region of the His tag, three different arginine residues were replaced in VP3 C-terminal domain (Arg-248, Arg-245, and Arg-242), by aspartic acid (relative positions are shown in the scheme, **Fig. 7**). With this approach the charge of every residue potentially involved in this interaction was replaced by a residue with an opposite ionic character. The loss of the ability to assembly in T=13 VLP, of different rVVs would indicate that the altered residue is probably implicated in viral capsid formation.

The analysis of the different single mutants, rVV/PolyR248D, rVV/PolyR245D and rVV/PolyR242D by sucrose gradient and ultracentrifugation (**Fig. 10A, 10B and 10C**), shows that Arg-248 of VP3 Ct domain change does not alter the proper assembly of T=13 VLPs, similar to viral capsids. Furthermore, results of the biochemical analysis were similar to those obtained with the wild-type polyprotein. The R245D mutation renders a wild-type biochemical pattern, structures observed are more labile and highly prone to collapse, than wild-type T=13 capsids. The R242D mutant leads to the accumulation of structures in the upper fraction of the gradient, the electron microscopy analysis showed the presence of capsid-like structures smaller than T=13, probably corresponding to T=7 VLP. These results with the rVV system indicate that within the basic region of VP3, basic residues Arg-245 and Arg-242 are essential and probably implicated in IBDV capsid assembly probably by an electrostatic interaction with a non-determined region of VP2.

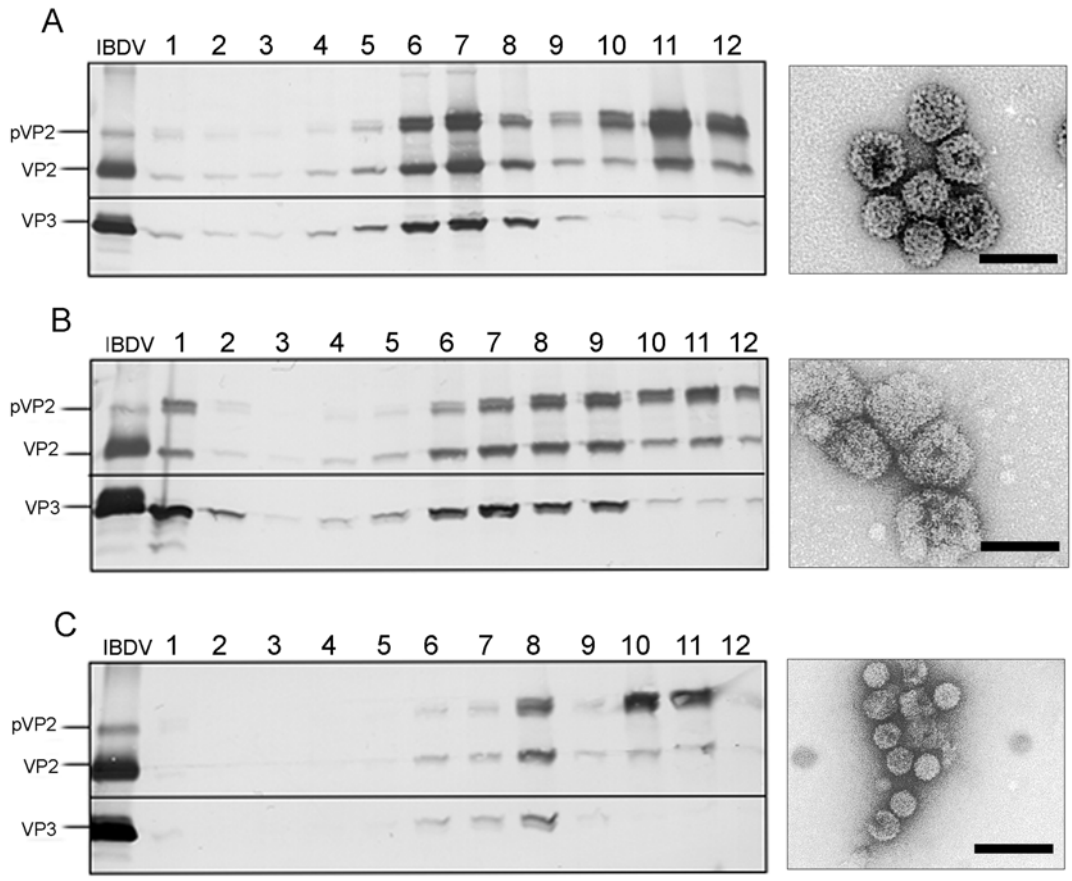


**Fig. 10**. **The role of the basic segment of VP3 C-t ends in viral assembly**. (**A**) VT7/POLYR3D assemblies were purified by ultracentrifugation on sucrose gradients. Gradients were collected into 12 fractions, concentrated by ultracentrifugation, and analyzed by SDSPAGE and Western blot using anti-VP2 and anti-VP3 serum. The direction of sedimentation was right to left, with fraction 12 representing the gradient top. The image shown on the right corresponds to a representative electron microscopy micrograph (negative staining). (**B**)VT7/POLYR6D and (**C**) VT7/POLYR9D assemblies were analyzed as described. Bars=100 nm.

### 4.1.3. Interaction between VP3-based triggering factor and the pVP2 molecular switch

The acid character of VP3 C-terminal domain is necessary for the correct assembly of T=13 VLP and its role in viral assembly tempts to suggest the hypothesis of an electrostatic interaction with VP2 amphiphatic α–helix, where some basic residues are located. These electrostatic interactions may be the initial event in the adoption of different pVP2 conformational states.

To dilucidate if there is any electrostatic interaction between VP3 acid residues and the VP2 amphiphatic α-helix, different point mutations were generated in HT-VP2-466 and CtVP3-VP2-466 recombinant genes. First, Lys-445 or Arg-449 was replaced by aspartic acid residues, in the amphiphatic α-helix. Second, Asp-11 and Asp-13 located in the spacer arm of the His tag, were replaced by two Arg residues, in BV/HT-VP2466. A similar approach was carried out for BV/CtVP3-VP2-466 in which Asp-13 (**VP3** Asp-252) or Asp-15 (**VP3** Asp-254) of VP3 DEDLE region, were exchanged by Arg residues. The modification of charged residues potentially involved in the electrostatic interaction, by a residue with the opposite ionic character would eventually lose the ability to assembly in T=13 capsids. With this hypothesis the recovery of capsid formation would be provided by the generation of double mutants, in which the electrostatic change has been compensated; e.g. in HT-VP2-466, in which Asp-13 has been mutated to a Arg residue, could be eventually compensated by the change of Arg-449 by Asp residue (a summary of all single mutants and double combinations generated is shown in **Fig. 11).**

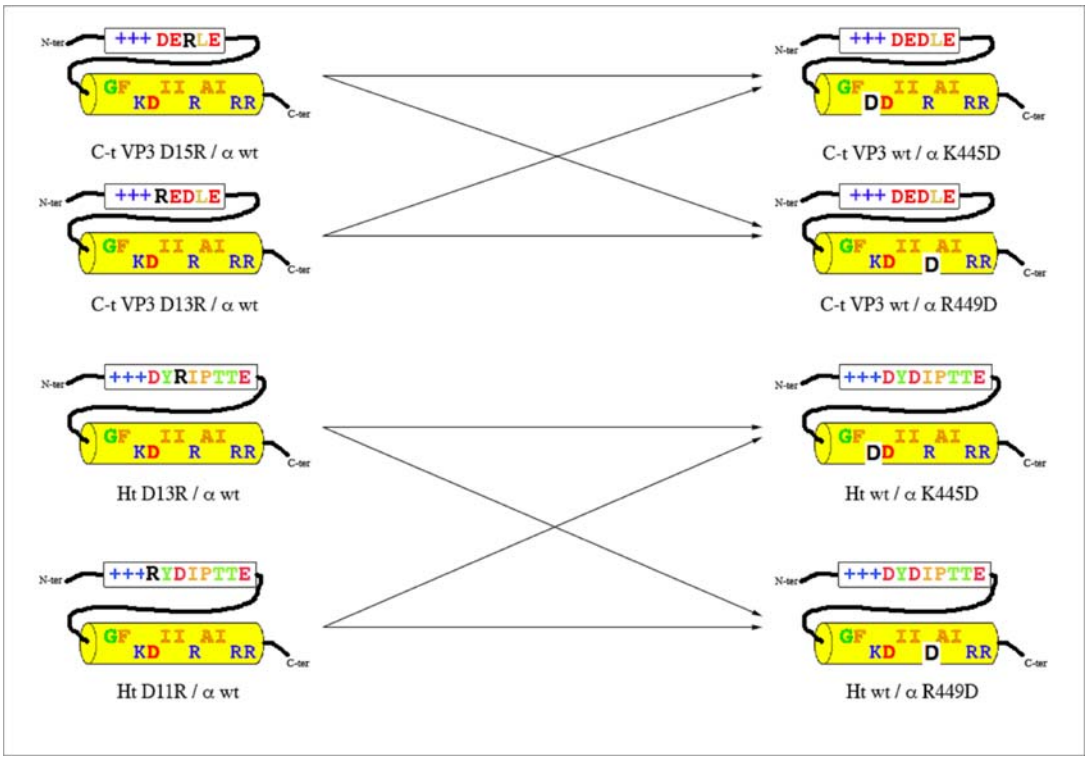


**Fig. 11**. **Analysis of a possible interaction between the acid regions of VP3 C-terminal domain with basic residues of the amphiphatic α-helix 442-453**. The proposed charge complementarity between the amphipathic α-helix and the last five residues of VP3 C-terminal region (**upper panel**) (or the aligned VP3 similar region of the His tag) (**lower panel**) used in this study are shown. VP3 and His tag sequences are shown in the opposite direction, from C-terminal to N-terminal ends. Residue mutated in each case is shown in black and the different double combinations can be followed by arrows.

H5 insect cells were infected by single mutants, and at 48 hp.i corresponding extracts were harvested and used for the isolation of IBDV derived assemblies using a sucrose gradient-based purification protocol followed by electron microscopy and biochemical analysis with Coomassie staining. The analysis of single mutants shows that mutations on the amphiphatic α–helix of VP2, in BV/HT-VP2-466 and BV/CtVP3-VP2-466 chimeric proteins, prevent the formation of T=13 capsids. Particulated material is accumulated at the bottom part of the gradient and by electron microscopy only large tubular structures with an hexagonal lattice are observed (**Fig. 12 and 14B**). When any acid residues of VP3 C-terminus or His tag spacer arm is replaced, the structure that could be recovered are mostly T=1 SVP accumulated at the upper gradient fractions (**Fig. 12 and 14C**). This suggests that all mutated residues are potentially involved in T=13 correct assembly, probably by their implication in stabilizing the electrostatic interaction.

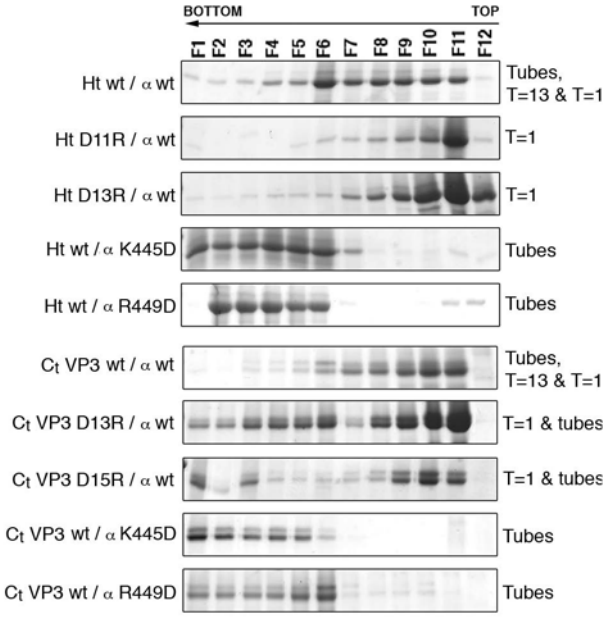


**Fig. 12. Analysis of single mutants**. Single mutants assemblies were purified by ultracentrifugation on sucrose gradients. Gradients were collected into 12 fractions, concentrated by ultracentrifugation, and analyzed by SDS-PAGE and Coomassie staining. The direction of sedimentation was right to left, with fraction 12 representing the gradient top. The kind of assemblies that are yielded with each mutant is indicating on the right side.

Double mutations in rBVs were carried out in order to rescue the proper T=13 capsid assembly. Mutants in the Ct region of VP3 or His tag in which one Asp residue

was replaced by Arg, were compensated with Lys-445 and Arg-449 mutations, and vice versa (**Fig. 11**). H5 insect cells infected by these rBVs and their corresponding extracts harvested and used for the isolation of IBDV derived assemblies. Mutants HTD11R-VP2-466R449D, HTD13R-VP2-466K445D, CtVP3/D13R-VP2466K445D, CtVP3/D13R-VP2466R449D, CtVP3/D15R-VP2466K445D, accumulate particulated material at the bottom fractions of the gradient, which was composed of tubular structures with a hexagonal lattice. Whilst the recovery of T=13 capsids was consistently observed when HT/D13R-VP2-466 and CtVP3/D15R-VP2466 were conjugated with R449D (**Fig. 13**), where VLP in the middle gradient fractions are observed by electron microscopy. T=13 capsids are also obtained with mutant HT/D11R-VP2-466K445D (**Fig. 13 and 14A**).

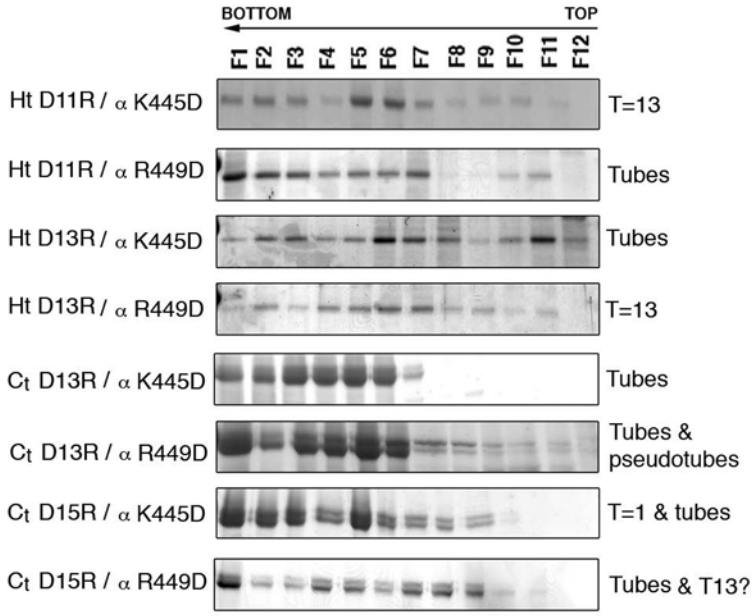


**Fig. 13. Analysis of double mutants**. Double mutants assemblies were purified by ultracentrifugation on sucrose gradients. Gradients were collected into 12 fractions, concentrated by ultracentrifugation, and analyzed by SDS-PAGE and Coomassie staining. The direction of sedimentation was right to left, with fraction 12 representing the gradient top. The kind of assemblies that are yielded with each mutant is indicating on the right side.

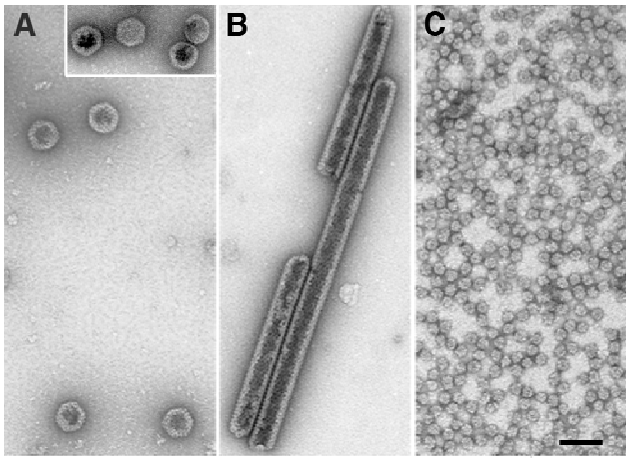


**Fig. 14**. Representative EM micrographs (negative staining) of (**A**) T=13 capsids of HTD13R-VP2-466R449D mutant, squared IBDV virions, (**B**) rigid tubules with an hexagonal lattice of CtVP3D13R mutant and (**C**) T=1 SVPs of the same mutant. Bars = 100 nm.

Taken together, the results of these analyses suggest that all mutated residues are implicated in the correct assembly of T=13 capsids probably due to a temporary electrostatic interaction between the acid region of the triggering factor, the VP3 C-terminus and the His tag, and the VP2 amphiphatic α-helix. As result of mutant analyses, in which T=13 VLP are only recovered in mutants HT/D13R-VP2-466R449, CtVP3/D15R-VP2-466R449D and HT/D11R-VP2-466K445D, it can be dilucidiate that this temporary electrostatic bond corresponds to an interaction between Arg-449 of the amphiphatic α-helix with Asp-254 of VP3 Ct domain and possibly between residues Lys-445 of VP2 with Asp-252 of VP3 in the context of the chimeric proteins analyzed.

## 4.2. Maturation of pVP2

### 4.2.1. VP2 candidates as catalytic residues for autoproteolysis

VP2 S and B domains share a high degree of structural similarity with noda- and tetravirus β-protein. Both coat protein precursors, pVP2 and α-protein; suffer an ulterior proteolytic event which confers stability and infectivity to the virion by rearrangement of the procapsid intermediate. As cleavage sites are deeply buried inside the capsid shell, and thus sheltered from possible attacks by cellular proteases. It has been described for noda- and tetravirus that the coat proteins is processed by an autoproteolytic event mediated by an acid residue (Taylor and Johnson, 2005; Zlotnick et al., 1994).

Searching for possible candidates in VP2, its atomic structure was fitted into the three-dimensional cryo-electron microscopy map of IBDV T=1 SVP allowing to identify at least two conformations for its C-terminal region (molecular swapping) (Luque et al., 2007). These structural considerations suggested that Asp391 and/or Asp431 might be good catalytic candidates capable to trigger a hydrolytic cleavage either on its own scissile bond or on that from a neighbouring pVP2 molecule (**Fig. 15**).

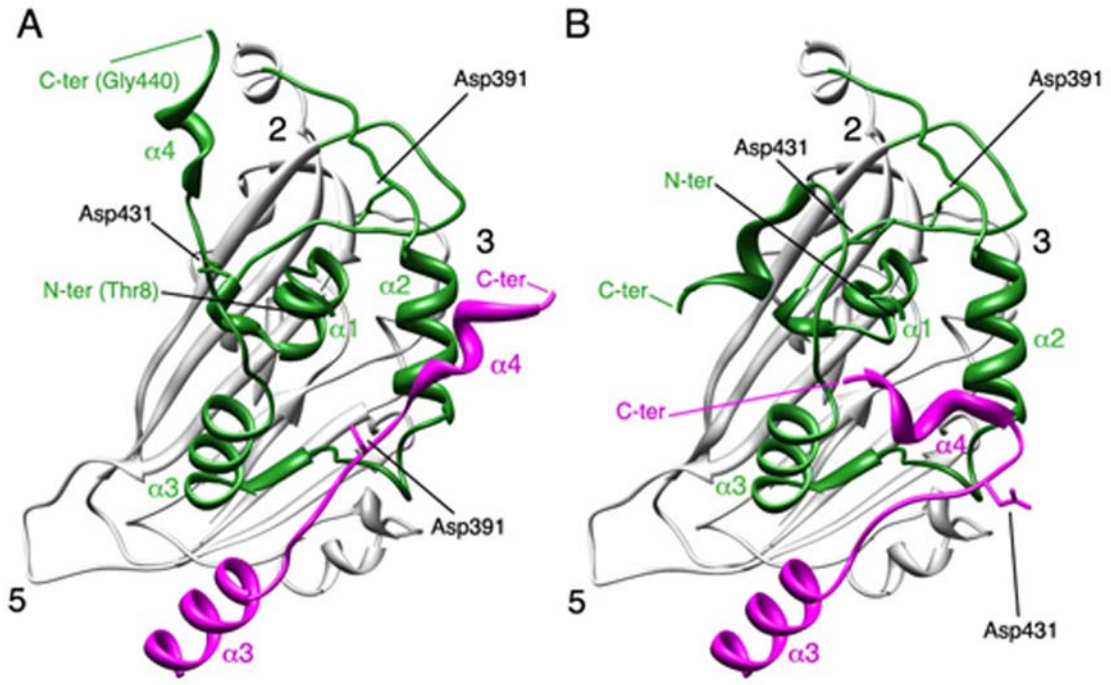


**Fig. 15**. **Conformational flexibility of VP2 C-terminal α-helix around its cleavage site**. (**A**) Bottom view, facing the inner surface of the viral capsid, of the VP2 protein X-ray model (PDB entry 2GSY). α-helices (1-4) of domain B (green) are indicated for a VP2 chain; the candidate catalytic residues Asp-391 and Asp-431 are also indicated. α3 and α4 helices of the closer neighbouring VP2 chain (magenta) that projects towards the three-fold axis of the trimer are shown and, to simplify the view, only its Asp-391 residue is indicated. The locations of five-fold, three-fold, and two-fold axes of icosahedral symmetry are indicated (**B**) Same as panel A, but the C-terminal α4 helices of VP2 chains were remodelled after fitting the X-ray model into an equivalent cryo-electron microscopy map (Luque et al., 2007).

Furthermore, some indirect evidences suggest that a maturation and rearrangement process may be required similar to noda- and tetravirus for the correct IBDV assembly. The IBDV polyprotein expressed by an inducible rVV provided an excellent framework to analyze IBDV maturation. The use of this system allows the accumulation of pVP2 and VP2, and the efficient assembly of VLP, structurally undistinguishable from IBDV virions at 72hp.i., whereas at 48 hp.i the expression of

rVV/Poly only collapsed structures can be recovered when is purified by the same purification protocol; although biochemical analysis of purified fractions by WB and Coomassie staining, at different post-infection hours are similar (Fig. 16) (Caston, 2008; Lombardo et al., 1999).

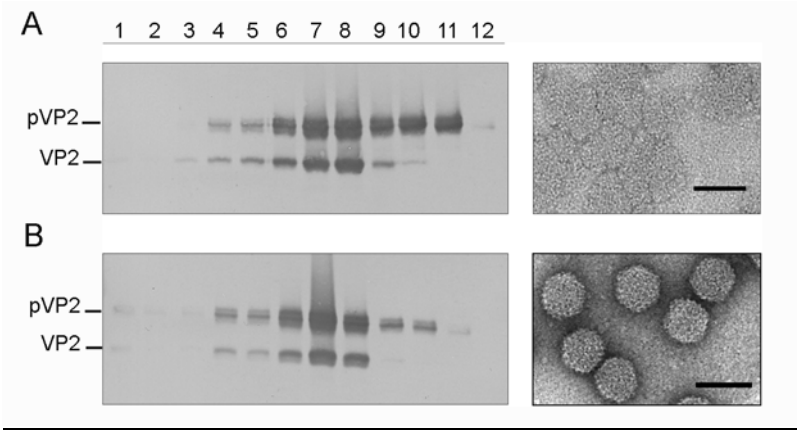


**Fig. 16. Maturation intermediates** (**A**) VT7/Poly at 48 hp.i. assemblies were purified by ultracentrifugation on sucrose gradients. Gradients were collected into 12 fractions, concentrated by ultracentrifugation, and analyzed by SDSPAGE and Western blot using anti-VP2. The direction of sedimentation was right to left, with fraction 12 representing the gradient top. The image shown on the right corresponds to a representative electron microscopy micrograph (negative staining) of partially collapsed structures present at middle fractions. (B) VT7/Poly at 72 hp.i. assemblies were analyzed as described above. The image shown on the right corresponds to a representative electron microscopy micrograph (negative staining) of T=13 capsid like structures in the middle fractions. Bars=100 nm.

### 4.2.2. Effect of mutations on VP2 Asp-431 and Asp-391

(p)VP2 residues D391 and D431 appeared to be likely candidates to trigger a nucleophilic attack on the pVP2 441-442 scissile bond. Two single-point mutant versions of the IBDV polyprotein gene were generated and used to construct the corresponding rVV, called VT7LacOI/D431N and VT7LacOI/D391N, respectively, in which Asp residues under study were replaced by Asn residues. Cultures infected with these two rVV were harvested at different times postinfection (pi, 24, 48, and 72 h), and the corresponding extracts analyzed by Western blot using VP2-specific serum. As a control for this experiment, cultures were also infected with VT7LacOI/POLY, a rVV expressing the wild-type polyprotein gene (Lombardo et al., 1999).

Although expression of wild-type and D391N polyproteins led to accumulation of both pVP2 and VP2 polypeptides, samples from cells expressing polyprotein D431N

showed equivalent pVP2 levels but did not contain detectable VP2 (**Fig. 17A**). These results, strongly suggesting that the D431N substitution specifically abrogates pVP2 proteolytic processing, were further confirmed using an alternative experimental approach. QM7 cells were infected with the three described rVV and, at 19 h pi, the cultures were metabolically labelled with [$^{35}$S] methionine for 1h. Thereafter, cultures were extensively washed and incubated with fresh medium supplemented with an excess of cold methionine. At different times postlabeling (0, 24, 48 and 72 h), cells were harvested, and the corresponding extracts subjected to IP using anti-VP2 antiserum. The results of this analysis (**Fig. 17B**) demonstrate that whilst in cells infected with VT7LacOI/POLY and VT7LacOI/D391N-infected cells, the pVP2 polypeptide is progressively processed to mature VP2, the pVP2 polypeptide encoded by VT7LacOI/D431N remains intact for the duration of the experiment (72 h after its synthesis). Taken together, these results demonstrate that the conservative D431N substitution causes a complete blockade on pVP2→VP2 proteolytic maturation.

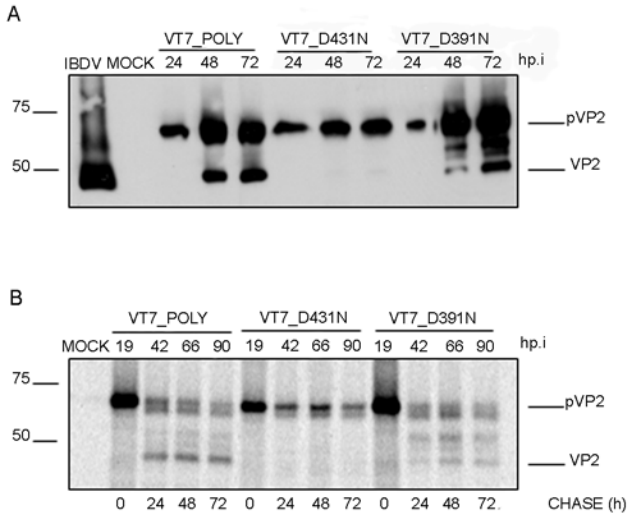


**Fig. 17**. **Effect of conservative mutations of residues Asp-431 and Asp-391 on pVP2/VP2 proteolytic maturation.** (**A**) Western blot analysis of proteins expressed in cells infected with rVV VT7LacOI/POLY, VT7LacOI/D431N or VT7LacOI/D391N, respectively. Infected cultures were harvested at 24, 48 and 72 h pi, respectively. The corresponding extracts were subjected to SDS-PAGE and Western blot using anti-VP2 serum. (**B**) QM7 cells infected with rVV VT7LacOI/POLY, VT7LacOI/D431N or VT7LacOI/D391N were metabolically pulse-labelled with [$^{35}$S]Met for 1h at 19 h pi. The radioactivity was chased with by adding fresh medium containing an excess of cold methionine. Cultures were harvested at 0, 24, 48 and 72 h post-labelling, and the corresponding extracts immunoprecipitated using anti-VP2 serum. The resulting samples were subjected to SDS-PAGE followed by autoradiography. Molecular weight markers (expressed in kDa, left) and bands corresponding to proteins pVP2 and VP2 (right) are indicated.

### 4.2.3. Decrease of IBDV infectivity by D431N substitution

In view of the results described above, it was important to assess the relevance of the D431 on IBDV infectivity. This analysis was carried out using a reverse genetics approach using plasmids pT7_SA_Rz and B pT7_SB_Rz containing the cDNA sequences corresponding to IBDV segments A and B, respectively, and plasmid pT7_SA/D431N_Rz, harbouring a mutant version of segment A containing the D431N substitution.

The results obtained demonstrate that the D431N substitution completely abolishes the production of an infectious IBDV progeny (**Table 7**). Western blot analysis indicated that cells transfected with plasmids pT7_SA/D431N_Rz and pT7_SB_Rz, and infected with a rVV expressing the T7 polymerase, failed to trigger the assembly of infectious IBDV. This finding, in agreement with the observations described above, highlights the critical importance of the VP2 D431N residue on IBDV infectivity.

**Table 7**. Virus titres obtained by reverse genetics.

| Coinfections | Virus titres (pfu/ml) | | |
|---|---|---|---|
| | First round | Second round | Third round |
| pT7-SA-Rz/ pT7-SB-Rz | $1.3\pm0.5x10^2$ | $9.0\pm1.3x10^4$ | $6.0\pm1.5x10^7$ |
| pT7-SA(D431N)-Rz/ pT7-SB-Rz | 0 | 0 | 0 |

### 4.2.4. pVP2 an intramolecular proteolytic processing

To get a better understanding of the pVP2 maturation mechanism, it was important to determine whether the pVP2→VP2 cleavage is the result of an intra- (*cis*-cleavage) or intermolecular (*trans*-cleavage) event.

To discriminate between these two possibilities, a polyprotein mutant containing an intact D431 residue but resistant to self-proteolytic processing was required. Such mutant would be used for co-expression analysis with the polyprotein D431N mutant to provide the pVP2→VP2 proteolytic activity in *trans*. With this aim, three polyprotein

genes, containing one or two amino acid substitutions affecting either one or both amino acid at the pVP2 scissile bond (Ala-441-Phe-442), were generated. The mutant genes contain the following substitutions: i)A441G; ii) F442G; and iii) A441G/F442G.

Mutant genes were then inserted within the VV genome giving rise to rVV VT7LacOI/A441G, VT7LacOI/F442G and VT7LacOI/A441G/F442G, respectively. The effect of the described mutations on pVP2 processing was analyzed by Western blot and pulse-chase/IP analysis. As shown in **Fig. 18**, whilst single substitutions cause a major but partial pVP2→VP2 blockade, the double mutation, A441G/F442G, completely abolishes pVP2 processing. Accordingly, this mutant gene was selected for subsequent experiments.

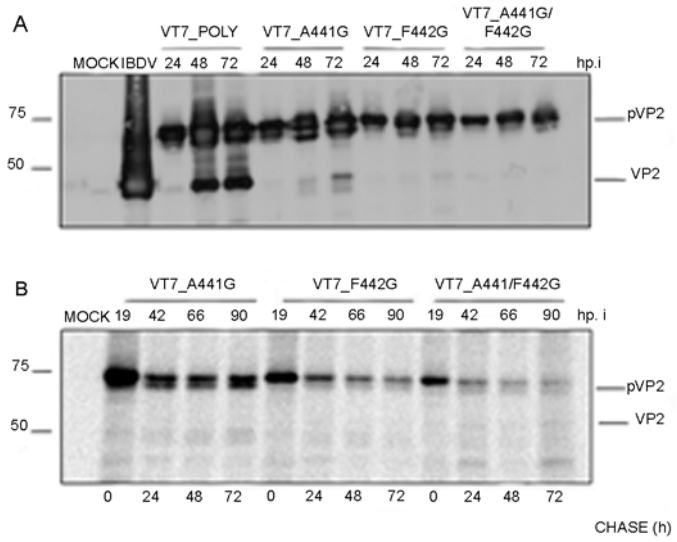


**Fig. 18**. **Analysis of the pVP2 cleavage site Ala 441-Phe 442**. (**A**) Western blot analysis of proteins expressed in cells infected with rVV VT7LacOI/POLY, VT7LacOI/A441G, VT7LacOI/F442G and VT7LacOI/A441G/F442G, respectively. Infected cultures were harvested at 24, 48 and 72 h pi. (**B**) QM7 cells were infected with different recombinants VT7LacOI/A441G, VT7LacOI/F442G or VT7LacOI/A441G/F442G were pulse-labelled with [$^{35}$S] Met for 1h at 19 h pi. The radioactivity was chased with by adding with fresh medium containing an excess of cold methionine. Cultures were harvested at 0, 24, 48 and 72 h post-labeling, and the corresponding extracts immunoprecipitated using anti-VP2 serum. The resulting samples were subjected to SDS-PAGE followed by autoradiography. Molecular weight markers (expressed in kDa, left) and bands corresponding to proteins pVP2 and VP2 (right) are indicated.

Next, cells were coinfected with VT7LacOI/POLY and VT7LacOI/D431N, VT7LacOI/POLY and VT7LacOI/A441G/F442G, or VT7LacOI/D431N and VT7LacOI/A441G/F442G. Cultures were harvested at 48 and 72 h pi, and the

corresponding extracts analyzed by Western blot. As shown in **Fig. 19**, the presence of mature VP2 was exclusively detected in samples from cells expressing the wt polyprotein gene that provides both the catalytic D431 residue and the intact cleavage site. Coinfection with VT7LacOI/D431N and VT7LacOI/A441G/F442G showed that pVP2-D431N remains uncleaved and is not proteolytically processed in *trans* by the wild-type pVP2, thus strongly suggesting that pVP2 processing is the result of a monomolecular *cis*-cleavage reaction.

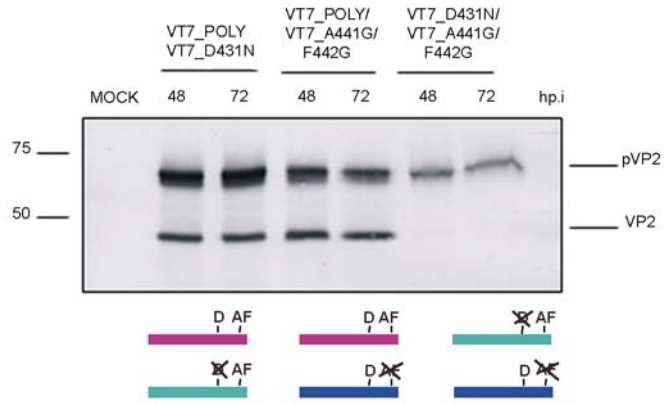


**Fig. 19**. **pVP2 intramolecular proteolytic processing**. Western blot analysis of proteins expressed in QM7 cells coinfected with VT7LacOI/POLY and VT7LacOI/D431N, VT7LacOI/POLY and VT7LacOI/A441G/F442G, or VT7LacOI/A441G/F442G and VT7LacOI/D431N, respectively. Infected cultures were harvested at 48 and 72 h pi, re4spectively. A scheme indicating the combinations of rVV used in this experiment (mutated positions are crossed out) is shown at the bottom.

## 4.3.Implication of the catalytic D431 in viral assembly

### 4.3.1. Influence of pVP2→VP2 maturation blockade on assembly of IBDV-particles

IPNV morphogenesis involves the assembly of provirions containing a high proportion of pVP2 molecules. Provirion maturation appears to be associated to pVP2 proteolytic processing (Villanueva et al., 2004). Hence, it seemed feasible that blocking pVP2→VP2 processing might favor the accumulation and isolation of IBDV provirions. To test this possibility, QM7 cultures were infected with VT7LacOI/POLY or VT7LacOI/D431N, respectively. Expression of the IBDV polyprotein in avian cells using an inducible rVV results in the accumulation of abundant levels of VLP with

similar size and shape to those of authentic IBDV particles (Lombardo et al., 1999). Remarkably, the assemblies produced with the rBV system in insect cells were nevertheless structurally varied, and in general, the formation of IBDV-like particles was rather inefficient. Insect cells might, therefore, have an important cellular factor(s) that interferes negatively with VLP assembly (*e.g.* cellular proteins and/or host environment). Cultures harvested at two different times (36 and 72 h pi), and the corresponding extracts used for the isolation of IBDV derived assemblies using a sucrose gradient-based purification protocol followed by electron microscopy and Western blot analyses of the collected fractions. As described previously, extracts from cells infected with the rVV expressing the wild-type polyprotein gene contained abundant icosahedral VLPs with a relatively high VP2/pVP2 ratio (Lombardo et al., 1999). In contrast, no IBDV-derived assemblies were detected in samples from VT7LacOI/ D431N-infected cells.

The use of gentler extraction conditions and/or alternative purification protocols yielded similar results. The same results were observed with extracts from cells infected with the three rVVs expressing polyprotein genes containing mutations on the pVP2 cleavage site described above (data not shown).

### 4.3.2. The assembly of D431N VP2 trimers

VP2 trimers constitute the building block of the IBDV-related icosahedral capsids with different triangulation numbers (T) as well as different tubular structures with helical symmetry (Luque et al., 2007; Saugar et al., 2005). Therefore, it seemed likely that the results described above might be caused by a deficiency on trimer assembly induced by a putative VP2 conformational change generated as a result of the D431N mutation. Such conformational change might prevent both the assembly of IBDV provirions and the subsequent pVP2 proteolytic processing event.

Expression of chimerical VP2 genes in insect cells leads to the spontaneous assembly of T=1 SVP, built by 20 VP2 trimers arranged into pentamers (Caston et al., 2001; Coulibaly et al., 2005; Lee et al., 2006). We have exploited this system to determine the effect of the D431N mutation on the assembly of VP2 trimers. A VP2 gene with the N-terminal 452 residues harbouring the D431N substitution was generated, VP2-452_D431N, inserted into the pFastBac1 transfer vector, and then used

to generate the corresponding recombinant baculovirus (rBV), rBV/VP2-452_D431N. Extracts from cells infected with rBV/VP2-452_D431N were used for SVP purification. As shown in **Fig. 20**, expression of the VP2-452D431N gene results in the assembly of T=1 SVP undistinguishable under electron microscopy from those assembled by wild-type protein.

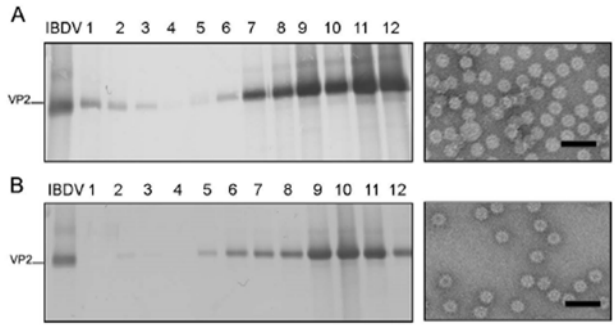


**Fig. 20**. **VP2 with the D431N substitution assembles as T=1 subviral particleVP2 trimers**. **(A**) Wild type VP2-452 SVP were purified by ultracentrifugation on sucrose gradients. Gradients were collected into 12 fractions, concentrated by ultracentrifugation, and analyzed by SDS-PAGE and Western blot using anti- VP2 serum. The direction of sedimentation was right to left, with fraction 12 representing the gradient top. The image shown on the right corresponds to a representative electron microscopy micrograph (negative staining) of wild-type SVP, present at the upper gradient fractions. (**B**) Mutant VP2-452-D431N assemblies were analyzed as described above. The image shown on the right corresponds to a representative electron microscopy micrograph (negative staining) of mutant VP2-452-D431N SVP present at the upper gradient fractions. Bars=100 nm.

The possibility nevertheless existed that the mutation D431N might somehow affect the formation of VP2 hexamers formed by VP2 trimers. To analyze this possibility we took advantage of a previous observation. We have shown that expression of VP2 long forms in a rBV expression system leads to the assembly of tubular structures formed exclusively by hexamers built by pVP2 intermediate precursor trimers (Caston et al., 2001; Saugar et al., 2005). Therefore, the D431N gene was subcloned into pFB/VP2-501, and the resulting plasmid, pFB/VP2-501_D431N, used to generate the corresponding rBV. As shown in **Fig. 21**, expression of VP2-501_D431N in insect cells results in the assembly of rigid tubules with an identical morphology to that of tubules purified from cells expressing wild-type VP2-501 gene. The results of this series of experiments demonstrate that the D431N substitution does prevent neither trimer assembly nor the subsequent formation of pentamers and hexamers.

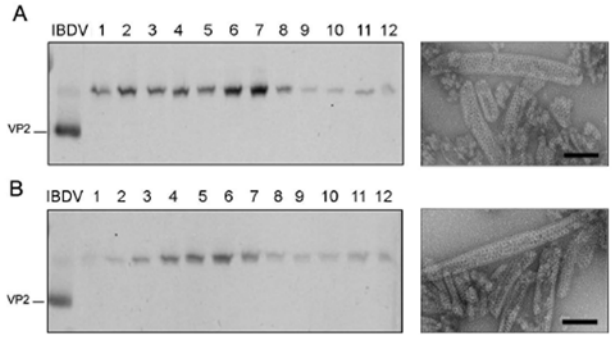


**Fig. 21. pVP2 variant with the D431N substitution assembles as tubular assemblies with hexagonal symmetry**. (**A**) Wild type pVP2-501 assemblies were purified by ultracentrifugation on sucrose gradients. Gradients were collected into 12 fractions, concentrated by ultracentrifugation, and analyzed by SDSPAGE and Western blot using anti-VP2 serum. The direction of sedimentation was right to left, with fraction 12 representing the gradient top. The image shown on the right corresponds to a representative electron microscopy micrograph (negative staining) of wild-type tubular structures present at the lower fractions. (**B**) Mutant pVP2-501-D431N assemblies were analyzed as described above. The image shown on the right corresponds to a representative electron microscopy micrograph (negative staining) of pVP2-501-D431N rigid tubules at the lower fractions. Bars=100 nm.

Finally, to rule out the possibility that the D431N substitution might induce conformational changes on the VP2 polypeptide undetectable by electron microscopy, the crystal structure of VP2-452_D431N-derived SVP was determined at 3.1 Å resolution. The root mean square deviation (rmsd) of the superimposition of all 428 equivalent C-α atoms from VP2, in the structures of native and D431N SVP is 0.20 Å, showing that these structures are essentially identical in conformation. This similarity is also maintained within the flexible linker, between helices α3 and α4 (residues 428-435), containing the D431N mutation (**Fig. 22**).

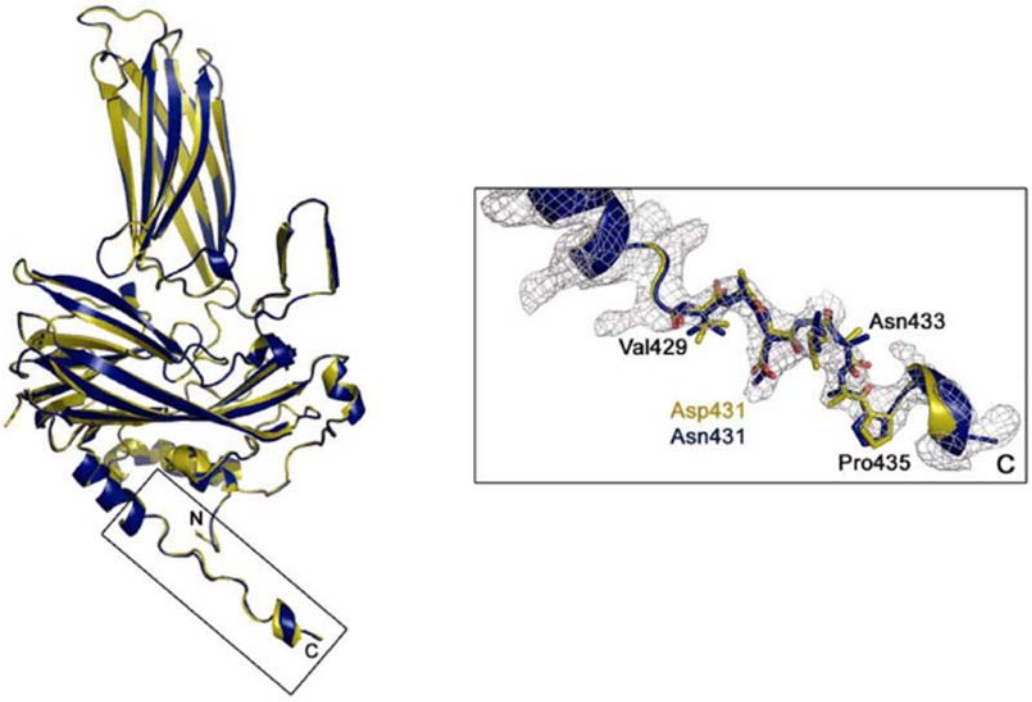


**Fig. 22. Structure of the VP2 D431N T=1 SVP monomer**. Ribbon diagrams of wild-type (yellow) and mutant D431N (blue) VP2 proteins. The superposition was performed using all the 428 residues of both molecules. On the right, electron density map of the VP2 C-terminal boxed region around residue Asp431. Residues from Val429 to Pro435 are shown as sticks and explicitly labelled every two residues.

### 4.3.3. D431N substitution in the context of HT-VP2-466 chimeric protein

The point mutation in the catalytic residue Asp-431 prevents T=13 VLP formation, although this change allows the correct assembly of VP2 pentamers and hexamers. To rule out the possibility that this might be due to a putative blockade of an interaction with another viral protein, the D431N mutation was placed in the HT-VP2-466 construct previously described system (Saugar et al., 2005). The expression of this wild-type recombinant yields efficient T=13 VLP (**Fig. 23A**) by the interaction of the His tag with the C-terminal of VP2. Unexpectedly, the results obtained with the HT-VP2-466-D431N shows that the formation of T=13 VLP is prevented whilst the only structure that could be rescued were small capsids similar to T=1 SVPs (**Fig. 23B**).

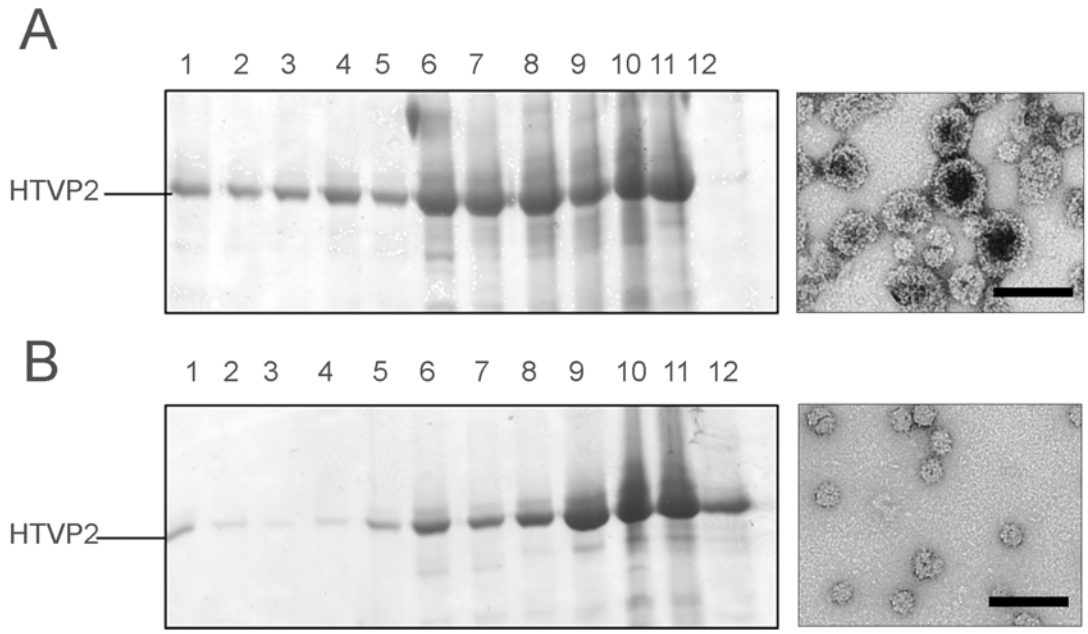


**Fig. 23**. **D431N substitution in the context of HT-VP2-466 chimeric protein**. **(A)** Wild type HTVP2-466 assemblies were purified by ultracentrifugation on sucrose gradients. Gradients were collected into 12 fractions, concentrated by ultracentrifugation, and analyzed by SDS-PAGE and Coomassie staining. The direction of sedimentation was right to left, with fraction 12 representing the gradient top. The image shown on the right corresponds to a representative electron microscopy micrograph (negative staining) of wild-type HTVP2-466 capsids, present at the middle and the top gradient fractions. (**B**) Mutant HTVP2-466-D431N assemblies were analyzed as described above. The image shown on the right corresponds to a representative electron microscopy micrograph (negative staining) of the upper fractions. Bars = 100 nm.

In an attempt to explain this observation, Asp-431, in addition to its proteolytic role, should be involved in other aspects that preclude T=13 particle assembly.

## 4.4.The role of a cellular protease

### 4.4.1. The VP2-452 intermediate is required for IBDV correct assembly

Polyprotein expression in insect cells with rBV vectors leads to an extremely inefficient VLP assembly (Chevalier et al., 2002; Martinez-Torrecuadrada et al., 2000). In particular, the use of IBDV polyprotein-derived rBVs results in the exclusive assembly of large tubule-like structures formed by hexamers of pVP2 trimers (Da Costa et al., 2002; Martinez-Torrecuadrada et al., 2000) identical to type I tubules isolated from IBDV-infected cells.

IBDV capsid is composed of pentamers and hexamers of (p) VP2 coat protein trimers; hexamers are provided by rBV/Poly, the other component necessary for a theoretical assembly of a VLP is the finding of a donor for pentamers. As previously described, short forms of VP2 spontaneously assemble into SVP, composed exclusively by pentameric units. Thus, it was rationalized that coinfections of rBV/Poly and rBV expressing short forms of VP2, i.e. VP2-441 (Saugar et al., 2005) or VP2-452, could eventually yield T=13 VLP. Additionally, the use of different short forms of VP2 could provide information about the requirement of the VP2 amphiphatic α-helix for T=13 capsid assembly.

We carried out different infections and coinfections in insect cells rBV/Poly, rBV/Poly and rBV/VP2-452, rBV/Poly and rBV/VP2-441. Extracts were harvested at 48hp.i and subjected to purification by sucrose gradient and ultracentrifugation and the resulting assemblies were analyzed. The infection with a rBV that express the wild-type Poly leads to the accumulation of particulated material in the bottom part of the gradient corresponding to large tubes (**Fig. 24A**). The coinfection of this rBV/Poly and the rBV/VP2-441 allows the detection of structures along the gradient. The bottom fractions contain tubular elements and in the upper fractions T=1 capsids. The middle fractions, where T=13 VLP are expected to migrate, T=1 SVP aggregations are observed, due to the sticky characteristic of VP2 P domain (**Fig. 24B**). On the other hand, the coinfection of rBV/Poly with a rBV/VP2-452 allows the accumulation of tubules, T=1 capsids, and in the middle fractions the presence of T=13 VLP. Not only the 452-VP2 form can be detected in these fractions, but also the VP2-441 form showing that these capsids were correctly processed because they could render the mature form of VP2. Also, it should be noticed that two different VP3 forms could be detected (**Fig. 24C**, framed in a red square). Polyprotein expression in insect cells leads to the accumulation of two VP3 species with different electrophoretic mobilities: a 29-kDa product, which is the wild type protein; and a truncated 27-kDa product, produced by proteolytic cleavage at the C-terminal end of the protein, probably generated by a cellular protease(s) (Maraver et al., 2003). In our results, there is a high amount of VP3 wild type accumulation probably because it has been protected from the cellular proteases by after encapsidation.

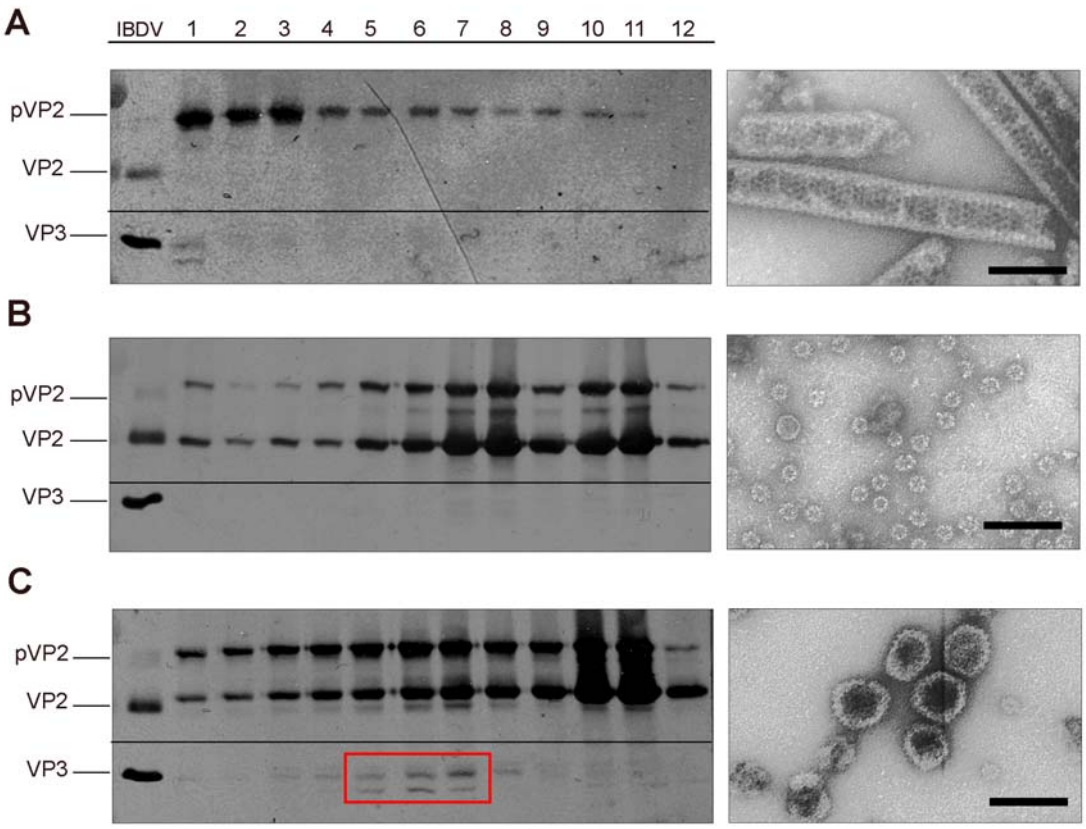


**Fig. 24**. **VP2-452 form is required for IBDV correct assembly.** (**A**) Wild type rBV/POLY assemblies were purified by ultracentrifugation on sucrose gradients. Gradients were collected into 12 fractions, concentrated by ultracentrifugation, and analyzed by SDSPAGE and Western blot using anti-VP2 and anti-VP3 serum. The direction of sedimentation was right to left, with fraction 12 representing the gradient top. The image shown on the right corresponds to a representative electron microscopy micrograph (negative staining) of wild-type tubular structures present at the lower fractions. (**B**) Coinfection rBV/POLY and rBV/VP2-441 and (**C**) coinfection rBV/POLY and rBV/VP2-452 assemblies were analyzed as described above. The image shown on the right corresponds to a representative electron microscopy micrograph (negative staining) of the middle fractions. Bars=100 nm.

Some previous results obtained in our laboratory, in which the Arg-452 and Arg-453 of VP2 were replaced by alanine residues in a rVV expressing the polyprotein (**Fig. 25A**) shows that Arg-452 residue is essential for VP2 assembly, as it can be observed by confocal analysis, where VP2 and VP3 are not interacting with themselves and any recognizable structure is visualized (**Fig. 25B**). Whereas the mutation of Arg-453 leads to the assembly of large tubules, in which VP2 and VP3 are colocalizing, but any viroplasmatic structure is detected (**Fig. 25B**).

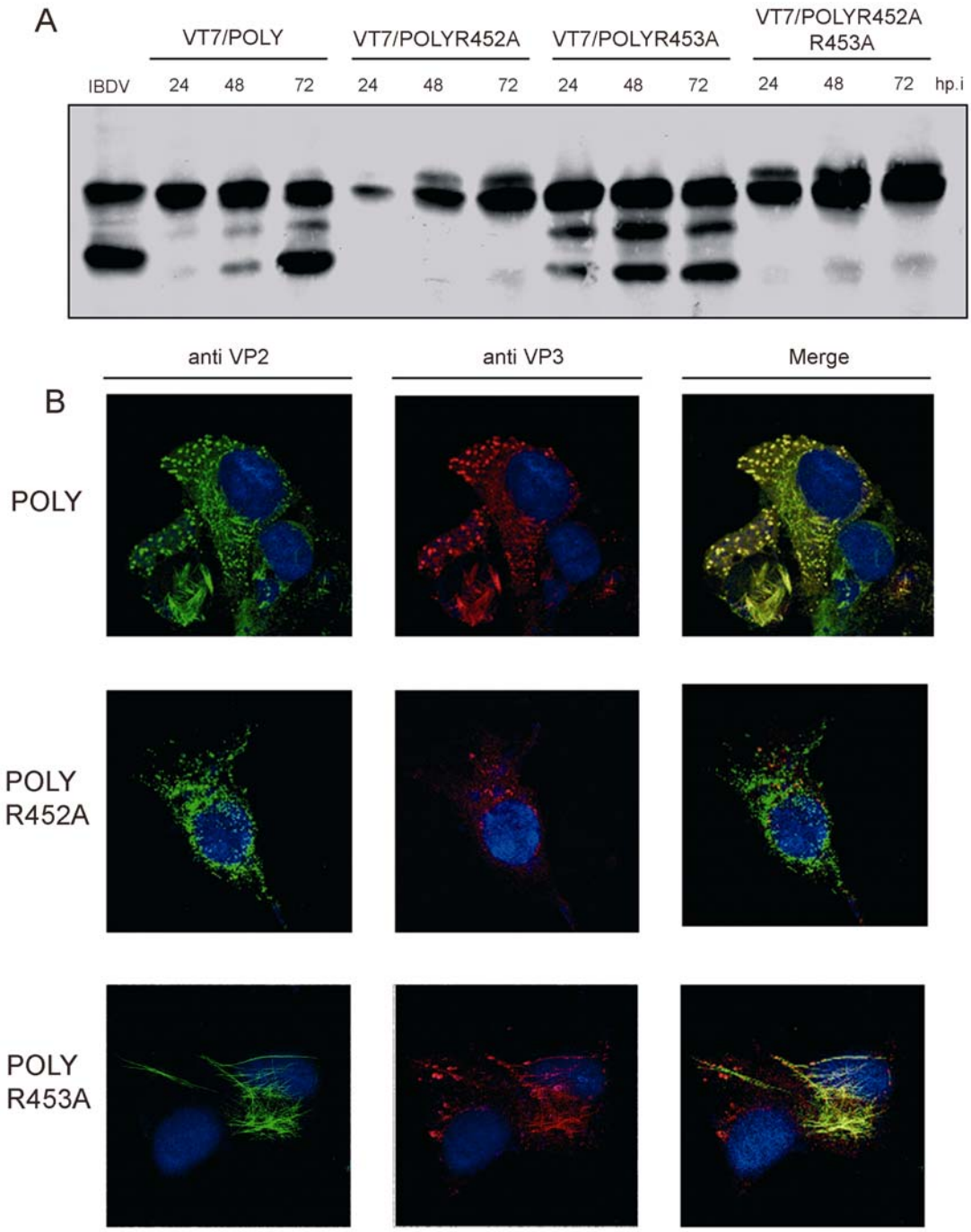


**Fig. 25**. **The presence of an intermediate band.** (**A**) Western blot analysis of VP2 expressed in BSC-40 cells infected with the different rVV mutants: VT7/POLY, VT7/POLYR452A, VT7/POLYR453A and VT7/POLYR452AR453A. Infected cultures were harvested at 24, 48 and 72 h.pi. (**B**) Digital confocal images of BSC-40 cells infected with three different rVVs. At 48 hp.i, cells were fixed and incubated with rabbit anti-VP2 and rat anti-VP3 followed by incubation with goat anti-rabbit immunoglobulin coupled to Alexa-488 (green) and goat anti-rat immunoglobulin coupled to Alexa-594 (red).

These results strongly suggest that the presence of VP2-452 forms in the viral capsid are essential for the correct T=13 assembly, probably conforming the capsid pentamers and by its interaction with the scaffolding protein VP3.

A band migrating between pVP2 (512aa) and VP2 (441aa) can be observed in SDS-PAGE (**Fig. 26**), when QM7 cell extracts are analyzed after having been infected with IBDV at 48 hp.i. Furthermore, this band is specifically recognized by anti-VP2 serum and co-migrates with the band corresponding to the (VP2 452aa) form, suggesting that the mature virion could eventually contain small amounts of this VP2 molecular form.

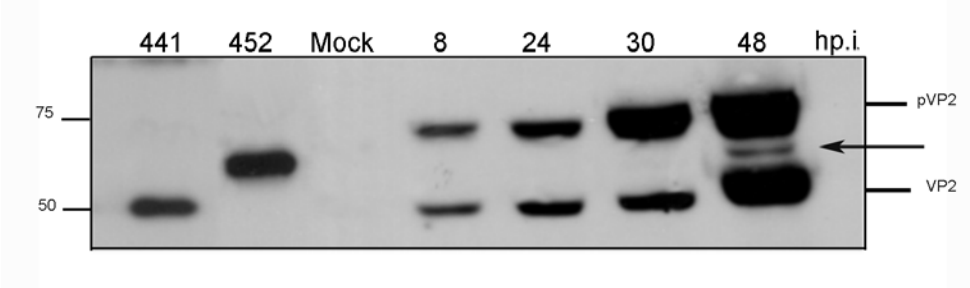


**Fig. 26**. **The presence of an intermediate band**. Western blot analysis of VP2 expressed in QM7 cells infected with IBDV. Infected cultures were harvested at 8, 12, 24, 30 and 48 h. pi. Bands corresponding to VP2-441aa and VP2-452aa are also shown. The intermediate band is indicated by an arrow. Molecular weight markers (expressed in kDa, left) and bands corresponding to proteins pVP2 and VP2 (right) are indicated.

## 4.4.2. Searching for the VP2-452 origin

Although the presence of a VP2-452 form is necessary for the correct assembly of the T=13 capsid in the context of rBV, the origin of this VP2 form remains unclear. Whereas the viral protease VP4 has as catalytic targets at alanine dipeptides (Sanchez and Rodriguez, 1999), the autocatalytic residue Asp-431 is also excluded since its scissile bond is located in the Ala-441-Phe-442. As no more viral protease activities have been reported, we thought about the possibility of a cellular protease involved in the cleavage of the Arg-452-Arg-453 dipeptide. To ascertain whether possible candidates were described in the literature, we scanned the Merops protease database (Sanger Institute UK) (Rawlings et al., 2008). A list of candidates is shown in **Table 8**. The cytosol alanylaminopeptidase, also known as puromycin sensitive aminopeptidase (PSA), was selected for further studies. PSA was first described in *Gallus gallus* when

full length cDNAs from chicken bursal lymphocytes were analyzed. Interestingly, these bursal lymphocytes are the cell target of IBDV (Caldwell et al., 2005).

**Table 8**. Several candidates as cellular proteases.

| **Protease name:** | **Cleavage site:** |
|---|---|
| 1.Trypsin 1 | Peptide Arg+ Arg Peptide |
| 2.Cathepsin L | Peptide Arg+ Arg Peptide |
| 3.Trytase beta | Peptide Arg+ Arg Peptide |
| 4.Kallikrein 1 | Peptide Arg+ Arg Peptide |
| 5.Thrombin | Peptide Arg+ Arg Peptide |
| 6.Plasmin | Peptide Arg+ Arg Peptide |
| 7.Lactoferrin | Peptide Arg+ Arg Peptide |
| 8.Intestinal Arg-specific endopeptidase | Peptide Arg+ Arg Peptide |
| 9.Puromycin sensitive aminopeptidase (PSA) | Arg+ Arg |

PSA is an ubiquitous 100 kDa, $Zn^{+2}$ metallopeptidase. It has been proposed that plays a role in a number of essential cellular processes including neuropeptides metabolism (Hersh and McKelvy, 1981; Hersh et al., 1980), processing of antigenic peptides for presentation on MHC Class I molecules (Stoltze et al., 2000) and hydrolysis of proteasomal products (Botbol and Scornik, 1983; Saric et al., 2004). This protease exhibits a broad specifity against various N-terminal residues with some preference for basic and hydrophobic amino acids (Constam et al., 1995; Johnson and Hersh, 1990; Stoltze et al., 2000).

### 4.4.3. Determination of the presence of the PSA in different IBDV- susceptible cell lines

We first determined the presence of the PSA in different cell lines routinely used in the laboratory that support correct T=13 capsid assembly. For the detection of mRNAs of PSA, primers were designed against highly conserved regions of this protein, determined by the alignment of PSA sequence from *Homo sapiens sapiens*, *Pan troglodytes* and *Gallus gallus* (**Fig. 27A**).

RNA from different cell lines was extracted. Different cell lines tested were: **DT40** cells (bursal lymphocytes as positive control); **DF1** cells (chicken fibroblasts);

**QM7** (quail muscle cells); **BSC 40** (green monkey kidney epithelial cells) as susceptible to allow the correct assembly of the capsid and **H5** insect cells as a possible candidate for a negative control since VLPs assembly is highly inefficient. cDNAs were generated by reverse transcription with random primers and a later PCR was set up with the conserved region primers. This analysis showed that the mRNAs corresponding to PSA were present in all the cell lines in which IBDV can correctly assemble apart from H5 insect cells (**Fig. 27B**).

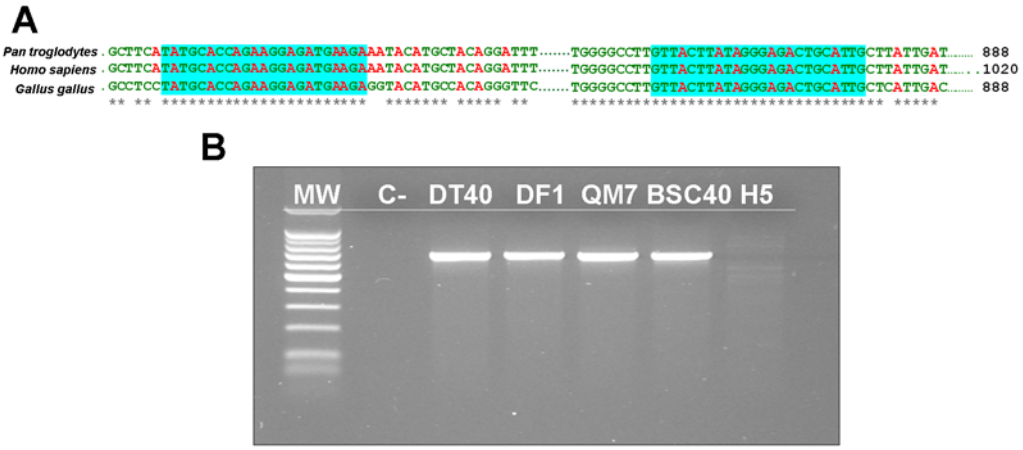


**Fig. 27. Determination of the presence of PSA in different cell lines**. (**A**) Alignment of the DNA sequence of PSA of three different organisms (*Pan troglodytes* accession number, NC-006484, *Homo sapiens* accession number AJ132583 and *Gallus gallus* accession number AJ851657). Highlighted in blue highly conserved domains used for oligonucleotides design. (**B**) Agarose gel of the PCR to determine the presence or absence of the cellular protease in different cell lines, DT40, DF1, QM7, BSC-40 and H5, respectively. As molecular weight marker 1-kb ladder.

### 4.4.4. Coexpression of PSA in H5 insect cells and its implication in VLP assembly

PSA can not be detected in H5 insect cells. To analyze its function when it is expressed in insect cells, a new rBV was generated (rBV/PSA). To clone the protease, DT40 cDNA was amplified by flanking primers in a PCR reaction and then inserted in a pFastBac vector which expressed a His tag. This would allow detecting the protein by immunological techniques and its ulterior purification if necessary.

H5 insect cells were infected with a rBV/Poly and by immunofluorescence analysis at 48 hp.i, a tubular pattern of VP2 coat protein is observed (**Fig. 28A**). When H5 are coinfected with rBV/Poly and rBV/PSA, the distribution of VP2 becomes more diffuse similar to the typical pattern exhibited when viroplasms are formed (Ona et al.,

2004), suggesting that the coat protein is not completely assembled in tubes (**Fig. 28B**). These assembles were purified by sucrose gradient and ultracentrifugation at 72 hp.i and different fractions obtained were analyzed by WB and electron microscopy. The comparison of biochemical patterns observed in the purification of IBDV-derived structures of rBV/Poly or the co-infection rBV/Poly-rBV/PSA revealed some differences. Whilst with rBV/Poly infection, the particulated material, exclusively composed by pVP2, is accumulated in the bottom part of the gradient (**Fig. 28C**); in the coinfection rBV/Poly and rBV/PSA, the mature form of VP2 (VP2-441) and a non-truncated VP3 specimen can be detected in the middle fractions suggesting the presence of capsids(**Fig. 28D**). By electron microscopy differences are more noticeable, structures observed with rBV/Poly, as expected, are pVP2 rigid tubes with an hexagonal lattice (**Fig. 28C**), whereas in middle fractions of the co-infection rBV/Poly-rBV/PSA some particles with a size and morphology similar to genuine T=13 virion particles can be purify, although some of them are partially collapsed probably due to its fragility (**Fig. 28D**).

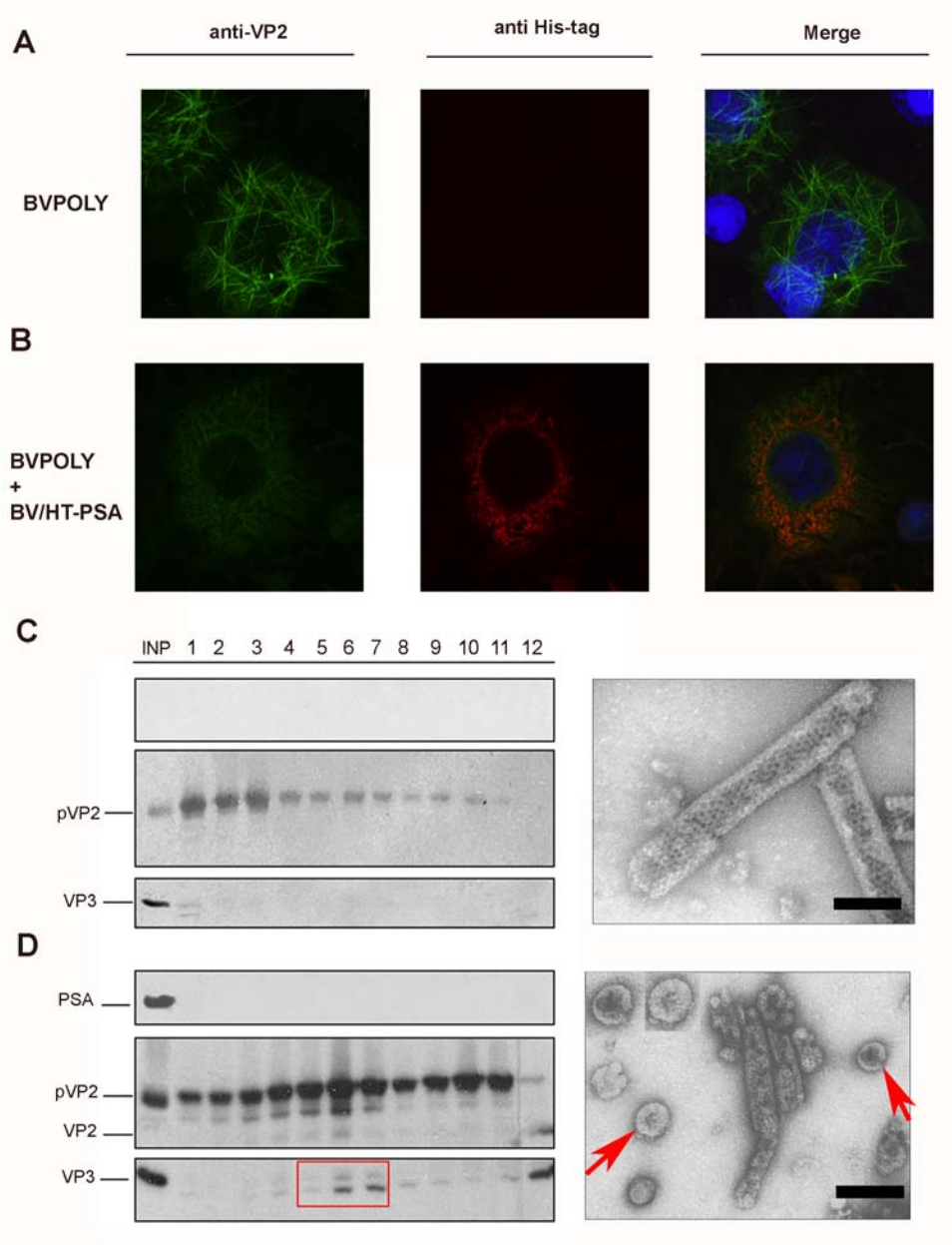


**Fig. 28. Implication of PSA in IBDV capsid assembly when is expressed in H5 insect cells. (A and B)** Digital confocal images of H5 cells infected with two different rBVs. At 48 hp.i, cells were fixed and incubated with rabbit anti-VP2 and mouse anti-His tag followed by incubation with goat anti-rabbit immunoglobulin coupled to Alexa-488 (green) and goat anti-mouse immunoglobulin coupled to Alexa-594 (red). (**A**). H5 insect cells infected with rBV/Poly and (**B**) H5 insect cells infected with rBV/Poly and rBV/HT-PSA. (**C**) Wild type rBV/POLY assemblies were purified by ultracentrifugation on sucrose gradients. Gradients were collected into 12 fractions, concentrated by ultracentrifugation, and analyzed by SDSPAGE and Western blot using anti-His tag, anti-VP2 and anti-VP3 serum. The direction of sedimentation was right to left, with fraction 12 representing the gradient top. The image shown on the right corresponds to a representative electron microscopy micrograph (negative staining) of wild-type tubular structures present at the lower fractions. (**D**) Coinfection of rBV/POLY and rBV/His tag-PSA; the image shown on the right corresponds to a representative electron microscopy of the middle fractions, where VLP purified are shown with an arrow. VP3 recovered inside the capsids are squared in red

Furthermore, to confirm the target of this cellular protease at the Arg-452-Arg-453, different mutants in the polyprotein gene were carried out. Arg-452 or Arg-453 was mutated to Ala residues. Insect cells were infected with the corresponding rBV/Poly R452A and rBV/PolyR453A Cultures harvested at 72hp.i, and the corresponding extracts used for the isolation of IBDV derived assemblies using a sucrose-gradient purification protocol. Any particulated material was recovered from rBV/PolyR452A infection. rBV/PolyR453A biochemical analysis shows a similar pattern to rBV/Poly, i.e., rigid tubules indistinguishable from rBV/Poly ones are observed by electron microscopy and confocal analysis (**Fig. 29A and 29C**). Coinfection of rBV/PolyR453A with rBV/PSA prevents the formation of capsid like structures. The biochemical pattern does not change regarding the non-protease added, and by electron microscopy and immunofluorescence analysis only large tubular structures are visualized (**Fig. 29B and 29D**).

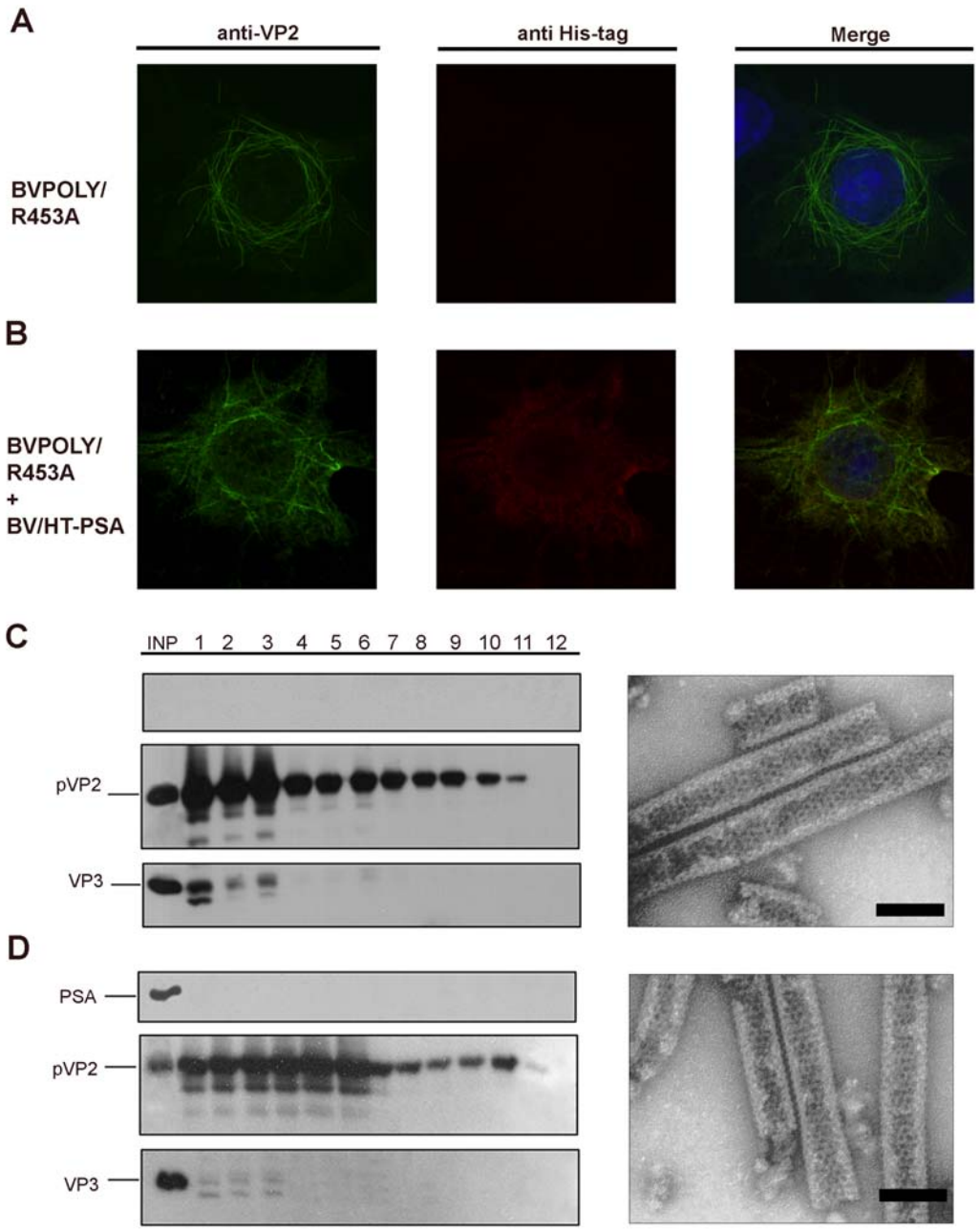


**Fig. 29. Implication of PSA in IBDV capsid assembly when is expressed in H5 insect cells. (A and B)** Digital confocal images of H5 cells infected with two different rBVs. At 48 hp.i, cells were fixed and incubated with rabbit anti-VP2 and mouse anti-His tag followed by incubation with goat anti-rabbit immunoglobulin coupled to Alexa-488 (green) and goat anti-mouse immunoglobulin coupled to Alexa-594 (red). (**A**). H5 insect cells infected with rBV/PolyR453A and (**B**) H5 insect cells infected with rBV/PolyR453A and rBV/HT-PSA. (**C**) rBV/PolyR453A assemblies were purified by ultracentrifugation on sucrose gradients. Gradients were collected into 12 fractions, concentrated by ultracentrifugation, and analyzed by SDSPAGE and Western blot using anti-His tag, anti-VP2 and anti-VP3 serum. The direction of sedimentation was right to left, with fraction 12 representing the gradient top. The image shown on the right corresponds to a representative electron microscopy micrograph (negative staining) of tubular structures present at the lower fractions. (**D**)Coinfection of rBV/POLYR453A and rBV/His tag-PSA.

These results suggest that the formation of T=13 VLP can be rescued in the baculovirus system, when PSA cellular protease, naturally absent in these cells, is expressed. There is also strong evidence, although a structural change is not excluded, that the cleavage site of the PSA cellular protease are the basic residues, Arg-452-Arg-453.

### 4.4.5. The role of the cellular protease in viral infection context

#### 4.4.5.1. Silencing of PSA in DF1 cells

To analyze the influence of the PSA in the context of IBDV real infection, some silencing experiments were carried out in DF1 cells (chicken fibroblasts). Four different retroviruses were generated, three of them with a sequence of short hairpin RNA (shRNA) susceptible to be cleaved by siRNA induced silencing complex (RISC complex), called DF1-sh1, DF1-sh2 and DF1-sh3, and an empty vector used as a positive control for the cellular protease, referred as DF1 control cells. Retroviruses used in this study contain a puromycin resistance gene. Thus stably silenced cells were established by the addition of the antibiotic to the media. To quantify the inhibitory effect of the shRNAs, a quantitative real time PCR (qRT PCR) with specific primers for the cellular protease was performed. As an internal control, the gen coding for the glyceraldehyde-3-phosphate dehydrogenase (GAPDH) of *Gallus gallus* was used.

As observed in **Fig. 30**, the inhibitory effect of siRNAs ranged near 90% in DF1-sh1 and DF1-sh3, whereas the amount of GAPDH is maintained in a constant level in all cell lines.

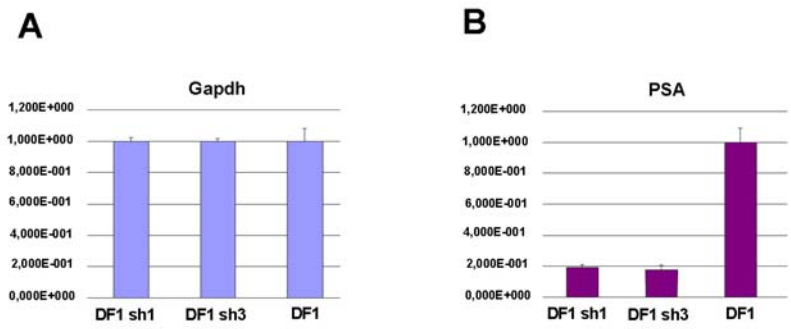


**Fig. 30**. **Silencing of PSA in DF1 cells.** Quantitative real time PCR (qRT PCR) to quantify the inhibitory effect of shRNAs in silenced cells (DF1-control, DF1-sh1 and DF1-sh3) for PSA. Bars have been scaled to a maximum of one and error deviations are also shown for each one. (**A**) Quantification by qRT PCR of the amount of GAPDH cDNA for each cell line. (**B**) Quantification by qRT PCR of the amount of PSA for silenced cells.

### 4.4.5.2. Effect of silencing in IBDV infection

Silenced cell lines were infected with IBDV at MOI 0.05 pfu/cell. At 30 hp.i cells were fixed and analyzed by immunofluorescence with an anti-VP2 antiserum. All DF1-control cells are infected, showing a characteristic viroplasmatic pattern in their cytoplasm (**Fig. 31**). In contrast with DF1-control cells, a small amount of DF1-sh1 and DF1-sh3 cells are susceptible to be infected by IBDV (**Fig. 31**).

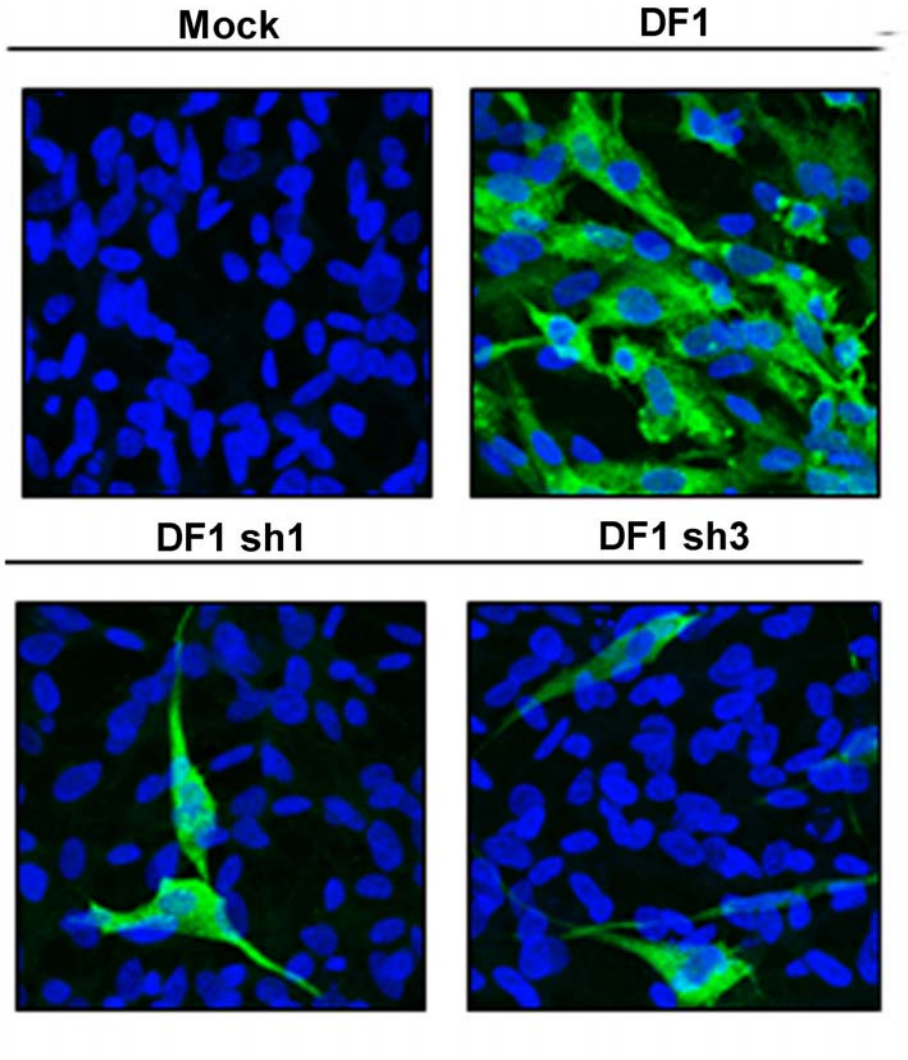


**Fig. 31**. **Effect of silencing in IBDV infection**. Digital confocal images of silenced cells infected with IBDV. At 30hp.i, cells were fixed and incubated with rabbit anti-VP2 followed by incubation with goat anti-rabbit immunoglobulin coupled to Alexa 488 (green).

At 48 hp.i silenced cells were infected with IBDV at MOI 0.05 pfu/cell, in the absence and presence of puromycin. Puromycin antibiotic has been described to be an inhibitor of PSA at low concentrations (Fidler et al., 1978). Cells were harvested and analyzed by Western Blot with an anti-VP2 antiserum. An accumulation of pVP2 and a prevention of the cleavage pVP2→VP2 can be observed in all infected silenced cells, probably because the coat protein has not been properly assembled in viral capsids (**Fig. 32**). This effect was more noticeable in the presence of puromycin (**Fig. 32**).

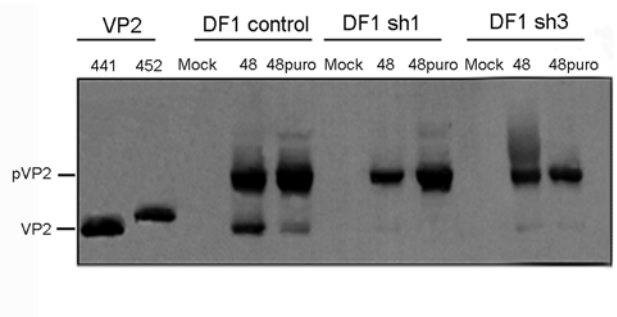


**Fig. 32**. **Effect of silencing in IBDV infection**. Western blot analysis of proteins using an anti-VP2 antiserum expressed in DF1 silenced cells infected with IBDV. Infected cultures were harvested at 48 h.pi in the absence and presence of puromycin (which is marked as puro).

To analyze the viability and production of IBDV virions in silenced cells. They were infected by IBDV, in the absence and presence of puromycin, at MOI 2 pfu/cells. The supernatant was collected at 12 hp.i and titrated by serial dilutions in QM7 cells. Viral titres were determined by an immunostaining assay against VP2 capsid protein. Viral titres reduction was dramatically high in DF1-sh1 and DF1-sh3 silenced cells, almost reaching a 90% (**Fig. 33**). It exists a clearly correlation between the silencing obtained by each cellular type and its capacity in viral production (**Fig. 33**). DF1-control cells were clearly affected by the addition of puromycin to the media, where viral titre was reduced to a half respect to the one obtained by DF1-control cells without antibiotic treatment.

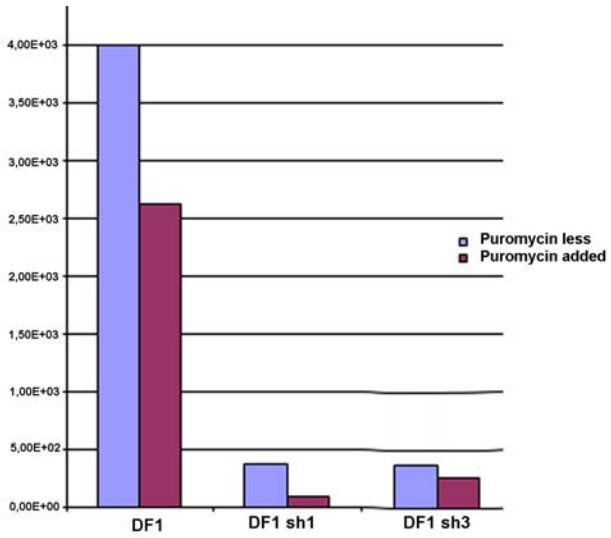


**Fig. 33**. **Effect of silencing in IBDV infection**: IBDV titration. Silenced cells were infected by IBDV in the absence or presence of puromycin. At 12hp.i supernatants were collected and titrated by serial dilutions in QM7 cells. Titres were determined by immunostaining and counting of plaque formation units. For each cell line bars in violet are for non-puromycin and in magenta for the addition of the antibiotic.

It seems that a previous cleavage of pVP2 by this cellular protease is required for a correct IBDV production. A drastic reduction of PSA, by silencing experiments prevents IBDV progeny in a 90%. As it has been previously suggested, the cleavage of pVP2 on Arg-452 would donate short forms of VP2 that could assembly spontaneously in pentamers. As they have not lose their amphiphatic α-helix yet, they could interact with VP3 conforming a first nucleation factor of the whole capsid by the addition of the hexamers of pVP2.

# DISCUSSION

## 5. INSIGHTS IN IBDV ASSEMBLY:

Structural polymorphism and transient conformations are common in multiprotein assemblies, such as those described during cyclic reactions of chaperones (Ranson et al., 2006), dynamic biomachines such as ribosomes (Mitra and Frank, 2006), spliceosomes (Stark and Luhrmann, 2006), and virus capsid assembly and maturation (Steven et al., 2005). Structural studies have provided some clues as to how capsid proteins determine the conformation that they must adopt (Abrescia et al., 2004), although the underlying mechanism is not yet fully understood.

The viral capsid structures provide a paradigm in the analysis of non-equivalent interactions among identical subunits. Structural polymorphism, together with the extensive use of symmetry, is an example of nature's efficient use of limited coding capacity (Harrison, 2001). We have analyzed the molecular basis of the conformational polymorphism of the IBDV coat protein VP2. IBDV has a single T=13 *levo* capsid (Böttcher et al., 1997; Coulibaly et al., 2005; Saugar et al., 2005) formed by 260 VP2 trimers, making 12 pentamers and 120 hexamers. The IBDV capsid is a fully quasi-equivalent shell built of a single protein. From strict geometric considerations, VP2 trimers adopt five distinct conformations (**a-e**) (**Fig. 34**). A number of T=13 capsids have been described for different dsRNA viruses.

VP2 is synthesized as part of a large polyprotein (ca. 110 kDa) that is cotranslationally self-cleaved releasing three polypeptides, namely pVP2 (the VP2 precursor), VP4 (the protease), and VP3 (a polypeptide with scaffolding activity among others). pVP2 (512 residues, 54,4 kDa) undergoes subsequent processing events mediated by VP4 at three secondary targets (positions 487, 494 and 501) (Sanchez and Rodriguez, 1999). The resulting intermediates are further cleaved twice between Arg452-Arg453 and Ala441-Phe442, probably in this order, to yield VP2 (47 kDa). The released C-terminal peptides (accounting for 7.4 kDa) remain inside the capsid (Da Costa et al., 2002) and appear to be involved in the entry mechanism by promoting the disruption of host cell membranes (Galloux et al., 2007). Here, we have also shed light on how these two late processing events occur, which are performed by a viral and, probably, by a cellular protease, respectively.

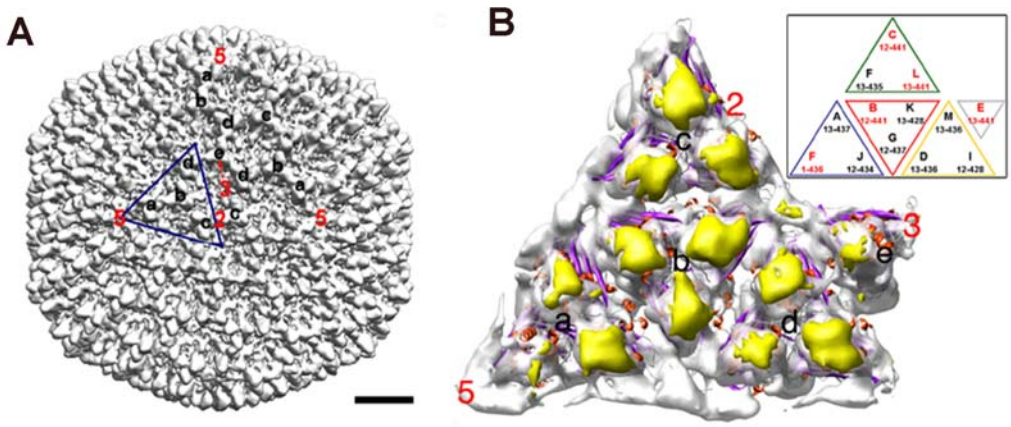


**Fig. 34**. **Fit of the IBDV X-ray model into the virion cryo-EM map**. (**A**) Complete capsid virion (white), rendered at ~10 Å. The five VP2 trimer types are indicated by letters a to e; the blue triangle indicates the limits of a G4 triangle. The locations of fivefold, threefold, and twofold axes are also indicated. Bar = 100 Å. (**B**) View from inside the capsid of the asymmetric unit X-ray model fitted into the corresponding region of the cryo-EM map. White surfaces show densities according to the X-ray model, displayed at a contour slightly lower than that of the cryo-EM map. Even at this threshold for the filtered atomic model, with P and S domains being well matched, the solid yellow densities correspond to empty cryo-EM virion densities; these densities probably arise from disordered VP2 N-terminal segments. A scheme of the asymmetric unit, seen from the inner surface, is shown in the inset. The first and last residues visible in the X-ray model are indicated for each of the 13 VP2 chains (A to M).

## 5.1. Conformational polymorphism of the IBDV major coat protein

Studies of the structures resulting from the expression of VP2 or pVP2 alone showed that VP2 spontaneously forms T=1 subviral particles (SVP), an all-pentamer capsid. In contrast pVP2 or intermediate pVP2 variants assemble into tubular structures with a hexagonal lattice (Caston et al., 2001). These IBDV-related structures are nevertheless formed by the same structural building block, (p)VP2 trimers. These results suggested that the inherent molecular switch controlling VP2 polymorphism resides in the temporally bound, 71-residue C-terminal sequence, which is removed when its function is completed. For this reason, no vestige remains in the mature capsid indicating how this event occurred. In addition, it has been shown that VP3 plays an essential role allowing pVP2 to acquire different conformations through its interaction with the pVP2 C-terminal end (Ona et al., 2004).

The role of the pVP2 C-terminal end was analyzed by generating a series of pVP2 C-terminal deletion mutants. These molecular forms were also expressed with a His tag bound covalently at their N-termini. Interestingly, some VP2 C-terminal deletions could correspond to naturally occurring intermediates involved in virus assembly (Saugar et al., 2005). The primary sequence, circular dichroism, and NMR analyses indicate that residues 443-GFKDIIRAIR-452 of pVP2 C-terminal domain, forms an amphiphilic α-helix. In the absence of VP3, efficient T=13 capsid-like assembly can be restored by the presence of a His tag at the VP2 N-terminus, suggesting that the His tag mimics VP3 function during virion assembly (Saugar et al., 2005). Comparative three-dimensional cryo-EM analyses of virions and chimeric His-tagged VP2 proteins (e.g., His-VP2-466 capsid) revealed that VP3 acts as a canonical scaffolding protein rather than as a permanent component of the mature capsid, and its function is successfully restored by the His tag. The pVP2 443-452 sequence is nearly identical to a *Lm*TIM amphipathic α-helix, whose hydrophobic side is buried, while leaving surface-exposed hydrophilic side-chains. The hydrophilic side of residues 443-452 is constituted of basic residues, although the same restrictions apply to the hydrophobic side of the VP2 peptide. Accordingly, this side would be buried by interaction with other VP2 region(s), although interactions with other protein(s) cannot be ruled out by the available data.

Furthermore, more additional functions have been attributed to the VP2 C-terminal domain. IBDV presents four characteristic structural peptides derived from pVP2CTD, termed pep46, pep7a, pep7b and pep11 and being 46,7,7 or 11 amino acids in length, respectively, associated to the virus particle (Da Costa et al., 2002) (**Fig. 35**). Pep46 deforms biological membranes, leading to the formation of pores. Its structure has been determined by NMR analysis (Galloux et al., 2007). In this peptide three different domains can be defined: a central hydrophobic domain flanked by two domains mainly constituted by both hydrophobic and charged residues. Whereas the N-terminal domain, is positively charged, where the amphiphatic α-helix is located, the C-terminal is somewhat negatively charged. The sequence similarity between pep46 of different IBDV strains and different birnaviruses is higher at the N-terminal than at the C-terminal domain, suggesting an important role for this α-helix in the viral cycle as it has been established during the present work. Moreover, the identification of the membrane-active domain of pep46 has been mapped within its first 15 residues, which

includes the amphiphatic α-helix until residue 452. Correlating the results that we have reported, point mutations in this region, using reverse genetics, Lys-445 and Arg-452 prevent the rescue of IBDV virus.

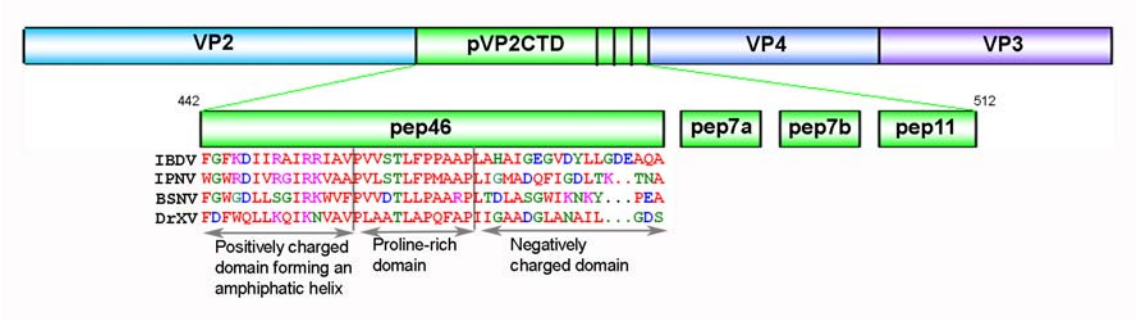


**Fig. 35**. IBDV polyprotein and the four structural peptides pep46, pep7a, pep7b, and pep11 derived from the C-terminal domain of pVP2, are represented. Numbering refers to the residue positions in the polyprotein. Hydrophobic residues are red, acidic in blue and basic in pink. The main characteristics of the pep46 domains are indicated.

## 5.2.Molecular switch and triggering factors

The distinct conformational states of capsid proteins may be controlled by flexible protein regions (loops, N- and C-termini), ds- or ssRNA, metal ions, pH, or combinations of these (Johnson, 1996). These factors, referred to as molecular switches, may be insufficient, especially when large T number capsids are considered, and might require one or more auxiliary proteins that acting as a molecular effectors (scaffold, minor capsid or enzymatic proteins) (Dokland, 2000). The presence of a His tag in different pVP2 variants is essential for assembly of genuine virus-like structures. His tag and VP3 sequence comparisons show that the last five residues in the VP3 C-terminal align with the similar His tag region. No other similarities are found, confirming the importance and uniqueness of this region. We have shown that the substitution of the His tag by the VP3 C-terminal domain also yields T=13 VLP indicating that the His tag is really emulating this VP3 region. Moreover, the deletion of the acid region (residues 11 to 25) in HT-VP2-466 prevents the VLP formation thus confirming the previous observations suggesting that the acidic segment of the VP3 C-terminal region was essential for correct capsid assembly. Hence, VP3 mutants with altered or deleted C-terminal residues (Chevalier et al., 2004), or entirely lacking the

last 13 residues (Maraver et al., 2003b) fail to assemble into T=13 capsids, and hexagonal tubular or aberrant assemblies are formed.

It is also noticeable, that both acidic segments in the His tag and the VP3 C-terminal residues are preceded by a basic segment that could also have an additional function. In the HT-VP2-466 construct, the deletion of the basic region, which includes all His residues, abolishes the T=13 VLP formation. This indicates that the basic region of VP3 C-terminal domain is necessary for the correct assembly of viral capsids. Moreover, point mutations in Arg residues of this basic region yields partially collapsed structures (VP3 Arg-245) or the production of a majority of T=7 capsids (VP3 Arg-242), reinforcing the importance of the VP3 basic region in virions.

Following these results, a charge complementarity between basic residues of the VP2 amphiphatic α-helix and the acid region of VP3 Ct domain could be necessary for the correct T=13 VLP assembly. In view of the alignment, it is tempting to suggest that electrostatic interactions may be the initial event in the adoption of different conformational states. Structural polymorphism might be achieved by electrostatic interactions between these two separate polypeptide elements that can be disengaged in the recombinant baculovirus system, with the HT-VP2-466 and CtVP3-VP2-466 gene. It has been established that an electrostatic interaction is established between VP2 Arg-449 and VP3 Asp-254 and a possible interaction between VP2 Lys-445 and VP3 Asp-252.

We postulate that this electrostatic interaction is transmitted to the rest of VP2, inducing the correct conformational change. Similar changes have been described at atomic detail for the allosteric regulation of integrins, which transmit conformational changes after activation by ligand binding (Xiao et al., 2004). We are currently focused on modifications of the His tag and the proposed counterpart to obtain new VP2 chimerical proteins able to successfully assemble T=13 shells with higher efficiency.

In addition, a possible electrostatic interaction between the basic region of VP3 C-terminal domain and the acid domain of pVP2 C-terminal domain corresponding to helix-α6 (Galloux et al., 2007) can not be ruled out at this point.

It is nonetheless intriguing that VP3 stoichiometry inside the virion remains constant at ~600 copies, in our purifications and those of others (Dobos et al., 1979). A plausible reason may be its temporal stabilizing role, carried out by a non-icosahedral but regular scaffold structure (Zandi et al., 2004; Zlotnick, 2004), capable of maintaining an unstable capsid made up of 780 (p)VP2 copies, i.e., a procapsid-like assembly.

## 5.3. Proteolytic processing of the capsid protein precursor

The progressive processing of pVP2 seems to avoid the natural tendency of mature VP2 to assemble into all-pentameric T=1 SVP. An effective assembly pathway that avoids the dominance of aberrant assemblies would be provided by a post-assembly maturation step, in which virions are initially assembled as a procapsid that matures through structural transitions. Biochemical studies of IPNV, a closely related birnavirus, showed the existence of a provirion (Villanueva et al., 2004) that matures by pVP2 processing.

Post assembly maturation has been described for noda- and tetraviruses, which assemble as provirions with a T=3 (Schneemann et al., 1998) and T=4 (Canady et al., 2000) lattice composed of a single α-protein, respectively. Provirion maturation is relatively slow, and takes place through the autocatalytic cleavage of the α-protein (Zlotnick et al., 1994), mediated by a single acidic residue. This yields the mature CP β–protein and the γ-peptide, and leads to the rearrangement of the capsid subunits. Considering the functional links (Ahlquist, 2005), and the unexpectedly high structural similarity between the CP of IBDV and noda- and tetravirus (Coulibaly et al., 2005), as well as their similarities in the assembly pathway, it was postulated that VP2 autoproteolysis is the final processing event rendering the mature VP2 protein. Based on the VP2 X-ray structure, we examined the role of two likely candidate residues, Asp-391 and Asp-431, for catalyzing the last proteolytic event that occurs during capsid maturation. These residues were selected taking into account the existing structural similarities of domains S and B CP from IBDV, noda- and tetraviruses (**Fig. 36**).

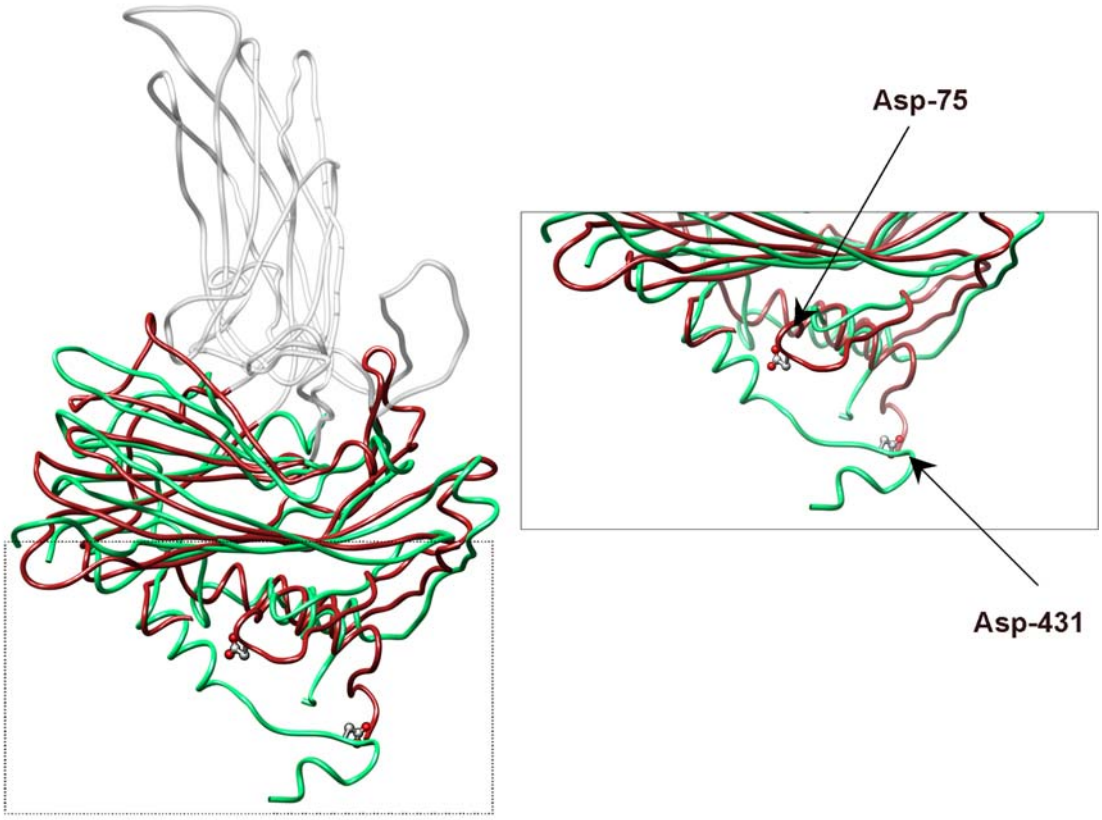


**Fig. 36. Structural relationships between capsid proteins of (+) ssRNA and dsRNA viruses.** Structural comparison of the crystallographic structure of protein β of FHV, a nodavirus (PDB 2Q26) (coloured in red), with VP2 of IBDV (PDB 2GSY) (coloured in green). Autoproteolytic residues are marked in balls and spheres, Asp-75 for FHV and Asp-431 for IBDV, as it can be observed both residues, although lacking of a sequence similarity, posses a similar localization in the S domain of the CP.

Our results indicate that the D431N mutation blocks the pVP2→VP2 proteolytic trimming and affects the assembly of stable IBDV particles. Assembly of VLPs with the proper size and morphology, i.e. the T=13 capsid, was not detected in cells expressing the polyprotein gene harbouring the D431N mutation. Expression of pVP2 intermediate polypeptides carrying the D431N point mutation nonetheless leads to the assembly of either as pentameric (T=1 SVP), or tubular structures with a hexagonal lattice. The isolation of these assembly products excluded a possible misfolding of the polypeptide since they are built by the same structural block, VP2 trimers (Saugar et al., 2005). The crystal structure of the mutant D431N VP2 protein provides additional experimental evidence supporting this interpretation. Similarly, mutations on the scissile bond Ala-441-Phe-442 yielded no production of particles. Furthermore, combinations of VP2 polypeptides containing mutations affecting either the scissile bond or the catalytic site

revealed that pVP2 proteolytic processing is the result of a monomolecular *cis*-cleavage reaction, similar to that previously described for the nodavirus CP (Zlotnick et al., 1994). Moreover, reverse genetics analyses demonstrate that pVP2 self-processing is essential for the assembly of an infectious IBDV progeny (Chevalier et al., 2002).

In this context, it is easily envisioned how the D431N mutation is not only unable to cleavage the Ala-441-Phe-442 scissile bond, but also might preclude or alter the interaction of VP3 with the helical region of VP2 at the inner basement of the VP2 S domain. Furthermore, we believe that the interaction of the VP3 C-terminal segment with the pVP2 amphipathic α-helix might be necessary to temporally inhibit the last proteolytic event since, probably being the Asp-431 blocked by one or more basic residues of the Ct domain of VP3 until the icosahedral capsid has been correctly assembled. Moreover, it can not be discarded that an activation of Asp-431 promoted by the VP3 basic environment, may be required for its autocatalytic function.

It should be also pointed out that CP, which ensures the successful propagation of viral genomes by sheltering them from a hostile environment, and guiding them through the interaction with specific cell receptors, in their journey to reach an appropriate milieu for a successful replication process, can also play other important roles. In addition to the Asp- or Glu-based proteolytic activities associated to birna-, noda- and tetravirus, other CP such that of Semliki Forest virus, an enveloped (+ss) RNA virus, exhibits a self-cleaving serine protease activity (Morillas et al., 2008). Enzymatic activities associated to CP, in most known examples found in fully assembled virus particles, are not exclusively restricted to protease activities. The CP of Leishmania RNA virus, a dsRNA virus that persistently infects the parasitic protozoan *Leishmania*, possesses a site specific RNA endoribonuclease activity that cleaves viral positive-sense RNA (MacBeth and Patterson, 1995a, MacBeth and Patterson, 1995b). L-A virus, another dsRNA virus that infects the yeast *Saccharomyces cerevisiae*, has a CP that removes the m7GMP caps from host cellular mRNAs and covalently attaches them to a His residue on the capsid outer surface (Blanc et al., 1994; Tang et al., 2005). Unfortunately, the lack of specific sequence consensus motifs complicates the search for CP-associated enzymatic activities.

## 5.4. IBDV assembly model

Results from our group indicate that the amphipathic α-helix is bound to the flexible VP2 C-terminal end (Luque et al., 2007). In the IBDV assembly model the spatial conformation of the (p) VP2 C-terminal region defines whether a pentamer or a hexamer is formed.

### 5.4.1. Pentamer assembly

Although SVP pentamer assembly is independent from other viral components, the corresponding virion capsid pentamers are built in a more physiological context, and additional factors must be considered. Comparison of almost identical pentamers from the various structures analyzed (T=1, T=7 and T=13 capsids of VP2 and chimeric VP2 monomers, (Caston et al., 2001; Luque et al., 2007; Saugar et al., 2005) suggests that the relatively large pVP2 C-terminal domain would interfere with the five-fold contacts. The structure of the T=13 His-VP2-466 capsid indicates that the VP2 C-terminal domain is processed sufficiently to allow contacts for those VP2 chains at the five-fold axis. In virion assembly, this rapid processing would preclude (or release) the VP3 interaction, resulting in α-helical bundle formation.

This is reminiscent of basic concepts from the well-established nodavirus assembly system (Schneemann et al., 1998b). The different lattice geometry (T=13 versus T=3), together with increased complexity, indicates a more sophisticated assembly pathway for IBDV. The nodavirus capsid is formed by 60 trimers, and the CP forms two different contacts: (i) those related by icosahedral twofold symmetry axes form 60 flat contacts with a 180° dihedral angle, and (ii) those related by quasi-twofold symmetry axes form 120 bent contacts with a 144° dihedral angle. Flat contacts are due primarily to insertion of an ordered RNA duplex and, to a lesser extent, to the presence of an ordered N-terminal peptide arm in the groove between subunits (Fisher and Johnson, 1993). Kinetic studies suggested that 120 bent subunits are cleaved at a higher rate than the remaining 60 flat subunits (Gallagher and Rueckert, 1988). In the T=13 lattice, the contacts between VP2 trimers at the fivefold axis are similarly bent, with a dihedral angle of ~140° (**Fig. 37A and 37C**). Rapid processing would lead to helical

bundle formation that, once again, is similar to the pentameric helical bundle made by the γ-peptide in the nodavirus capsid (Cheng et al., 1994). In this model, VP2 pentamers could act as nucleating centres for capsid assembly after joining additional VP2 trimers with flat contacts (hexamers).

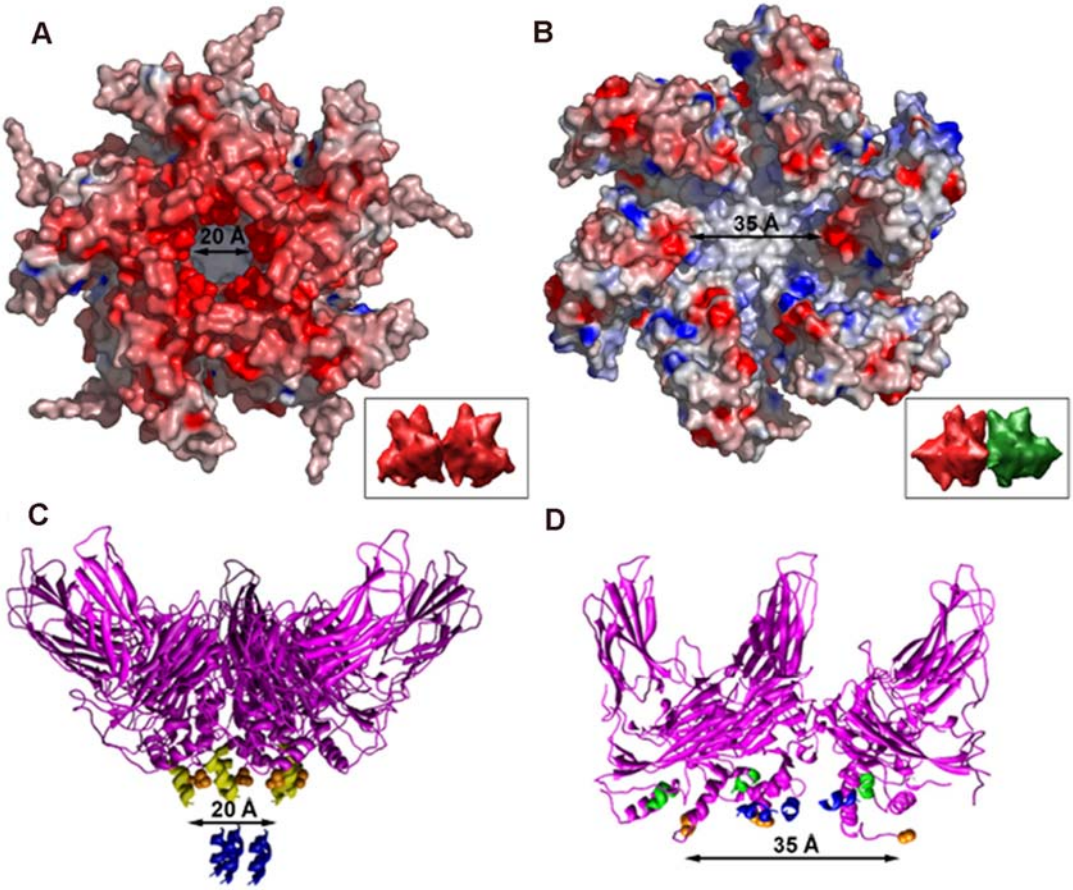


**Fig. 37**. **Structural conformations of pVP2 amphipathic α-helix**. (**A and B**) Inner surfaces of a pentamer (**A**) and a hexamer (**B**). Surfaces are represented with electrostatic potentials calculated with the GRASP program, showing the distributions of negative (red) and positive (blue) charges. Note the narrow channel (diameter,~20 Å) formed by five α−3 helices around the five-fold axis, in contrast with the broader channel at the quasi-six-fold axis (diameter,~35 Å). The insets indicate the two classes of contacts between adjacent VP2 trimers, namely, bent at the five-fold axis (two pentameric trimers in red) or flat at the local six-fold axis (a pentameric red trimer and a hexameric green trimer). (**C and D**) Side views of ribbon diagrams of a VP2 pentamer (**C**) and a hexamer (**D**). For simplicity, the hexamer front half has been removed. The amphipathic α-helices are shown in blue. VP2 chains are shown in magenta, except for the last visible C-terminal amino acid, which is represented as an orange sphere.

Our current hypothesis is that the VP2 molecular form required for the correct formation of pentamers is provided by the cleavage of VP2 between residues 452-453 by a cellular protease, the puromycin sensitive aminopeptidase (PSA). VP2-452 leads to an helical bundle formation by the amphiphatic α-helix in the pentameric axes. Finally, these amphiphatic helices would be partially removed when the correct capsid conformation has been set up as part of the maturation process. Some of the reminiscences of this process can be observed when an intermediate band of 452 amino acids can be detected in IBDV mature virions.

The necessity of these helical bundles in pentamers by amphiphatic α-helices 443-452 was shown when coinfections in insect cells with the rBV/Poly, as an hexamer donor, and the rBV/VP2-441, which provides pentamers, prevented the correct formation of T=13 capsid like structures; whereas with the rBV/VP2-452, IBDV VLPs were assembled.

Aditionally, the VP3 proteolytic degradation in insect cells (Maraver et al., 2003b) was prevented as the protein was interacting with VP2 and protected by its encapsidation. Although it has been reported that coexpression of VP1 prevents VP3 trimming and restores VLP formation in insect cells (Maraver et al., 2003a), as the formation of VP3-VP1 complexes (Lombardo et al., 1999) might hinder the VP3 cleavage site, and thus protect the VP3 C-terminal tail against proteolysis; the quantity of VLPs using this experimenta approach is less significant than that observed in cells coinfected with of rBV/Poly and rBV/VP2-452. It is also significant the absence of PSA RNA in H5 insect cells, where IBDV VLP formation is prevented when the polyprotein is expressed; suggesting the lack of this cellular protease in this cell line.

PSA is an ubiquitous 100 kDa, $Zn^{+2}$ metallopeptidase present at high concentrations in mammalian brain especially cerebellum; (Karsten et al., 2006) from which it was initially purified as an enkephalin-degrading aminopeptidase (Hersh et al., 1980). PSA exists primarily in soluble form in the cytosol and nucleus, but is also found in a membrane-bound form, and associated with the microtubule-spindle apparatus during mitosis (Constam et al., 1995). It has been proposed that it plays a role in a number of processes including neuropeptide metabolism (Hersh and McKelvy, 1981; Hersh et al., 1980), regulation of the cell cycle (Constam et al., 1995), processing of

antigenic peptides for presentation on MHC Class I molecules (Stoltze et al., 2000) and hydrolysis of proteasomal products (Botbol and Scornik, 1983; Saric et al., 2004). PSA exhibits a broad specifity against various N-terminal residues with some preference for basic and hydrophobic amino acids (Constam et al., 1995; Johnson and Hersh, 1990; Stoltze et al., 2000). Silencing of the *Caenorhabditis elegans* ortholog of PSA causes defects in embryogenesis and reproduction (Brooks et al., 2003). The homozygous PSA knockout mice show dwarfism and impairment of reproductive functions in both sexes (Osada et al., 2001a; Osada et al., 2001b). Interestingly, the PSA-deficient mice also show altered locomotor activity, increased anxiety and impaired response to pain (Osada et al., 1999). Perhaps these behavioural and neurological abnormalities are related to the failure to metabolize polyQ proteins by PSA (Bhutani et al., 2007), which when overproduced can be toxic.

Coinfections in H5 insect cells with rBV/Poly and rBV/PSA result in the recovery of T=13 VLP, suggesting that the polyprotein has a PSA-specific cleavage site in its sequence. When a mutant rBV/Poly was generated, in which Arg-453 was substituted by an Ala residue, PSA coexpression did not rescue VLP assembly, showing that the protease target must be this arginine dipeptide. Furthermore, the same mutation in the heterologous system of rVV, which leads to high production of VLPs, only yielded pVP2 type I tubules, suggesting that this residue is critical for proper pentamer assembly.

The role of PSA in the viral infection context was analyzed using a RNA interference approach, showing that PSA silencing in DF1 cells (chicken fibroblasts) dramatically reduces the viral production over 90% with a large accumulation of VP2 precursor (pVP2) forms.

It should be also noticed the endopeptidase PSA activity, which has always been described as an exopeptidase, acting against various N-terminal residues, with some preference for basic and hydrophobic amino acids (Constam et al., 1995; Johnson and Hersh, 1990; Stoltze et al., 2000). This is not the only peptidase that having been described as an exopeptidase can degrade proteins “from inside”. Some other examples like the tripeptidyl peptidase II (TPPII), a cytosolic subtilisin-like peptidase that exhibits enhanced activity in proteasome inhibitor-adapted cells and degrades polypeptides by

exo- as well as predominantly trypsin-like endoproteolytic cleavage (Geier et al., 1999; Wang et al., 2000) and aminopeptidase N (PepN), characterized as the sole alanine aminopeptidase in *Escherichia coli* (Chandu et al., 2003), have been found.

PepN is very efficient as an aminopeptidase in cleaving after alanine, leucine, tyrosine and phenylalanine. The cleavage of endopeptidase substrates by PepN was much slower than aminopeptidase substrates, revealing a preference for hydrophobic and basic residues. PepN belongs to the M1 family of metallopeptidases (Hooper, 1994; Rawlings and Barrett, 1995) and its homologues are ubiquitous and present in all kingdoms, as PSA (**Fig. 38**). PepN and its homologues possess the conserved exopeptidase, GXMEN motif (Vazeux et al., 1998) and three Zn2+- binding ligands present within the $HEXXHX_{18}E$ motif (Hooper, 1994; Rawlings and Barrett, 1995; Rudberg et al., 2002), which is the metallopeptidase one. Although the endopeptidase motif has not been determined yet, the deletion of 312 bp encompassing catalytically important residues in the M1 family disrupts endopeptidase activity.


**Fig. 38**. **Sequence alignment of the region harbouring the catalytically important residues from PepN *E.coli* and PSA *Gallus gallus***. Asterisks represent identical residues, whereas colons and single dots represent conserved and semi-conserved substitutions. Boxes highlight the exopeptidase motif (in green) and the M1 family metallopeptidase motif (in blue); the glutamate residue important in catalysis is also shown in blue. Gen Bank™ accession numbers of sequences are as follows: PepN, *E. coli* (M15273) and PSA, *Gallus gallus* (AJ851657).

As described above, the cleavage site of the cellular protease is Arg-452-Arg-453. This motif of dibasic amino acids in this position is highly conserved in all analyzed IBDV strains (**Fig. 39A**) as well as in different members of the *Birnaviridae*

family (**Fig. 39B**). This also suggests a kind of host dependence, as IBDV VLP are not correctly assembled in cell lines that are not susceptible to infection, as insect cells.

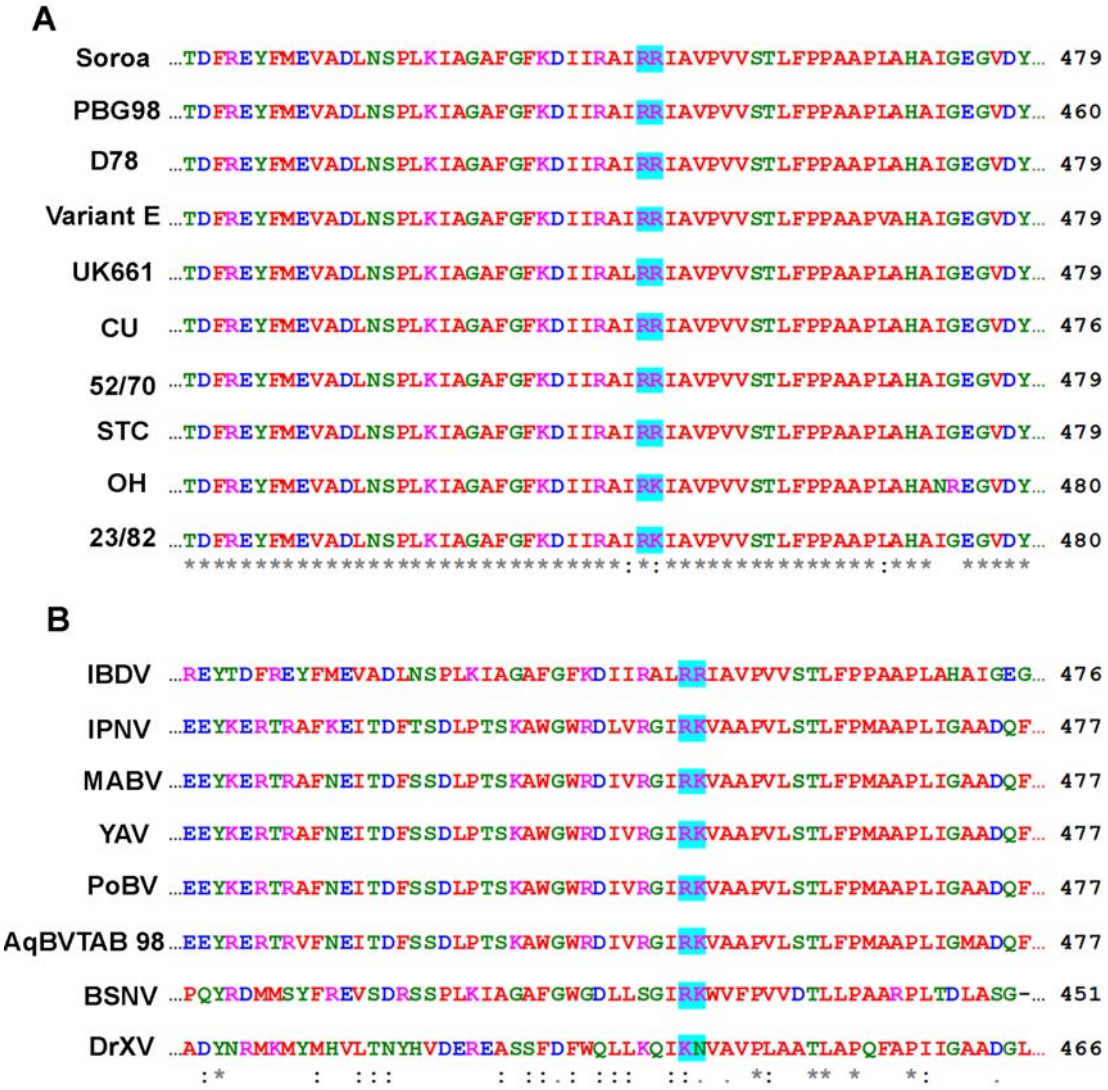


**Fig. 39**. **Sequence alignment of protein VP2 of the region harbouring the cleavage site of the cellular protease**. **A**. Alignment of different IBDV strains: Soroa (accession number AAD30136), PBG98 (BAA00741), D78 (AA015768), Variant E (AAD32617), UK661 (NP690838), CU (AAK51522), 52/70 (BAA00745), STC (BAA00391), OH (AAC55351), 23/82 (CAI4863) **B**. Alignment of different *Birnaviridae* members: IBDV (accession number AAD30136), Infectious Pancreatic Necrosis Virus (IPNV; AJ622822), Marine Aquabirnavirus (MABV; BAA31999), Yellowtail Ascites Virus (YAV; NP690805), *Paralichthys olivaceus* birnavirus (PoBV, YP001514404), Aquabirnavirus TAB 98 (AqBVTAB98, ACD64976), Blotched Snakehead Virus (BSNV; AJ459382) and *Drosophila* X Virus (DrXV, U60650). The scissile bond is highlighted in blue. Asterisks represent identical residues, whereas colons and single dots represent conserved and semi- conserved substitutions.

Although it has not been reported previously the implication of a cellular protease in the assembly of the birnaviruses. This is a common strategy used by some

viruses. Some recent findings report that for example, during the course of Hepatitis A virus particle assembly and RNA packaging, immature procapsids might be targeted to early lysosomes where they encounter cellular proteases including cathepsin L that remove 2A peptide, and thereby fully mature the particles (Morace et al., 2008). In flavivirus, just prior to release, the proteolytic cleavage of prM protein by furin triggers the conversion of the immature virions into slightly smaller mature particles with high infectivity (Junjhon et al., 2008). Hepatitis C virus, with a positive-sense ssRNA genome, that encodes a polyprotein of ca. 3000 amino acids, which is cleaved both co- and post-translationally by viral and cellular proteases to render mature viral proteins (Moradpour et al., 2007; Penin et al., 2004). In the case of core protein, complete maturation requires further cleavage within the core-E1 signal peptide by signal peptide peptidase (SPP) (Targett-Adams et al., 2008).

### 5.4.2. Hexamer assembly

Coplanar contacts are formed by VP2 trimers within a G4 triangle and those made by the e trimer. In our model, insertion of the VP2 amphipatic α-helix into the highly hydrophobic grooves that form the broad cavity at the quasi six-fold axes would preclude the bending of these contacts. The amphipathic α-helix has an Asp residue (Asp-446) between its hydrophobic and enriched basic residue sides, which could further stabilize the dominant hydrophobic interactions (**Fig. 37A and 37D**). Amphipathic α-helix behaviour would resemble that of the ordered N-terminal peptide arm of the nodavirus CP. Previous analysis of pVP2 polypeptides with C-terminal extensions of variable length showed that the longer the C-terminal domain the more probable is hexamer formation which would produce primarily tubular structures (Saugar et al., 2005a). Accordingly, the C-terminal domain cleavage would be slower, and would be stabilized by its interaction with VP3.

Furthermore, analysis restricted to His-VP2-466 capsid particles. similar in size to IBDV virions, from a sample containing heterogeneous assemblies in equilibrium, represents an arrested morphogenetic intermediate, and may constitute a set of conformationally metastable particles. This interpretation is reflected in the density

arms around the quasi six-fold axis, which are not identical and one of which is absent (**Fig. 37A**).

We show a scheme that summarizes our model for the IBDV assembly pathway (**Fig. 40**). Structural analysis of CP topology, virion architecture, and assembly between evolutionally distant viruses reveal unexpected similarities (Bamford et al., 2005). Our data for the IBDV assembly pathway reinforces the recently suggested evolutionary relationships between birnavirus and positive-strand ssRNA viruses. The IBDV capsid assembly is controlled by scaffolding (VP3) and proteolytic proteins (VP4, VP2 and a cellular protease, PSA) that degrade short CP-specific sequences in consecutive events. This, together with the VP2 C-terminal flexibility, triggers interactions of the amphipathic α-helix for VP2 assembly into hexamers and pentamers. Interactions via amphipathic α-helices may be a common feature of macromolecular complex activation (Johnston et al., 2005) and, as found in HIV assembly (Ternois et al., 2005), may serve as an attractive target for future antiviral strategies.

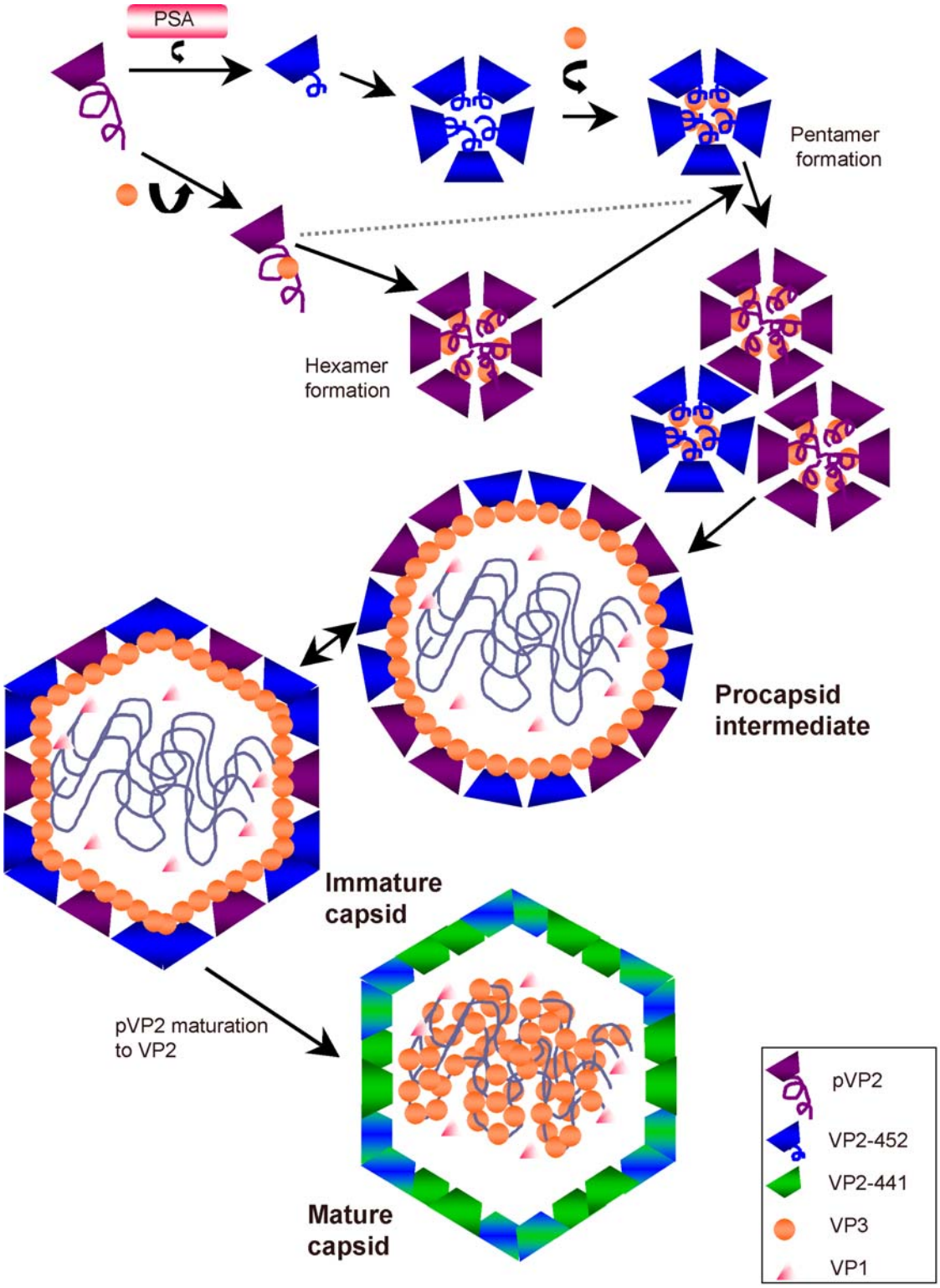


**Fig. 39. Hypothetical scheme of IBDV assembly**. After the release of pVP2, VP3 and VP4 by the cleavage of the polyprotein; some pVP2 peptides are further cleaved by PSA in Arg-452-Arg-453 scissile bond. Amphiphatic α-helices (443-452) interact with themselves forming a helical bundle forming the pentameric conformation; these α-helices can probably interact with VP3 C-terminal domain stabilizing the pentamers. On the other hand, pVP2 will probably interact with VP3 leading to coplanar contacts that form hexamers. Preformed pentamers and hexamers could interact by VP3 oligomerization domain assembling a "procapsid" intermediate. Another possibility is that the pentamer could act as a nucleation

factor with which pVP2-VP3 complexes could interact by VP3 contacts. Similar to noda- and tetravirus assembly model, this spherical "procapsid" intermediate could adopt a reversible state ("immature capsid") depending on pH until a CP small amount has been cleaved. Finally, the capsid matures when VP2 C-terminal domain is released by the cleavage of Ala-441-Phe-442 by Asp-431, rendering VP3 inside the capsid. Which is the signal that originates the cleavage of the CP still unknown, probably the higher density of dsRNA and their interaction with VP3 forming the RNP complexes provokes the dissociation of pVP2 and VP3 and the further maturation of the CP.

# CONCLUSIONS

1. VP2 structural polymorphism is based on two peptide components: the pVP2 C-terminal amphipathic α-helix, acting as a conformational molecular switch, and the VP3 C-terminal domain, acting as a molecular triggering factor. Acid and basic residues of VP3 C-terminal domain are required for the correct assembly of IBDV capsid. Structural polymorphism is achieved by electrostatic interactions between these two peptide components.

2. VP2 Asp-431, lying in a flexible loop preceding the C-terminal (helix α-4), is responsible for the endopeptidase activity that cleaves the Ala-441-Phe-442 bond to generate the mature VP2 polypeptide. pVP2 proteolytic processing is the result of a monomolecular *cis*-cleavage reaction.

3. VP2 self-processing is essential for the assembly of an infectious IBDV progeny.VP2-452 intermediate precursors are essential to pentamer assembly, which act as capsid nucleation factors. A cellular protease, puromycin sensitive aminopeptidase, is responsible *in vivo* to provide VP2-452 polypeptide.

1. El polimorfismo estructural de VP2 se basa en dos componentes peptídicos: la hélice-α anfipática del dominio C-terminal de VP2 que actúa como un interruptor molecular conformacional, y el dominio C-terminal de VP3, que actúa como un factor efector molecular. Los residuos ácidos y básicos del dominio C-terminal de VP3 se requieren para el correcto ensamblaje de la cápsida de IBDV. El polimorfismo estructural se consigue debido a una interacción electrostática entre estos dos componentes peptídicos.

2. Asp-431 de VP2, localizado en un "loop" flexible (hélice α-4), es responsable de la actividad endopeptidasa que procesa el enlace Ala-441-Phe-442 para generar el polipéptido maduro de VP2. El proceso proteolítico de pVP2 es el resultado de una reacción monomolecular de corte en *cis*.

3. El autoprocesamiento de pVP2 es esencial para el ensamblaje de una progenie infecciosa de IBDV:
4. Los precursores intermedios de VP2-452 son esenciales para el ensamblaje de pentámeros, los cuales actúan como factores nucleadores de la cápsida. Una proteasa celular, una aminopeptidasa sensible a puromicina (PSA), es la responsable *in vivo* de proveer el polipéptido VP2-452.

# BIBLIOGRAPHY

Abrescia, N. G., Cockburn, J. J., Grimes, J. M., Sutton, G. C., Diprose, J. M., Butcher, S. J., Fuller, S. D., San Martin, C., Burnett, R. M., Stuart, D. I., *et al.* (2004). Insights into assembly from structural analysis of bacteriophage PRD1. Nature *432*, 68-74.

Adamson, C. S., and Freed, E. O. (2007). Human immunodeficiency virus type 1 assembly, release, and maturation. Adv Pharmacol *55*, 347-387.

Agirrezabala, X., Velazquez-Muriel, J. A., Gomez-Puertas, P., Scheres, S. H., Carazo, J. M., and Carrascosa, J. L. (2007). Quasi-atomic model of bacteriophage t7 procapsid shell: insights into the structure and evolution of a basic fold. Structure *15*, 461-472.

Ahlquist, P. (2005). Virus evolution: fitting lifestyles to a T, Vol 15).

Antin, P. B., and Ordahl, C. P. (1991). Isolation and characterization of an avian myogenic cell line. Dev Biol *143*, 111-121.

Bamford, D. H., Grimes, J. M., and Stuart, D. I. (2005). What does structure tell us about virus evolution? Curr Opin Struct Biol *15*, 655-663.

Berger, B., Shor, P. W., Tucker-Kellogg, L., and King, J. (1994). Local rule-based theory of virus shell assembly. Proc Natl Acad Sci U S A *91*, 7732-7736.

Berget, P. B. (1985). Pathways in viral morphogenesis. (Boston, Jones and Bartlett Publishers).

Bhutani, N., Venkatraman, P., and Goldberg, A. L. (2007). Puromycin-sensitive aminopeptidase is the major peptidase responsible for digesting polyglutamine sequences released by proteasomes during protein degradation. Embo J *26*, 1385-1396.

Birghan, C., Mundt, E., and Gorbalenya, A. E. (2000). A non-canonical lon proteinase lacking the ATPase domain employs the ser-Lys catalytic dyad to exercise broad control over the life cycle of a double-stranded RNA virus. Embo J *19*, 114-123.

Blanc, A., Ribas, J. C., Wickner, R. B., and Sonenberg, N. (1994). His-154 is involved in the linkage of the Saccharomyces cerevisiae L-A double-stranded RNA virus Gag protein to the cap structure of mRNAs and is essential for M1 satellite virus expression. Mol Cell Biol *14*, 2664-2674.

Botbol, V., and Scornik, O. A. (1983). Peptide intermediates in the degradation of cellular proteins. Bestatin permits their accumulation in mouse liver in vivo. J Biol Chem *258*, 1942-1949.

Bothner, B., Taylor, D., Jun, B., Lee, K. K., Siuzdak, G., Schultz, C. P., and Johnson, J. E. (2005). Maturation of a tetravirus capsid alters the dynamic properties and creates a metastable complex. Virology *334*, 17-27.

Bottcher, B., Kiselev, N. A., Stel'Mashchuk, V. Y., Perevozchikova, N. A., Borisov, A. V., and Crowther, R. A. (1997). Three-dimensional structure of infectious bursal disease virus determined by electron cryomicroscopy. J Virol *71*, 325-330.

Brandt, M., Yao, K., Liu, M., Heckert, R. A., and Vakharia, V. N. (2001). Molecular determinants of virulence, cell tropism, and pathogenic phenotype of infectious bursal disease virus. J Virol *75*, 11974-11982.

Brockman, W. W., and Nathans, D. (1974). The isolation of simian virus 40 variants with specifically altered genomes. Proc Natl Acad Sci U S A *71*, 942-946.
Brooks, D. R., Hooper, N. M., and Isaac, R. E. (2003). The Caenorhabditis elegans orthologue of mammalian puromycin-sensitive aminopeptidase has roles in embryogenesis and reproduction. J Biol Chem *278*, 42795-42801.

Brown, M. D., and Skinner, M. A. (1996). Coding sequences of both genome segments of a European 'very virulent' infectious bursal disease virus. Virus Res *40*, 1-15.

Brünger, A. T. (1998). Acta Crystallogr Sect D Biol Crystallogr *54*, 905-921.

Caldwell, R. B., Kierzek, A. M., Arakawa, H., Bezzubov, Y., Zaim, J., Fiedler, P., Kutter, S., Blagodatski, A., Kostovska, D., Koter, M., *et al.* (2005). Full-length cDNAs from chicken bursal lymphocytes to facilitate gene function analysis. Genome Biol *6*, R6.

Canady, M. A., Tihova, M., Hanzlik, T. N., Johnson, J. E., and Yeager, M. (2000). Large conformational changes in the maturation of a simple RNA virus, nudaurelia capensis omega virus (NomegaV). J Mol Biol *299*, 573-584.

Casanas, A., Navarro, A., Ferrer-Orta, C., Gonzalez, D., Rodriguez, J. F., and Verdaguer, N. (2008). Structural insights into the multifunctional protein VP3 of birnaviruses. Structure *16*, 29-37.

Caspar, D. L. (1956). Structure of bushy stunt virus. Nature *177*, 475-476.

Caspar, D. L., and Klug, A. (1962). Physical principles in the construction of regular viruses. Cold Spring Harb Symp Quant Biol *27*, 1-24.

Caston, J., Rodriguez, JF, Carrascosa, JL (2008). Segmented Doubled-stranded RNA Viruses, Caister Academic Press).

Caston, J. R., Martinez-Torrecuadrada, J. L., Maraver, A., Lombardo, E., Rodriguez, J. F., Casal, J. I., and Carrascosa, J. L. (2001). C terminus of infectious bursal disease virus major capsid protein VP2 is involved in definition of the T number for capsid assembly. J Virol *75*, 10815-10828.

Constam, D. B., Tobler, A. R., Rensing-Ehl, A., Kemler, I., Hersh, L. B., and Fontana, A. (1995). Puromycin-sensitive aminopeptidase. Sequence analysis, expression, and functional characterization. J Biol Chem *270*, 26931-26939.

Conway, J. F., Duda, R. L., Cheng, N., Hendrix, R. W., and Steven, A. C. (1995). Proteolytic and conformational control of virus capsid maturation: the bacteriophage HK97 system. J Mol Biol *253*, 86-99.

Coulibaly, F., Chevalier, C., Gutsche, I., Pous, J., Navaza, J., Bressanelli, S., Delmas, B., and Rey, F. A. (2005). The birnavirus crystal structure reveals structural relationships among icosahedral viruses. Cell *120*, 761-772.

Crick, F. H., and Watson, J. D. (1956). Structure of small viruses. Nature *177*, 473-475.
Chandu, D., Kumar, A., and Nandi, D. (2003). PepN, the major Suc-LLVY-AMC-hydrolyzing enzyme in Escherichia coli, displays functional similarity with downstream processing enzymes in Archaea and eukarya. Implications in cytosolic protein degradation. J Biol Chem *278*, 5548-5556.

Chang, J. R., Spilman, M. S., Rodenburg, C. M., and Dokland, T. (2009). Functional domains of the bacteriophage P2 scaffolding protein: identification of residues involved in assembly and protease activity. Virology *384*, 144-150.

Chen, H. Y., Yang, J., Lin, C., and Yuan, Y. A. (2008). Structural basis for RNA-silencing suppression by Tomato aspermy virus protein 2b. EMBO Rep *9*, 754-760.

Cheng, R. H., Reddy, V. S., Olson, N. H., Fisher, A. J., Baker, T. S., and Johnson, J. E. (1994). Functional implications of quasi-equivalence in a T = 3 icosahedral animal virus established by cryo-electron microscopy and X-ray crystallography. Structure *2*, 271-282.

Chettle, N., Stuart, J. C., and Wyeth, P. J. (1989). Outbreak of virulent infectious bursal disease in East Anglia. Vet Rec *125*, 271-272.

Chevalier, C., Galloux, M., Pous, J., Henry, C., Denis, J., Da Costa, B., Navaza, J., Lepault, J., and Delmas, B. (2005). Structural peptides of a nonenveloped virus are involved in assembly and membrane translocation. J Virol *79*, 12253-12263.

Chevalier, C., Lepault, J., Da Costa, B., and Delmas, B. (2004). The last C-terminal residue of VP3, glutamic acid 257, controls capsid assembly of infectious bursal disease virus. J Virol *78*, 3296-3303.

Chevalier, C., Lepault, J., Erk, I., Da Costa, B., and Delmas, B. (2002). The maturation process of pVP2 requires assembly of infectious bursal disease virus capsids. J Virol *76*, 2384-2392.

Da Costa, B., Chevalier, C., Henry, C., Huet, J. C., Petit, S., Lepault, J., Boot, H., and Delmas, B. (2002). The capsid of infectious bursal disease virus contains several small peptides arising from the maturation process of pVP2. J Virol *76*, 2393-2402.

Delmas, B., Kibenge, F.S.B., Leong, J.C., Mundt E., Vakharia, V.N., Wu J.L. (2004). Birnaviridae. In *Virus Taxonomy, Eighth report of the International Committee on Taxonomy of Viruses*, pp. 561-569.

Diprose, J. M., Burroughs, J. N., Sutton, G. C., Goldsmith, A., Gouet, P., Malby, R., Overton, I., Zientara, S., Mertens, P. P., Stuart, D. I., and Grimes, J. M. (2001). Translocation portals for the substrates and products of a viral transcription complex: the bluetongue virus core. Embo J *20*, 7229-7239.

Dobos, P. (1993). In vitro guanylylation of infectious pancreatic necrosis virus polypeptide VP1. Virology *193*, 403-413.

Dokland, T. (1999). Scaffolding proteins and their role in viral assembly. Cell Mol Life Sci *56*, 580-603.

Dokland, T. (2000). Freedom and restraint: themes in virus capsid assembly. Structure *8*, R157-162.

Dokland, T., and Murialdo, H. (1993). Structural transitions during maturation of bacteriophage lambda capsids. J Mol Biol *233*, 682-694.

DuBridge, R. B., Tang, P., Hsia, H. C., Leong, P. M., Miller, J. H., and Calos, M. P. (1987). Analysis of mutation in human cells by using an Epstein-Barr virus shuttle system. Mol Cell Biol *7*, 379-387.

Dulbecco, R., and Freeman, G. (1959). Plaque production by the polyoma virus. Virology *8*, 396-397.

Earl, P. L. a. M. B. (1993). Generation of recombinant vaccinia viruses., Vol 2 (New York, F.M. Ausubel, R. Brent, R.E. Kingston, D.D. More, J.G. Seidman, J.A. Smith and K. Struhl).

Emsley, P. C., K. (2004). Coot: Model- Building Tools for Molecular Graphics. Acta Crystallogr Sect D Biol Crystallogr *60*, 2126-2132.

Evans, P. (1994). Proceedings of the CCP4 study weekend. Data collection and processing. Acta Crystallogr Sect D Biol Crystallogr *50*, 760-763.

Fauquet, C. M., and Fargette, D. (2005). International Committee on Taxonomy of Viruses and the 3,142 unassigned species. Virol J *2*, 64.

Feldman, A. R., Lee, J., Delmas, B., and Paetzel, M. (2006). Crystal structure of a novel viral protease with a serine/lysine catalytic dyad mechanism. J Mol Biol *358*, 1378-1389.

Fernandez-Arias, A., Martinez, S., and Rodriguez, J. F. (1997). The major antigenic protein of infectious bursal disease virus, VP2, is an apoptotic inducer. J Virol *71*, 8014-8018.

Fernandez-Arias, A., Risco, C., Martinez, S., Albar, J. P., and Rodriguez, J. F. (1998). Expression of ORF A1 of infectious bursal disease virus results in the formation of virus-like particles. J Gen Virol *79 (Pt 5)*, 1047-1054.

Fidler, I. J., Gersten, D. M., and Hart, I. R. (1978). The biology of cancer invasion and metastasis. Adv Cancer Res *28*, 149-250.

Fisher, A. J., and Johnson, J. E. (1993). Ordered duplex RNA controls capsid architecture in an icosahedral animal virus. Nature *361*, 176-179.

Gallagher, T. M., and Rueckert, R. R. (1988). Assembly-dependent maturation cleavage in provirions of a small icosahedral insect ribovirus. J Virol *62*, 3399-3406.

Galloux, M., Libersou, S., Morellet, N., Bouaziz, S., Da Costa, B., Ouldali, M., Lepault, J., and Delmas, B. (2007). Infectious bursal disease virus, a non-enveloped virus, possesses a capsid-associated peptide that deforms and perforates biological membranes. J Biol Chem *282*, 20774-20784.

Garriga, D., Navarro, A., Querol-Audi, J., Abaitua, F., Rodriguez, J. F., and Verdaguer, N. (2007). Activation mechanism of a noncanonical RNA-dependent RNA polymerase. Proc Natl Acad Sci U S A *104*, 20540-20545.

Garriga, D., Querol-Audi, J., Abaitua, F., Saugar, I., Pous, J., Verdaguer, N., Caston, J. R., and Rodriguez, J. F. (2006). The 2.6-Angstrom structure of infectious bursal disease virus-derived T=1 particles reveals new stabilizing elements of the virus capsid. J Virol *80*, 6895-6905.

Geier, E., Pfeifer, G., Wilm, M., Lucchiari-Hartz, M., Baumeister, W., Eichmann, K., and Niedermann, G. (1999). A giant protease with potential to substitute for some functions of the proteasome. Science *283*, 978-981.

Gertsman, I., Gan, L., Guttman, M., Lee, K., Speir, J. A., Duda, R. L., Hendrix, R. W., Komives, E. A., and Johnson, J. E. (2009). An unexpected twist in viral capsid maturation. Nature *458*, 646-650.

Gonzalez, D., Rodriguez, J. F., and Abaitua, F. (2005). Intracellular interference of infectious bursal disease virus. J Virol *79*, 14437-14441.

Gorbalenya, A. E., Pringle, F. M., Zeddam, J. L., Luke, B. T., Cameron, C. E., Kalmakoff, J., Hanzlik, T. N., Gordon, K. H., and Ward, V. K. (2002). The palm subdomain-based active site is internally permuted in viral RNA-dependent RNA polymerases of an ancient lineage. J Mol Biol *324*, 47-62.

Gouet, P., Diprose, J. M., Grimes, J. M., Malby, R., Burroughs, J. N., Zientara, S., Stuart, D. I., and Mertens, P. P. (1999). The highly ordered double-stranded RNA genome of bluetongue virus revealed by crystallography. Cell *97*, 481-490.

Granzow, H., Birghan, C., Mettenleiter, T. C., Beyer, J., Kollner, B., and Mundt, E. (1997). A second form of infectious bursal disease virus-associated tubule contains VP4. J Virol *71*, 8879-8885.

Grimes, J. M., Burroughs, J. N., Gouet, P., Diprose, J. M., Malby, R., Zientara, S., Mertens, P. P., and Stuart, D. I. (1998). The atomic structure of the bluetongue virus core. Nature *395*, 470-478.

Hanzlik, T. N., and Gordon, K. H. (1997). The Tetraviridae. Adv Virus Res *48*, 101-168.

Harlow, E. a. D. L. (1988). Antibodies: a laboratory manual (Cold Spring Habor, N.Y.).

Hellen, C. U., and Wimmer, E. (1992). The role of proteolytic processing in the morphogenesis of virus particles. Experientia *48*, 201-215.

Harrison, S. C. (2001). Principles of virus structure. In Fields virology, D. M. Knipe, P. M. Howley, D. E. Griffin, M. A. Martin, R. A. Lamb, B. Roizman, and S. E. Strauss, eds. (Philadelphia, Lippincott Williams & Wilkins), pp. 53-85.
Hendry, D. A. (1991). Nodaviridae of invertebrates. In *Viruses of Invertebrates* (New York: Marcel Dekker, Edited by E. Kurstak), pp. pp. 277 285.

Hersh, L. B., and McKelvy, J. F. (1981). An aminopeptidase from bovine brain which catalyzes the hydrolysis of enkephalin. J Neurochem *36*, 171-178.

Hersh, L. B., Smith, T. E., and McKelvy, J. F. (1980). Cleavage of endorphins to des-Tyr endorphins by homogeneous bovine brain aminopeptidase. Nature *286*, 160-162.

Himly, M., Foster, D. N., Bottoli, I., Iacovoni, J. S., and Vogt, P. K. (1998). The DF-1 chicken fibroblast cell line: transformation induced by diverse oncogenes and cell death resulting from infection by avian leukosis viruses. Virology *248*, 295-304.

Hjalmarsson, A., Carlemalm, E., and Everitt, E. (1999). Infectious pancreatic necrosis virus: identification of a VP3-containing ribonucleoprotein core structure and evidence for O-linked glycosylation of the capsid protein VP2. J Virol *73*, 3484-3490.

Hooper, N. M. (1994). Families of zinc metalloproteases. FEBS Lett *354*, 1-6.

Johnson, G. D., and Hersh, L. B. (1990). Studies on the subsite specificity of the rat brain puromycin-sensitive aminopeptidase. Arch Biochem Biophys *276*, 305-309.

Johnson, J. E. (1996). Functional implications of protein-protein interactions in icosahedral viruses. Proc Natl Acad Sci U S A *93*, 27-33.

Johnson, J. E., and Speir, J. A. (1997). Quasi-equivalent viruses: a paradigm for protein assemblies. J Mol Biol *269*, 665-675.

Johnston, C. A., Willard, F. S., Jezyk, M. R., Fredericks, Z., Bodor, E. T., Jones, M. B., Blaesius, R., Watts, V. J., Harden, T. K., Sondek, J., *et al.* (2005). Structure of Gα(i1) bound to a GDP-selective peptide provides insight into guanine nucleotide exchange. Structure *13*, 1069-1080.

Junjhon, J., Lausumpao, M., Supasa, S., Noisakran, S., Songjaeng, A., Saraithong, P., Chaichoun, K., Utaipat, U., Keelapang, P., Kanjanahaluethai, A., *et al.* (2008). Differential modulation of prM cleavage, extracellular particle distribution, and virus infectivity by conserved residues at nonfurin consensus positions of the dengue virus pr-M junction. J Virol *82*, 10776-10791.

Kaesberg, P. (1987). Organization of bipartite insect virus genomes: the genome of black beetle virus. In *The Molecular Biology of the Positive Strand RNA Viruses* (London: Academic Press, eds. Rowlands, D. J., Mayo, M. A. & Mahy, B. W. J.), pp. 207-218.

Karsten, S. L., Sang, T. K., Gehman, L. T., Chatterjee, S., Liu, J., Lawless, G. M., Sengupta, S., Berry, R. W., Pomakian, J., Oh, H. S., *et al.* (2006). A genomic screen for modifiers of tauopathy identifies puromycin-sensitive aminopeptidase as an inhibitor of tau-induced neurodegeneration. Neuron *51*, 549-560.

Kaufer, I., and Weiss, E. (1980). Significance of bursa of Fabricius as target organ in infectious bursal disease of chickens. Infect Immun *27*, 364-367.

Kochan, G., Gonzalez, D., and Rodriguez, J. F. (2003). Characterization of the RNA-binding activity of VP3, a major structural protein of Infectious bursal disease virus. Arch Virol *148*, 723-744.

Krol, M. A., Olson, N. H., Tate, J., Johnson, J. E., Baker, T. S., and Ahlquist, P. (1999). RNA-controlled polymorphism in the in vivo assembly of 180-subunit and 120-subunit virions from a single capsid protein. Proc Natl Acad Sci U S A *96*, 13650-13655.

Lawton, J. A., Estes, M. K., and Prasad, B. V. (1997). Three-dimensional visualization of mRNA release from actively transcribing rotavirus particles. Nat Struct Biol *4*, 118-121.

Lee, C. C., Ko, T. P., Chou, C. C., Yoshimura, M., Doong, S. R., Wang, M. Y., and Wang, A. H. (2006). Crystal structure of infectious bursal disease virus VP2 subviral particle at 2.6A resolution: implications in virion assembly and immunogenicity. J Struct Biol *155*, 74-86.

Lee, C. C., Ko, T. P., Lee, M. S., Chou, C. C., Lai, S. Y., Wang, A. H., and Wang, M. Y. (2003). Purification, crystallization and preliminary X-ray analysis of immunogenic virus-like particles formed by infectious bursal disease virus (IBDV) structural protein VP2. Acta Crystallogr D Biol Crystallogr *59*, 1234-1237.

Lee, J., Feldman, A. R., Delmas, B., and Paetzel, M. (2007). Crystal structure of the VP4 protease from infectious pancreatic necrosis virus reveals the acyl-enzyme complex for an intermolecular self-cleavage reaction. J Biol Chem *282*, 24928-24937.

Leslie, A. (1991). Macromolecular data processing, Vol 5 (Oxford. United Kingdom, Oxford University Press).

Li, H., Li, W. X., and Ding, S. W. (2002). Induction and suppression of RNA silencing by an animal virus. Science *296*, 1319-1321.

Liddington, R. C., Yan, Y., Moulai, J., Sahli, R., Benjamin, T. L., and Harrison, S. C. (1991). Structure of simian virus 40 at 3.8-A resolution. Nature *354*, 278-284.

Liu, M., and Vakharia, V. N. (2006). Nonstructural protein of infectious bursal disease virus inhibits apoptosis at the early stage of virus infection. J Virol *80*, 3369-3377.

Lombardo, E., Maraver, A., Cast n, J. R., Rivera, J., Fernandez-Arias, A., Serrano, A., Carrascosa, J. L., and Rodriguez, J. F. (1999). VP1, the putative RNA-dependent RNA polymerase of infectious bursal disease virus, forms complexes with the capsid protein VP3, leading to efficient encapsidation into virus-like particles. J Virol *73*, 6973-6983.

Lombardo, E., Maraver, A., Espinosa, I., Fernandez-Arias, A., and Rodriguez, J. F. (2000). VP5, the nonstructural polypeptide of infectious bursal disease virus, accumulates within the host plasma membrane and induces cell lysis. Virology *277*, 345-357.

Luckow, V. A., Lee, S. C., Barry, G. F., and Olins, P. O. (1993). Efficient generation of infectious recombinant baculoviruses by site-specific transposon-mediated insertion of foreign genes into a baculovirus genome propagated in Escherichia coli. J Virol *67*, 4566-4579.

Luque, D., Rivas, G., Alfonso, C., Carrascosa, J. L., Rodriguez, J. F., and Caston, J. R. (2009a). Infectious bursal disease virus is an icosahedral polyploid dsRNA virus. Proc Natl Acad Sci U S A *106*, 2148-2152.

Luque, D., Saugar, I., Rejas, M. T., Carrascosa, J. L., Rodriguez, J. F., and Caston, J. R. (2009b). Infectious Bursal disease virus: ribonucleoprotein complexes of a double-stranded RNA virus. J Mol Biol *386*, 891-901.

Luque, D., Saugar, I., Rodriguez, J. F., Verdaguer, N., Garriga, D., Martin, C. S., Velazquez-Muriel, J. A., Trus, B. L., Carrascosa, J. L., and Caston, J. R. (2007). Infectious Bursal Disease Virus capsid assembly and maturation by structural rearrangements of a transient molecular switch. J Virol.

MacBeth, K. J., and Patterson, J. L. (1995a). The short transcript of Leishmania RNA virus is generated by RNA cleavage. J Virol *69*, 3458-3464.

MacBeth, K. J., and Patterson, J. L. (1995b). Single-site cleavage in the 5'-untranslated region of Leishmaniavirus RNA is mediated by the viral capsid protein. Proc Natl Acad Sci U S A *92*, 8994-8998.

Maraver, A., Clemente, R., Rodriguez, J. F., and Lombardo, E. (2003a). Identification and molecular characterization of the RNA polymerase-binding motif of infectious bursal disease virus inner capsid protein VP3. J Virol *77*, 2459-2468.

Maraver, A., Ona, A., Abaitua, F., Gonzalez, D., Clemente, R., Ruiz-Diaz, J. A., Caston, J. R., Pazos, F., and Rodriguez, J. F. (2003b). The oligomerization domain of VP3, the scaffolding protein of infectious bursal disease virus, plays a critical role in capsid assembly. J Virol *77*, 6438-6449.

Martinez-Torrecuadrada, J. L., Caston, J. R., Castro, M., Carrascosa, J. L., Rodriguez, J. F., and Casal, J. I. (2000a). Different architectures in the assembly of infectious bursal disease virus capsid proteins expressed in insect cells. Virology *278*, 322-331.

Martinez-Torrecuadrada, J. L., Lazaro, B., Rodriguez, J. F., and Casal, J. I. (2000b). Antigenic properties and diagnostic potential of baculovirus-expressed infectious bursal disease virus proteins VPX and VP3. Clin Diagn Lab Immunol *7*, 645-651.

Martinez-Torrecuadrada, J. L., Saubi, N., Pages-Mante, A., Caston, J. R., Espuna, E., and Casal, J. I. (2003). Structure-dependent efficacy of infectious bursal disease virus (IBDV) recombinant vaccines. Vaccine *21*, 1952-1960.

McFerran, J. B., McNulty, M. S., McKillop, E. R., Connor, T. J., McCracken, R. M., Collins, D. S., and Allan, G. M. (1980). Isolation and serological studies with infectious bursal disease viruses from fowl, turkeys and ducks: demonstration of a second serotype. Avian Pathol *9*, 395-404.

Medawar PB, M. J. (1983). Aristotle to Zoos. A philosophical dictionary of biology. (Cambridge, Massachusetts, USA, Harvard University Press).

Mitra, K., and Frank, J. (2006). Ribosome dynamics: insights from atomic structure modeling into cryo-electron microscopy maps. Annu Rev Biophys Biomol Struct *35*, 299-317.

Morace, G., Kusov, Y., Dzagurov, G., Beneduce, F., and Gauss-Muller, V. (2008). The unique role of domain 2A of the hepatitis A virus precursor polypeptide P1-2A in viral morphogenesis. BMB Rep *41*, 678-683.

Moradpour, D., Penin, F., and Rice, C. M. (2007). Replication of hepatitis C virus. Nat Rev Microbiol *5*, 453-463.

Morgan, M. M., Macreadie, I. G., Harley, V. R., Hudson, P. J., and Azad, A. A. (1988). Sequence of the small double-stranded RNA genomic segment of infectious bursal disease virus and its deduced 90-kDa product. Virology *163*, 240-242.

Mori, K., Nakai, T., Muroga, K., Arimoto, M., Mushiake, K., and Furusawa, I. (1992). Properties of a new virus belonging to nodaviridae found in larval striped jack (Pseudocaranx dentex) with nervous necrosis. Virology *187*, 368-371.

Morillas, M., Eberl, H., Allain, F. H., Glockshuber, R., and Kuennemann, E. (2008). Novel enzymatic activity derived from the Semliki Forest virus capsid protein. J Mol Biol *376*, 721-735.

Muller, H., Islam, M. R., and Raue, R. (2003). Research on infectious bursal disease--the past, the present and the future. Vet Microbiol *97*, 153-165.

Muller, H., and Nitschke, R. (1987a). Molecular weight determination of the two segments of double-stranded RNA of infectious bursal disease virus, a member of the birnavirus group. Med Microbiol Immunol *176*, 113-121.

Muller, H., and Nitschke, R. (1987b). The two segments of the infectious bursal disease virus genome are circularized by a 90,000-Da protein. Virology *159*, 174-177.

Muller, H., Scholtissek, C., and Becht, H. (1979). The genome of infectious bursal disease virus consists of two segments of double-stranded RNA. J Virol *31*, 584-589.

Munshi, S., Liljas, L., Cavarelli, J., Bomu, W., McKinney, B., Reddy, V., and Johnson, J. E. (1996). The 2.8 A structure of a T = 4 animal virus and its implications for membrane translocation of RNA. J Mol Biol *261*, 1-10.

Negash, T., al-Garib, S. O., and Gruys, E. (2004). Comparison of in ovo and post-hatch vaccination with particular reference to infectious bursal disease. A review. Vet Q *26*, 76-87.

Newcomb, W. W., Trus, B. L., Cheng, N., Steven, A. C., Sheaffer, A. K., Tenney, D. J., Weller, S. K., and Brown, J. C. (2000). Isolation of herpes simplex virus procapsids from cells infected with a protease-deficient mutant virus. J Virol *74*, 1663-1673.

Ona, A., Luque, D., Abaitua, F., Maraver, A., Caston, J. R., and Rodriguez, J. F. (2004). The C-terminal domain of the pVP2 precursor is essential for the interaction between VP2 and VP3, the capsid polypeptides of infectious bursal disease virus. Virology *322*, 135-142.

Osada, T., Ikegami, S., Takiguchi-Hayashi, K., Yamazaki, Y., Katoh-Fukui, Y., Higashinakagawa, T., Sakaki, Y., and Takeuchi, T. (1999). Increased anxiety and impaired pain response in puromycin-sensitive aminopeptidase gene-deficient mice obtained by a mouse gene-trap method. J Neurosci *19*, 6068-6078.

Osada, T., Watanabe, G., Kondo, S., Toyoda, M., Sakaki, Y., and Takeuchi, T. (2001a). Male reproductive defects caused by puromycin-sensitive aminopeptidase deficiency in mice. Mol Endocrinol *15*, 960-971.

Osada, T., Watanabe, G., Sakaki, Y., and Takeuchi, T. (2001b). Puromycin-sensitive aminopeptidase is essential for the maternal recognition of pregnancy in mice. Mol Endocrinol *15*, 882-893.

Pan, J., Vakharia, V. N., and Tao, Y. J. (2007). The structure of a birnavirus polymerase reveals a distinct active site topology. Proc Natl Acad Sci U S A *104*, 7385-7390.

Paul, A. V., van Boom, J. H., Filippov, D., and Wimmer, E. (1998). Protein-primed RNA synthesis by purified poliovirus RNA polymerase. Nature *393*, 280-284.

Penin, F., Dubuisson, J., Rey, F. A., Moradpour, D., and Pawlotsky, J. M. (2004). Structural biology of hepatitis C virus. Hepatology *39*, 5-19.

Pitcovski, J., Goldberg, D., Levi, B. Z., Di-Castro, D., Azriel, A., Krispel, S., Maray, T., and Shaaltiel, Y. (1998). Coding region of segment A sequence of a very virulent isolate of IBDV--comparison with isolates from different countries and virulence. Avian Dis *42*, 497-506.

Prasad, B. V., and Prevelige, P. E., Jr. (2003). Viral genome organization. Adv Protein Chem *64*, 219-258.

Raleigh E.A., E. K., Brent R. (2003). Selected Topics from Classical Bacterial Genetics. In *Current Protocols in Molecular Biology* (Interscience).

Ranson, N. A., Clare, D. K., Farr, G. W., Houldershaw, D., Horwich, A. L., and Saibil, H. R. (2006). Allosteric signaling of ATP hydrolysis in GroEL-GroES complexes. Nat Struct Mol Biol *13*, 147-152.

Rawlings, N. D., and Barrett, A. J. (1995). Evolutionary families of metallopeptidases. Methods Enzymol *248*, 183-228.

Rawlings, N. D., Morton, F. R., Kok, C. Y., Kong, J., and Barrett, A. J. (2008). MEROPS: the peptidase database. Nucleic Acids Res *36*, D320-325.

Rossmann, M. G., and Johnson, J. E. (1989). Icosahedral RNA virus structure. Annu Rev Biochem *58*, 533-573.

Rudberg, P. C., Tholander, F., Thunnissen, M. M., and Haeggstrom, J. Z. (2002). Leukotriene A4 hydrolase/aminopeptidase. Glutamate 271 is a catalytic residue with specific roles in two distinct enzyme mechanisms. J Biol Chem *277*, 1398-1404.

Salunke, D. M., Caspar, D. L., and Garcea, R. L. (1989). Polymorphism in the assembly of polyomavirus capsid protein VP1. Biophys J *56*, 887-900.

Sanchez, A. B., and Rodriguez, J. F. (1999). Proteolytic processing in infectious bursal disease virus: identification of the polyprotein cleavage sites by site-directed mutagenesis. Virology *262*, 190-199.

Saric, T., Graef, C. I., and Goldberg, A. L. (2004). Pathway for degradation of peptides generated by proteasomes: a key role for thimet oligopeptidase and other metallopeptidases. J Biol Chem *279*, 46723-46732.

Saugar, I., Luque, D., Ona, A., Rodriguez, J. F., Carrascosa, J. L., Trus, B. L., and Caston, J. R. (2005). Structural polymorphism of the major capsid protein of a double-stranded RNA virus: an amphipathic alpha helix as a molecular switch. Structure *13*, 1007-1017.

Savithri, H. S., and Erickson, J. W. (1983). The self-assembly of the cowpea strain of southern bean mosaic virus: formation of T = 1 and T = 3 nucleoprotein particles. Virology *126*, 328-335.

Schneemann, A., Reddy, V., and Johnson, J. E. (1998). The structure and function of nodavirus particles: a paradigm for understanding chemical biology. Adv Virus Res *50*, 381-446.

Schneemann, A., Zhong, W., Gallagher, T. M., and Rueckert, R. R. (1992). Maturation cleavage required for infectivity of a nodavirus. J Virol *66*, 6728-6734.

Schwartz, R., Garcea, R. L., and Berger, B. (2000). "Local rules" theory applied to polyomavirus polymorphic capsid assemblies. Virology *268*, 461-470.

Shwed, P. S., Dobos, P., Cameron, L. A., Vakharia, V. N., and Duncan, R. (2002). Birnavirus VP1 proteins form a distinct subgroup of RNA-dependent RNA polymerases lacking a GDD motif. Virology *296*, 241-250.

Snyder, D. B. (1990). Changes in the field status of infectious bursal disease virus. Avian Pathol *19*, 419-423.

Spies, U., and Muller, H. (1990). Demonstration of enzyme activities required for cap structure formation in infectious bursal disease virus, a member of the birnavirus group. J Gen Virol *71 (Pt 4)*, 977-981.

Spies, U., Muller, H., and Becht, H. (1987). Properties of RNA polymerase activity associated with infectious bursal disease virus and characterization of its reaction products. Virus Res *8*, 127-140.

Stark, H., and Luhrmann, R. (2006). Cryo-electron microscopy of spliceosomal components. Annu Rev Biophys Biomol Struct *35*, 435-457.

Stehle, T., Gamblin, S. J., Yan, Y., and Harrison, S. C. (1996). The structure of simian virus 40 refined at 3.1 A resolution. Structure *4*, 165-182.

Stoltze, L., Schirle, M., Schwarz, G., Schroter, C., Thompson, M. W., Hersh, L. B., Kalbacher, H., Stevanovic, S., Rammensee, H. G., and Schild, H. (2000). Two new proteases in the MHC class I processing pathway. Nat Immunol *1*, 413-418.

Tacken, M. G., Peeters, B. P., Thomas, A. A., Rottier, P. J., and Boot, H. J. (2002). Infectious bursal disease virus capsid protein VP3 interacts both with VP1, the RNA-dependent RNA polymerase, and with viral double-stranded RNA. J Virol *76*, 11301-11311.

Tacken, M. G., Rottier, P. J., Gielkens, A. L., and Peeters, B. P. (2000). Interactions in vivo between the proteins of infectious bursal disease virus: capsid protein VP3 interacts with the RNA-dependent RNA polymerase, VP1. J Gen Virol *81*, 209-218.

Tang, J., Naitow, H., Gardner, N. A., Kolesar, A., Tang, L., Wickner, R. B., and Johnson, J. E. (2005). The structural basis of recognition and removal of cellular mRNA 7-methyl G 'caps' by a viral capsid protein: a unique viral response to host defense. J Mol Recognit *18*, 158-168.

Targett-Adams, P., Hope, G., Boulant, S., and McLauchlan, J. (2008). Maturation of hepatitis C virus core protein by signal peptide peptidase is required for virus production. J Biol Chem *283*, 16850-16859.

Taylor, D. J., and Johnson, J. E. (2005). Folding and particle assembly are disrupted by single-point mutations near the autocatalytic cleavage site of Nudaurelia capensis omega virus capsid protein. Protein Sci *14*, 401-408.

Taylor, D. J., Krishna, N. K., Canady, M. A., Schneemann, A., and Johnson, J. E. (2002). Large-scale, pH-dependent, quaternary structure changes in an RNA virus capsid are reversible in the absence of subunit autoproteolysis. J Virol *76*, 9972-9980.
Ternois, F., Sticht, J., Duquerroy, S., Krausslich, H. G., and Rey, F. A. (2005). The HIV-1 capsid protein C-terminal domain in complex with a virus assembly inhibitor. Nat Struct Mol Biol *12*, 678-682.

van den Berg, T. P., Eterradossi, N., Toquin, D., and Meulemans, G. (2000). Infectious bursal disease (Gumboro disease). Rev Sci Tech *19*, 509-543.

Vaughn, J. L., Goodwin, R. H., Tompkins, G. J., and McCawley, P. (1977). The establishment of two cell lines from the insect Spodoptera frugiperda (Lepidoptera; Noctuidae). In Vitro *13*, 213-217.

Vazeux, G., Iturrioz, X., Corvol, P., and Llorens-Cortes, C. (1998). A glutamate residue contributes to the exopeptidase specificity in aminopeptidase A. Biochem J *334 (Pt 2)*, 407-413.

Villanueva, R. A., Galaz, J. L., Valdes, J. A., Jashes, M. M., and Sandino, A. M. (2004). Genome assembly and particle maturation of the birnavirus infectious pancreatic necrosis virus. J Virol *78*, 13829-13838.

von Einem, U. I., Gorbalenya, A. E., Schirrmeier, H., Behrens, S. E., Letzel, T., and Mundt, E. (2004). VP1 of infectious bursal disease virus is an RNA-dependent RNA polymerase. J Gen Virol *85*, 2221-2229.

Walukiewicz, H. E., Banerjee, M., Schneemann, A., and Johnson, J. E. (2008). Rescue of maturation-defective flock house virus infectivity with noninfectious, mature, viruslike particles. J Virol *82*, 2025-2027.

Wang, E. W., Kessler, B. M., Borodovsky, A., Cravatt, B. F., Bogyo, M., Ploegh, H. L., and Glas, R. (2000). Integration of the ubiquitin-proteasome pathway with a cytosolic oligopeptidase activity. Proc Natl Acad Sci U S A *97*, 9990-9995.

Ward, G. A., Stover, C. K., Moss, B., and Fuerst, T. R. (1995). Stringent chemical and thermal regulation of recombinant gene expression by vaccinia virus vectors in mammalian cells. Proc Natl Acad Sci U S A *92*, 6773-6777.

Xiao, T., Takagi, J., Coller, B. S., Wang, J. H., and Springer, T. A. (2004). Structural basis for allostery in integrins and binding to fibrinogen-mimetic therapeutics. Nature *432*, 59-67.

Xu, H. T., Si, W. D., and Dobos, P. (2004). Mapping the site of guanylylation on VP1, the protein primer for infectious pancreatic necrosis virus RNA synthesis. Virology *322*, 199-210.

Yamaguchi, T., Ogawa, M., Inoshima, Y., Miyoshi, M., Fukushi, H., and Hirai, K. (1996). Identification of sequence changes responsible for the attenuation of highly virulent infectious bursal disease virus. Virology *223*, 219-223.

Zandi, R., Reguera, D., Bruinsma, R. F., Gelbart, W. M., and Rudnick, J. (2004). Origin of icosahedral symmetry in viruses. Proc Natl Acad Sci U S A *101*, 15556-15560.

Zhou, Z. H., Macnab, S. J., Jakana, J., Scott, L. R., Chiu, W., and Rixon, F. J. (1998). Identification of the sites of interaction between the scaffold and outer shell in herpes simplex virus-1 capsids by difference electron imaging. Proc Natl Acad Sci U S A *95*, 2778-2783.

Zlotnick, A., Reddy, V. S., Dasgupta, R., Schneemann, A., Ray, W. J., Jr., Rueckert, R. R., and Johnson, J. E. (1994). Capsid assembly in a family of animal viruses primes an

autoproteolytic maturation that depends on a single aspartic acid residue. J Biol Chem *269*, 13680-13684.

Zlotnick, A. (2004). Viruses and the physics of soft condensed matter. Proc Natl Acad Sci U S A *101*, 15549-15550.

# PUBLICATIONS

# BIBLIOGRAPHY

THE JOURNAL OF BIOLOGICAL CHEMISTRY VOL. 284, NO. 12, pp. 8064–8072, March 20, 2009


# Autoproteolytic Activity Derived from the Infectious Bursal Disease Virus Capsid Protein*[S]

Received for publication, November 25, 2008, and in revised form, December 19, 2008 Published, JBC Papers in Press, January 14, 2009, DOI 10.1074/jbc.M808942200

**Nerea Irigoyen**[‡1], **Damià Garriga**[§2], **Aitor Navarro**[‡], **Nuria Verdaguer**[§], **José F. Rodríguez**[‡], **and José R. Castón**[¶3]

*From the Departments of* [‡]*Molecular and Cellular Biology and* [¶]*Structure of Macromolecules, Centro Nacional de Biotecnología/Consejo Superior de Investigaciones Científicas (CSIC), Cantoblanco, 28049 Madrid, Spain and* [§]*Institut de Biologia Molecular de Barcelona/CSIC, Parc Científic de Barcelona, Josep Samitier 1-5, 08028-Barcelona, Spain*

**Viral capsids are envisioned as vehicles to deliver the viral genome to the host cell. They are nonetheless dynamic protective shells, as they participate in numerous processes of the virus cycle such as assembly, genome packaging, binding to receptors, and uncoating among others. In so doing, they undergo large scale conformational changes. Capsid proteins with essential enzymatic activities are being described more frequently. Here we show that the precursor (pVP2) of the capsid protein VP2 of the infectious bursal disease virus (IBDV), an avian double-stranded RNA virus, has autoproteolytic activity. The pVP2 C-terminal region is first processed by the viral protease VP4. VP2 Asp-431, lying in a flexible loop preceding the C-terminal most α-helix, is responsible for the endopeptidase activity that cleaves the Ala-441—Phe-442 bond to generate the mature VP2 polypeptide. The D431N substitution abrogates the endopeptidase activity without introducing a significant conformational change, as deduced from the three-dimensional structure of the mutant protein at 3.1 Å resolution. Combinations of VP2 polypeptides containing mutations affecting either the cleavage or the catalytic site revealed that pVP2 proteolytic processing is the result of a monomolecular *cis*-cleavage reaction. The D431N mutation does not affect the assembly of the VP2 trimers that constitute the capsid building block. Although VP2 D431N trimers are capable of assembling both pentamers and hexamers, expression of a polyprotein gene harboring the D431N mutation does not result in the assembly of IBDV virus-like particles. Reverse genetics analyses demonstrate that pVP2 self-processing is essential for the assembly of an infectious IBDV progeny.**

Multiprotein assemblies are the basic cellular entities controlling fundamental biological processes. Viral capsids represent an excellent framework for the analysis of "built-in" features such as structural polymorphism and transient conformations. In addition, complex capsids may require one or more auxiliary proteins (scaffold, accessory, and proteolytic proteins) to trigger structural and functional changes. In this context, assembly of birnavirus capsid has resulted in an appropriate process for studying the coordination of molecular factors involved that, like in many other viruses, rarely leads to aberrant assemblies *in vivo*.

Birnaviruses are a family of naked icosahedral viruses infecting rotifers, insects, fishes, and birds (1). Their genome, formed by two segments of double-stranded RNA (dsRNA),[4] encodes only five mature polypeptides. Although most of the research has been focused on the infectious bursal disease virus (IBDV), an important avian pathogen (2), available information suggests that all members of the family share similar replication strategies.

The IBDV particle possesses a relatively complex icosahedral capsid based on a triangulation number T = 13 *levo* lattice composed by a single polypeptide known as VP2. Whereas the simplest capsids are built from 60 identical subunits and assembled into pentamers (T = 1), those with more than 60 subunits are assembled into pentamers and hexamers and cannot have identical but "quasi-equivalent" environments (T > 1) (3). The T number also describes the number of different environments occupied by the protein subunit (4). The VP2 protein assembles into 260 trimers that form 12 pentamers and 120 hexamers (5–7). From strict geometric considerations, VP2 trimers have five distinct conformations.

VP2 is synthesized as part of a polyprotein (~110 kDa) that is cotranslationally self-cleaved, releasing three polypeptides, namely pVP2 (the VP2 precursor), VP4 (the protease), and VP3 (a polypeptide with scaffolding activity among others). pVP2 (512 residues, 54.4 kDa) undergoes subsequent, and much slower, processing events mediated by VP4 at three secondary targets (positions 487, 494, and 501) (8), and the resulting intermediates are further cleaved between residues Ala-441 and Phe-442 to yield VP2 (47 kDa) and several C-terminal fragments (accounting for 7.4 kDa). Both the mechanism and the

* This work was supported by Spanish Dirección General de Investigación (MEC) Grants BIO2006-09407, BFU2005-02376, and BFU2005–06487. The costs of publication of this article were defrayed in part by the payment of page charges. This article must therefore be hereby marked "*advertisement*" in accordance with 18 U.S.C. Section 1734 solely to indicate this fact.

[S] The on-line version of this article (available at http://www.jbc.org) contains supplemental Tables 1 and 2.

*The atomic coordinates and structure factors (code 3FBM) have been deposited in the Protein Data Bank, Research Collaboratory for Structural Bioinformatics, Rutgers University, New Brunswick, NJ (http://www.rcsb.org/).*

[1] Supported by "Residencia de Estudiantes" and Gobierno de Aragón and by an Formación de Personal Universitario fellowship from the Spanish Ministry of Education (MEC).

[2] Recipient of an I3P fellowship from Consejo Superior de Investigaciones Científicas.

[3] To whom correspondence should be addressed: Dpto. de Estructura de Macromoléculas, Centro Nacional de Biotecnología/CSIC, C/ Darwin no. 3, Cantoblanco, 28049-Madrid, Spain. Tel.: 34-91-5854971; Fax: 34-91-5854506; E-mail: jrcaston@cnb.csic.es.

[4] The abbreviations used are: dsRNA, double-stranded RNA; ssRNA, single-stranded RNA; IBDV, infectious bursal disease virus; IPNV, infectious pancreatic necrosis virus; CP, capsid protein; rBV, recombinant baculovirus; rVV, recombinant vaccinia virus; SVP, subviral particle; VLP, virus-like particle; DMEM, Dulbecco's modified Eagle's medium; pi, postinfection.

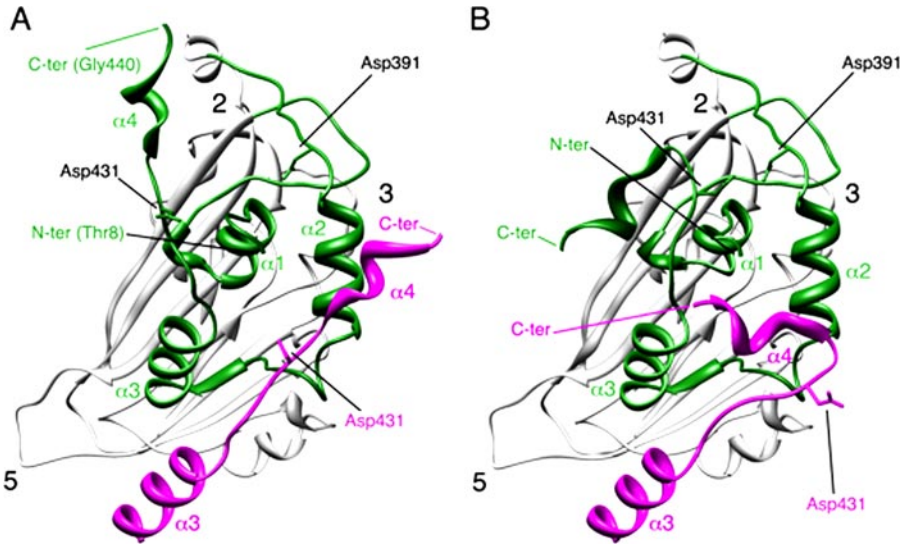


FIGURE 1. **Conformational flexibility of the VP2 C-terminal α-helix around its cleavage site.** *A*, bottom view, facing the inner surface of the viral capsid, of the VP2 protein x-ray model (PDB entry 2GSY). α-Helices (*1–4*) of domain B (*green*) are indicated for a VP2 chain; the candidate catalytic residues Asp-391 and Asp-431 are also indicated. α3 and α4 helices of the closer neighboring VP2 chain (*magenta*) that projects toward the 3-fold axis of the trimer are shown, and to simplify the view, only its Asp-391 residue is indicated. The locations of 5-, 3-, and 2-fold axes of icosahedral symmetry are indicated. *B*, same as *panel A*, but the C-terminal α4 helices of VP2 chains were remodeled after fitting the x-ray model into an equivalent cryo-electron microscopy map (21).

executor of the last pVP2 → VP2 proteolytic maturation remain unknown and are associated with the pVP2 assembly into a procapsid-like structure (9). The released C-terminal segments remain associated to the capsid (10) and appear to be involved in the entry mechanism by promoting the disruption of host cell membranes (11).

Studies carried out with another birnavirus, infectious pancreatic necrosis virus (IPNV), a pathogen of the aquatic fauna (12), suggest that the pVP2 → VP2 conversion is required for the maturation of quasi-spherical provirions into mature icosahedral virions (13). This maturation mechanism is reminiscent of the post-assembly proteolytic maturation that takes place during the morphogenesis of some ssRNA icosahedral viruses, and in particular to those of noda- and tetraviruses (14, 15). The capsid protein (CP) precursor, the α-protein, associates as a trimer, building a quasi-spherical provirion (16). At low pH, the α-protein is autocatalytically processed, rendering the mature CP, known as β-protein, and the C-terminal γ-peptide (17). This reaction is slow and dependent on a conserved Asp residue located in close proximity of the CP scissile bond (18). Maturation of the β-protein is accompanied by large conformational changes on the CP that irreversibly transforms the quasi-spherical (non-infectious) provirions into icosahedral infective virions (14, 17).

The molecular mechanisms that define the multimeric state of the mature VP2 as hexamers or pentamers have been intensively analyzed (7, 19–21). Expression of VP2 alone results in the spontaneous assembly of icosahedral T = 1 subviral particles (SVP), an all-pentamer capsid ~23 nm in diameter composed of 20 trimeric clusters of VP2. On the other hand, pVP2 expression leads to the assembly of tubular structures with a hexagonal lattice (7, 19). The pVP2 C-terminal processing events are abolished when this protein is expressed using a baculovirus-based system. Notably, the pVP2 C-terminal region contains an amphipathic α-helix that plays an important role in allowing the formation of multiple VP2 conformations. VP3 also participates in the inherent conformational polymorphism of pVP2 through interaction with the pVP2 C-terminal end, working as a canonical scaffolding protein.

The atomic structure of the VP2 polypeptide has been recently solved from T = 1 SVP (5, 22, 23). The VP2 subunit folds into three domains termed projection (P), shell (S), and base (B). Domains S and P are β barrels with a jelly roll topology, whereas the B domain is formed by α-helices facing the interior of the shell, corresponding to its N and C termini. The helical C-terminal arm of VP2 establishes a domain swapping and mediates interactions between adjacent VP2 trimers increasing their stability. S and B domains share a high degree of structural similarity with noda- and tetravirus α-protein. pVP2 and α-protein cleavage sites are deeply buried inside the capsid shell, thus sheltered from possible attacks by cellular proteases. Fitting the VP2 atomic structure into the three-dimensional cryo-electron microscopy map of IBDV T = 1 SVP allowed us to identify at least two conformations for its C-terminal region (19, 21). These structural considerations tempted us to suggest Asp-391 and/or Asp-431 as candidate catalytic residues capable of triggering a hydrolytic cleavage either on its own scissile bond or on that from a neighboring pVP2 molecule (Fig. 1). The results presented here demonstrate that residue Asp-431 is essential for pVP2 proteolytic maturation, thus leading us to propose that birnavirus pVP2 polypeptides are autocatalytically processed. This finding provides yet another piece of evidence reinforcing the hypothesis about a common ancestor linking icosahedral ssRNA and dsRNA viruses.

## EXPERIMENTAL PROCEDURES

*Cells and Viruses*—Recombinant vaccinia virus (rVV) VT7LacOI/POLY and recombinant baculoviruses (rBV) FB/VP2–452 and FB/VP2-501 were previously described (7, 24, 25). Expression experiments were carried out with BSC-1 mammalian cells or QM7 quail muscle cells for rVV infections and *Trichoplusia ni* (H5) insect cells (Invitrogen) for rBV infections. BSC-1 and QM7 cells were grown in Dulbecco's modified Eagle's medium (DMEM) containing 10% fetal calf serum. H5 cells were grown in TC-100 medium (Invitrogen) containing 10% fetal calf serum. rVVs and rBVs were grown and titrated as previously described (25, 26).

*Generation of the Recombinant Viruses VT7/LacOI*—Using PCR overlap extension five mutant pVP2 genes were constructed containing the following single and double muta-

tions: A441G, F442G, A441G/F442G, D431N, and D391N. PCR reactions were carried out using the pVP2 gene, cloned in the pFB/POLY plasmid as template, and the set of mutator primers (supplemental Table 1) in combination with primers 5′-GCCATCACAAGCCTCAGCGTTGG and 5′-GTGCACCGCGGAGTACCCCAG for A441G, F442G, and A441G/F442G. Primers 5′-GATGCCATCACAAGCCTCAGC and 5′-CGCAGTCGAGGTTGTGTGCAC were used for D431N and D391N. The resulting DNA fragments were digested with NdeI and SphI and used to replace the original NdeI-SphI fragment of the pVOTE.2/POLY plasmid previously described (25). The plasmids pVOTE/A441G, pVOTE/F442G, pVOTE/A441G/F442G, pVOTE/D391N, and pVOTE/D431N were used to obtain the recombinant vaccinia viruses VT7LacOI/A441G, VT7LacOI/F442G, VT7LacOI/A441G/F442G, VT7LacOI/D391N, and VT7LacOI/D431N. For this, BSC-1 cells were infected with the vaccinia virus recombinant VT7LacOI (27) and transfected with the previous plasmids. Selection and amplification of VT7LacOI/A441G, VT7LacOI/F442G, VT7LacOI/A441G/F442G, VT7LacOI/D391N, and VT7LacOI/D431N were carried out as previously described (28).

*Construction of Recombinant Baculoviruses*—rBV FB/VP2–452 and FB/VP2-501 were previously described (7, 19). The pVOTE.2/D431N and pVOTE.2/D391N plasmids were used as a template for PCR synthesis to generate rBV/VP2–452D431N, rBV/VP2–452D391N, and rBV/VP2-501D431N. PCR was performed with Vent DNA polymerase (New England Biolabs) with common 5′ and 3′ end primer (5′-GCGCAGATCTATGACAAACCTGTCAGATCAAACCC and 5′-GCGCAAGCTTACCTTATGGCCCGGATTATGTCTTTGAAGC). BglII-HindIII-digested PCR fragments were cloned into FastBac (Invitrogen) BamH1-HindIII polylinker sites for protein expression. Selection of derived bacmids from the DH10Bac *Escherichia coli* strain and preparation for Lipofectine transfection were performed according to the manufacturer's protocols (Invitrogen). The constructs were expressed in H5 insect cells (29).

*Immunoprecipitation of VP2*—QM7 cell monolayers were infected with the corresponding rVV at a multiplicity of infection of 2 plaque-forming units/cell and maintained in the presence of isopropyl β-D-thiogalactosidase. At 18 h postinfection (pi), cells were washed twice and metabolically labeled with methionine-free DMEM containing 125 μCi/ml [$^{35}$S]Met and isopropyl β-D-thiogalactosidase for 1 h. After this period cells were washed 3 times with DMEM containing a 10-fold concentration of cold methionine and then maintained in DMEM supplemented with isopropyl β-D-thiogalactosidase and 2% fetal calf serum. At 0, 24, 48, and 72 h post-labeling, cells were harvested, washed twice with phosphate-buffered saline, and resuspended in lysis buffer (50 mM Tris, pH 7.5, 100 mM NaCl, 5 mM EDTA, 0.5% IGEPAL CA-630). Immunoprecipitations were carried as described elsewhere (26). Immunoprecipitated samples were resuspended in Laemmli sample buffer to a 1× final concentration and subjected to 11% SDS-PAGE followed by autoradiography.

*Reverse Genetic Analysis*—DNA fragments containing cDNA versions corresponding to the complete positive strand RNAs of to the IBDV Soroa strain segments A and B, fused to the T7 bacteriophage promoter (in 5′ position with respect of the IBDV cDNAs), and a cDNA corresponding to the hepatitis delta virus ribozyme (in 3′ position with respect of the IBDV cDNAs) sequences were generated by *in vitro* gene synthesis (Genescript Co.) and inserted into the multiple cloning site of the pUC57 cloning plasmid (GenBank$^{TM}$/EMBL). These plasmids were named pT7-SA-Rz and pT7-SB-Rz, containing the cDNA corresponding to segment A and B, respectively.

Plasmid pVOTE/D431N, described above, was digested with SphI and NdeI and ligated to pT7-SA-Rz previously digested with the same enzymes. The resulting plasmid, pT7-SA(D431N)-Rz, was sequenced to determine the correctness of its sequence.

QM7 cells were transfected with a combination of either pT7-SA-Rz and pT7-SB-Rz or pT7-SA(D431N)-Rz and pT7-SB-Rz, respectively, using Lipofectamine (Invitrogen). 6 h after transfection cultures were infected with 1 plaque-forming unit/cell of VT7LacOI, an rVV inducibly expressing the T7 RNA polymerase. After infection, cultures were maintained at 37 °C in DMEM containing 10% fetal calf serum supplemented with 1 mM isopropyl β-D-thiogalactosidase. At 72 h pi, cultures were harvested and subjected to three freeze-thawing cycles. After removing cell debris by low speed centrifugation, supernatants were recovered and passed through 0.1-μm filters (Millipore) to eliminate contaminant rVV particles and used to infect fresh QM7 cell monolayers. Infections were performed in triplicate with undiluted and $10^{-1}$–$10^{-5}$ serial dilutions of the initial stocks. A set of infected cells was used to determine the IBDV titer at 72 h pi. Another set was harvested at 72 h pi, and the corresponding extracts were analyzed for the presence of VP1 and VP2 proteins. The absence of contaminant infecting rVV particles was also monitored by Western blot using the mAbC3. The third set was also harvested at 72 h pi and used to collect cells originally infected with the undiluted stocks. These samples were subjected to three freeze-thawing cycles, and the procedure described above was repeated, thus allowing the analysis of the initial virus stock and two subsequent virus amplification rounds.

*Purification of IBDV Polyprotein-derived Structures*—QM7 and H5 cells (2–5 × $10^8$ cells) were infected with appropriate rVV or rBV (multiplicity of infection 1–5 plaque-forming units/cell). At 72 h pi in rVV assays and at 48 h pi in rBV assays, cells were harvested, lysed in PES buffer (25 mM piperazine-*N*,*N*′-bis(2-ethanesulfonic acid), pH 6.2, 150 mM NaCl, and 20 mM $CaCl_2$) plus 1% IGEPAL CA-630 (Sigma) on ice, and processed on a 25% sucrose cushion and a linear 20–50% sucrose gradient (19). The particulate material containing polyprotein-derived structures was concentrated 20-fold by ultracentrifugation and used for SDS-PAGE, Western blot, and electron microscopy analysis.

*SDS-PAGE and Western Blot*—Infected cell extracts (25 μl) or concentrated sucrose gradient fractions (10 μl) were added to Laemmli' s sample buffer to a 1× final concentration and heated at 100 °C for 3 min. Electrophoresis was performed in 11% polyacrylamide gels. Western blot analyses were carried out using an anti-VP2 serum as described (26).

*Electron Microscopy*—2–5-μl samples of concentrated sucrose gradient fractions were applied to glow-discharged carbon-coated grids for 2 min and negatively stained with 2% aqueous uranyl acetate. Micrographs were recorded with a JEOL 1200 EXII electron microscope operating at 100 kV at a nominal magnification of 40,000×.

*Crystallization and Data Collection*—Cubic crystals belonging to space group P213 ($a = b = c = 326.72$ Å) were obtained by the vapor diffusion method in hanging drops at room temperature by mixing 2 volumes of VP2–452_D431N-derived SVP (1.6 mg/ml) and 1 volume of the reservoir solution containing 14–17% polyethylene glycol 4000, 0.1 M Tris, pH 9.0, and 5% isopropanol. Crystals were transferred to a cryoprotecting solution containing 20% glycerol in the crystallization buffer and incubated for 1 min before they were flash-frozen by immersion in liquid nitrogen. X-ray data were collected from a single crystal using synchrotron radiation at the European Synchrotron Radiation Facility, Grenoble, France (beamline ID14-2) to 3.1 Å resolution. Diffraction images were processed using MOSFLM (30) and internally scaled with SCALA (31).

*Structure Refinement*—Crystals of D431N-mutated SVP were isomorphous to the previously obtained of native VP2 SVPs (PDB code 2GSY (22)). The initial maps for D431N-mutant were obtained after a rigid body fitting of the coordinates of native SVPs (PDB code 2GSY) to the new unit cell. The D431N mutation and other subtle changes were manually rebuilt using Coot (32), and the structure was then refined with CNS (33) using the 20-fold non crystallographic symmetry as a restraint. The final refinement statistics are summarized in supplemental Table 2. The coordinates and structure factors have been deposited into the Protein Data Bank (code 3FBM).

## RESULTS

*Effect of Mutations on Asp Residues Potentially Involved on pVP2 → VP2 Proteolytic Maturation*—(p)VP2 residues Asp-391 and Asp-431 appeared to be likely candidates to trigger a nucleophilic attack on the pVP2 441–442 scissile bond. The IBDV polyprotein expressed by an inducible rVV provided an excellent framework to analyzing the possible role of residues Asp-391 and Asp-431 on pVP2 proteolytic maturation. As described above, the use of this system allows the accumulation of pVP2 and VP2 and the efficient assembly of virus-like particles (VLP), structurally undistinguishable from purified IBDV virions (26, 34). Hence, two single-point mutant versions of the IBDV polyprotein gene were generated and used to construct two rVV, called VT7LacOI/D431N and VT7LacOI/D391N, in which Asp residues under study at positions 431 and 391 were replaced by Asn residues, respectively. Cultures infected with these two rVV were harvested at different times pi (24, 48, and 72 h), and the corresponding extracts were analyzed by Western blot using VP2-specific serum. As a control for this experiment, cultures were also infected with VT7LacOI/POLY, a rVV expressing the wild-type polyprotein gene (26).

Although expression of wild-type and D391N polyproteins led to accumulation of both pVP2 and VP2 polypeptides, samples from cells expressing polyprotein D431N showed equivalent pVP2 levels but did not contain detectable VP2 (Fig. 2*A*). These results strongly suggested that the D431N substitution

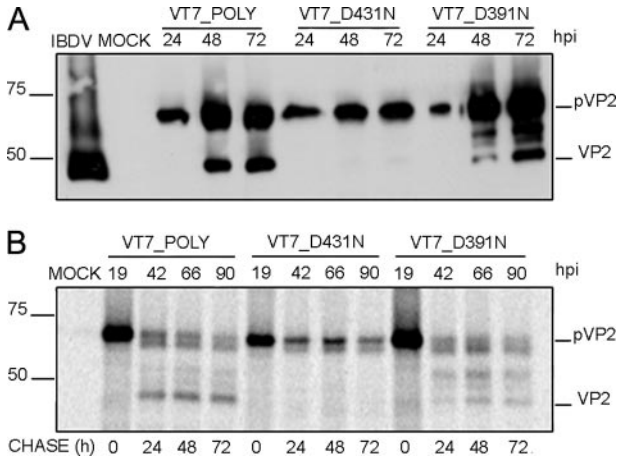


FIGURE 2. **Effect of conservative mutations of residues Asp-431 and Asp-391 on pVP2/VP2 proteolytic maturation.** *A*, Western blot analysis of proteins expressed in cells infected with rVV VT7LacOI/POLY, VT7LacOI/D431N, or VT7LacOI/D391N, respectively. Infected cultures were harvested at 24, 48, and 72 h pi, respectively. The corresponding extracts were subjected to SDS-PAGE and Western blot using anti-VP2 serum. *B*, QM7 cells infected with rVV VT7LacOI/POLY, VT7LacOI/D431N, or VT7LacOI/D391N were metabolically pulse-labeled with [$^{35}$S]Met for 1 h at 19 h pi (*hpi*). The radioactivity was chased with by adding fresh medium containing an excess of cold methionine. Cultures were harvested at 0, 24, 48, and 72 h post-labeling, and the corresponding extracts were immunoprecipitated using anti-VP2 serum. The resulting samples were subjected to SDS-PAGE followed by autoradiography. Molecular weight markers (expressed in kDa, *left*) and bands corresponding to proteins pVP2 and VP2 (*right*) are indicated.

specifically abrogated pVP2 proteolytic processing and were further confirmed using an alternative experimental approach. QM7 cells were infected with the three described rVV and, at 19 h pi, the cultures were metabolically labeled with [$^{35}$S]methionine for 1 h. Thereafter, cultures were extensively washed and incubated with fresh medium supplemented with an excess of cold methionine. At different times post-labeling (0, 24, 48, and 72 h), cells were harvested, and the corresponding extracts were subjected to immune precipitation using anti-VP2 antiserum. The results of this analysis (Fig. 2*B*) demonstrate that whereas in cells infected with VT7LacOI/POLY and VT7LacOI/D391N, the pVP2 polypeptide is progressively processed to mature VP2, the pVP2 polypeptide encoded by VT7LacOI/D431N remains intact for the duration of the experiment (72 h after its synthesis). Taken together, these results demonstrate that the conservative D431N substitution causes a complete blockade on pVP2 → VP2 proteolytic maturation.

*D431N Substitution Allows the Assembly of VP2 Trimers*—VP2 trimers constitute the building block of the IBDV-related icosahedral capsids with different T as well as different tubular structures with helical symmetry (19, 21). Therefore, it seemed likely that the results described above might be caused by deficiency on trimer assembly induced by a VP2 conformational change generated in the D431N mutant. Such a conformational change might prevent both the assembly of IBDV provirions and the subsequent pVP2 proteolytic processing event.

Expression of chimerical VP2 genes in insect cells leads to the spontaneous assembly of T = 1 SVP built by 20 VP2 trimers arranged into pentamers. We have exploited this system to determine the effect of the D431N mutation on the assembly of VP2 trimers. A VP2 gene with the N-terminal 452 residues

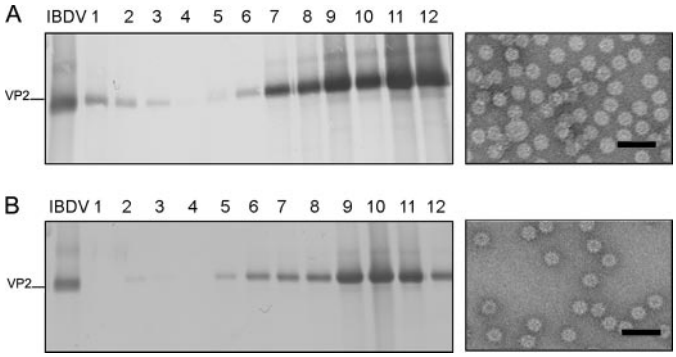


FIGURE 3. **VP2 with the D431N substitution assembles as T = 1 subviral particle VP2 trimers.** *A*, wild-type VP2–452 SVP were purified by ultracentrifugation on sucrose gradients. Gradients were collected into 12 fractions, concentrated by ultracentrifugation, and analyzed by SDS-PAGE and Western blot using anti-VP2 serum. The direction of sedimentation was *right* to *left*, with fraction 12 representing the gradient top. The image shown on the *right* corresponds to a representative electron microscopy micrograph (negative staining) of wild-type SVP, present at the upper gradient fractions. *B*, mutant VP2–452_D431N assemblies were analyzed as described above. The image shown on the *right* corresponds to a representative electron microscopy micrograph (negative staining) of mutant VP2–452_D431N SVP present at the upper gradient fractions. *Bars* = 100 nm.

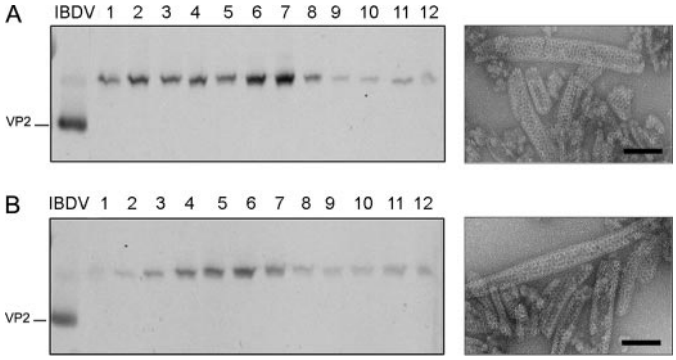


FIGURE 4. **pVP2 variant with the D431N substitution assembles as tubular assemblies with hexagonal symmetry.** *A*, wild-type p VP2-501 assemblies were purified by ultracentrifugation on sucrose gradients. Gradients were collected into 12 fractions, concentrated by ultracentrifugation, and analyzed by SDS-PAGE and Western blot using anti-VP2 serum. The direction of sedimentation was *right* to *left*, with fraction 12 representing the gradient top. The image shown on the *right* corresponds to a representative electron microscopy micrograph (negative staining) of wild-type tubular structures present at the lower fractions. *B*, mutant pVP2-501 _D431N assemblies were analyzed as described above. The image shown on the *right* corresponds to a representative electron microscopy micrograph (negative staining) of pVP2-501 _D431N rigid tubules at the lower fractions. *Bars* = 100 nm.

harboring the D431N substitution was generated, VP2–452_D431N, inserted into the pFastBac1 transfer vector, and then used to generate the corresponding rBV, rBV/VP2–452_D431N. Extracts from cells infected with rBV/VP2–452_D431N were used for SVP purification. As shown in Fig. 3, expression of the VP2–452D431N gene results in the assembly of T = 1 SVP that is undistinguishable under electron microscopy observation by negative staining from those produced by wild-type protein and D391N mutant (data not shown).

The possibility nevertheless existed that the mutation D431N might somehow affect the formation of VP2 hexamers formed by six VP2 trimers. To analyze this possibility we took advantage of a previous observation. As described above, we have shown that expression of VP2 long forms in a rBV expression system leads to the assembly of tubular structures formed exclusively by hexamers built by pVP2 intermediate precursor trimers (7, 19). Therefore, the D431N gene was subcloned into pFB/VP2-501, and the resulting plasmid, pFB/VP2-501_D431N, was used to generate the corresponding rBV. As shown in Fig. 4, expression of VP2-501 _D431N in insect cells results in the assembly of rigid tubules with an identical morphology to that of tubules purified from cells expressing wild-type VP2-501 gene. The results of this series of experiments demonstrate that the D431N substitution do not prevent either the trimer assembly or the subsequent formation of pentamers and hexamers.

Finally, to rule out the possibility that the D431N substitution might induce conformational changes on the VP2 polypeptide undetectable by electron microscopy, the crystal structure of VP2–452_D431N-derived SVP was determined at 3.1 Å resolution (supplemental Table S1). The root mean square deviation of the superimposition of all 428 equivalent C$\alpha$ atoms from VP2 in the structures of native and D431N SVP is 0.20 Å, showing that these structures are essentially identical in conformation. This similarity is also maintained within the flexible linker between helices $\alpha$3 and $\alpha$4 (residues 428–435), containing the D431N mutation (Fig. 5).

*pVP2 Undergoes an Intramolecular Proteolytic Processing*—To get a better understanding of the pVP2 maturation mechanism, it was important to determine whether the pVP2 → VP2 cleavage is the result of an intra- (*cis*-cleavage) or intermolecular (*trans*-cleavage) event.

To discriminate between these two possibilities, a polyprotein mutant containing an intact Asp-431 residue but resistant to self-proteolytic processing was required. Such a mutant would be used for co-expression analysis to provide the pVP2 → VP2 proteolytic activity in *trans*. With this aim, three polyprotein genes containing one or two amino acid substitutions affecting either one or both amino acids at the pVP2 scissile bond (Ala-441—Phe-442) were generated. The mutant genes contain the following substitutions: (i) A441G, (ii) F442G, and (iii) A441G/F442G. Mutant genes were then inserted within the vaccinia virus genome, giving rise to rVV VT7LacOI/A441G, VT7LacOI/F442G, and VT7LacOI/A441G/F442G, respectively. The effect of the described mutations on pVP2 processing was analyzed by Western blot and pulse-chase/immune precipitation analysis. As shown in Fig. 6, whereas single substitutions cause a major but partial pVP2 → VP2 blockade, the double mutation A441G/F442G completely abolishes pVP2 processing. Accordingly, this mutant gene was selected for subsequent experiments.

Next, cells were coinfected with VT7LacOI/POLY and VT7LacOI/D431N, VT7LacOI/POLY and VT7LacOI/A441G/F442G or VT7LacOI/D431N and VT7LacOI/A441G/F442G. Cultures were harvested at 48 and 72 h pi, and the corresponding extracts were analyzed by Western blot. As shown in Fig. 7, the presence of mature VP2 was exclusively detected in samples from cells expressing the wild-type polyprotein gene that provides both the catalytic Asp-431 residue and the intact cleavage site. Coinfection with VT7LacOI/D431N and VT7LacOI/A441G/F442G showed that pVP2-D431N remains uncleaved and is not proteolytically processed in *trans* by the wild-type pVP2, thus strongly suggesting that pVP2 processing is the result of a monomolecular *cis*-cleavage reaction.

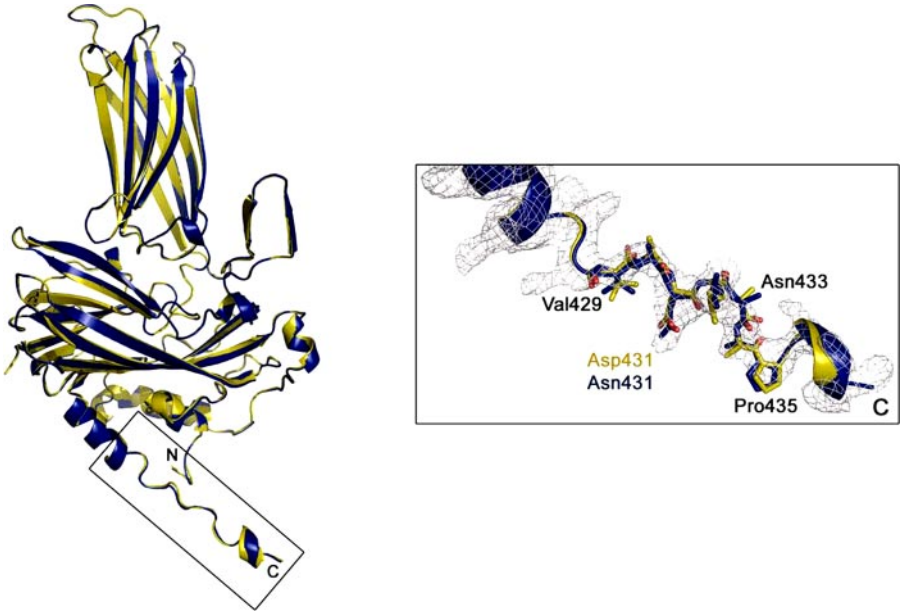


FIGURE 5. **Structure of the VP2 D431N T = 1 SVP monomer.** Ribbon diagrams of wild-type (*yellow*) and mutant D431N (*blue*) VP2 proteins. The superposition was performed using all the 428 residues of both molecules. Shown on the *right* is an electron density map of the VP2 C-terminal *boxed* region around residue Asp-431 . Residues from Val-429 to Pro-435 are shown as sticks and explicitly labeled every two residues.

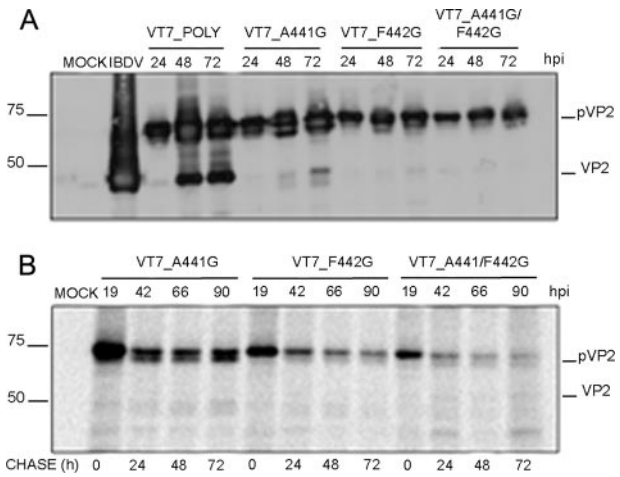


FIGURE 6. **Analysis of the pVP2 cleavage site Ala-441-Phe-442.** *A*, Western blot analysis of proteins expressed in cells infected with rVV VT7LacOI/POLY, VT7LacOI/A441G, VT7LacOI/F442G, and VT7LacOI/A441G/F442G. Infected cultures were harvested at 24, 48, and 72 h pi (*hpi*). *B*, QM7 cells were infected with different recombinants VT7LacOI/A441G, VT7LacOI/F442G, or VT7LacOI/A441G/F442G were pulse-labeled with [$^{35}$S]Met for 1 h at 19 h pi. The radioactivity was chased with by adding with fresh medium containing an excess of cold methionine. Cultures were harvested at 0, 24, 48, and 72 h post-labeling, and the corresponding extracts immunoprecipitated using anti-VP2 serum. The resulting samples were subjected to SDS-PAGE followed by autoradiography. Molecular weight markers (expressed in kDa, *left*), and bands corresponding to proteins pVP2 and VP2 (*right*) are indicated.

*D431N Substitution Completely Abolishes IBDV Infectivity*—It was important to assess the relevance of the Asp-431 on IBDV infectivity. This analysis was carried out using a reverse genetics approach using plasmids pT7_SA_Rz and B pT7_SB_Rz containing the cDNA sequences corresponding to IBDV segments A and B, respectively, and plasmid pT7_SA/D431N_Rz, harboring a mutant version of segment A containing the D431N substitution.

The results obtained demonstrate that the D431N substitution completely abolishes the production of an infectious IBDV progeny (Table 1). Western blot analysis indicated that cells transfected with plasmids pT7_SA/D431N_Rz and pT7_SB_Rz failed to trigger the generation of infectious IBDV. This finding, in agreement with the observations described above, highlights the critical importance of the VP2 D431N residue on IBDV infectivity.

*pVP2 → VP2 Maturation Blockade Prevents the Assembly of Stable IBDV-derived VLP*—IPNV morphogenesis involves the assembly of provirions containing a high proportion of pVP2 molecules. Provirion maturation appears to be associated to pVP2 proteolytic processing (13). Hence, it seemed feasible that blocking pVP2 → VP2 processing might favor the accumulation and isolation of IBDV provirions. To test this possibility, QM7 cultures were infected with VT7LacOI/POLY or VT7LacOI/D431N. Expression of the IBDV polyprotein in avian cells using an inducible rVV results in the accumulation of abundant levels of VLP with similar size and shape to those of authentic IBDV particles (26, 35). Remarkably, the assemblies produced with the rBV system in insect cells were nevertheless structurally varied, and in general, the formation of IBDV-like particles was rather inefficient. Insect cells might, therefore, have an important cellular factor(s) that interferes negatively with VLP assembly (*e.g.* cellular proteins and/or host environment).

Cultures harvested at 2 different times, 36 and 72 h pi, and the corresponding extracts were then used for the isolation of IBDV-derived assemblies using a sucrose gradient-based purification protocol followed by electron microscopy and Western blot analyses of the collected fractions. As described previously, extracts from cells infected with the rVV expressing the wild-type polyprotein gene contained abundant icosahedral VLPs with a relatively high VP2/pVP2 ratio (26). In contrast, no IBDV-derived assemblies were detected in samples from VT7LacOI/D431N-infected cells. The use of gentler extraction conditions and/or alternative purification protocols yielded similar results. The same results were observed with extracts from cells infected with the three rVVs expressing polyprotein genes containing mutations on the pVP2 cleavage site described above.

## DISCUSSION

We analyzed the protease activity of the IBDV CP VP2. The IBDV polyprotein is a fusion of capsid precursor pVP2 with the viral protease (VP4) and the scaffolding protein (VP3). pVP2, a 512-residue precursor, undergoes sequential C-terminal processing events mediated by the viral protease VP4 to render

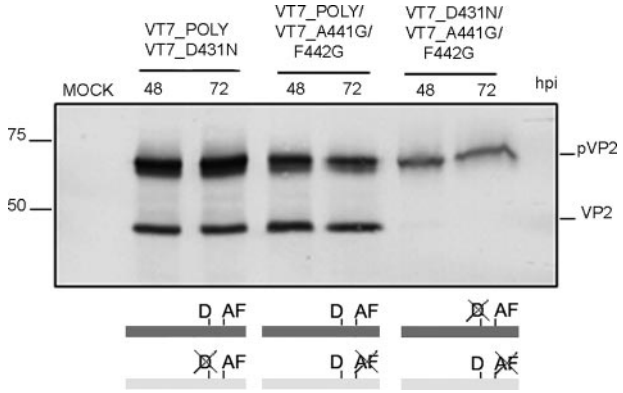


FIGURE 7. **pVP2 intramolecular proteolytic processing.** Western blot analysis of proteins expressed in QM7 cells coinfected with VT7LacOI/POLY and VT7LacOI/D431N, VT7LacOI/POLY and VT7LacOI/A441G/F442G, or VT7LacOI/A441G/F442G and VT7LacOI/D431N. Infected cultures were harvested at 48 and 72 h pi (*hpi*). A scheme indicating the combinations of rVV used in this experiment (mutated positions are *crossed out*) is shown at the *bottom*.

**TABLE 1**
**Virus titers obtained by reverse genetics**

| Coinfections | Virus titers | | |
|---|---|---|---|
| | First round | Second round | Third round |
| | | *pfu/ml* | |
| pT7-SA-Rz/pT7-SB-Rz | $1.3 \pm 0.5 \times 10^2$ | $9.0 \pm 1.3 \times 10^4$ | $6.0 \pm 1.5 \times 10^7$ |
| pT7-SA(D431N)-Rz/ pT7-SB-Rz | 0 | 0 | 0 |

shorter pVP2 polypeptides. These pVP2 intermediates with C-terminal extensions of variable length are further cleaved to render the mature VP2 (441 residues). Based on the VP2 x-ray structure, we examined the role of two likely candidate residues, Asp-391 and Asp-431, for catalyzing the last proteolytic event that occurs during capsid maturation. These residues were selected taking into account the structural analogies of domains S and B of IBDV CP to their counterparts in some positive-sense ssRNA viruses such as noda- and tetraviruses, in which the cleavage is mediated by acid residues, specifically Asp-75 of Flock House virus (FHV) (18) and Glu-103 of Nudaurelia capensis $\omega$ virus (36).

Our results indicate that he D431N mutation blocks the pVP2 → VP2 proteolytic trimming and affects the assembly of stable IBDV particles. Assembly of VLPs with the proper size and morphology, *i.e.* the T = 13 capsid, was not detected in cells expressing the polyprotein gene harboring the D431N mutation. Expression of pVP2 intermediate polypeptides with the point mutation D431N nonetheless can assemble either as all-pentamer structures (T = 1 SVP) or tubular structures built of pVP2 hexamers. The isolation of these assembly products excluded a possible misfolding of the polypeptide as they are built by the same structural block, VP2 trimers (19). The crystal structure of the mutant D431N VP2 protein provides additional experimental evidence supporting this interpretation. Similarly, mutations on the scissile bond Ala-441—Phe-442 yielded no production of particles.

We previously reported that the molecular switch controlling VP2 polymorphism resides in the C-terminal $^{443}$GFKDII-RAIR$^{452}$ segment that is organized as an amphipathic $\alpha$-helix (19). In addition, most of the temporally bound 71-residue C-terminal segment consists of $\alpha$-helices (11). Our working model assumes that assembly control of the complex IBDV T = 13 capsid requires the electrostatic interaction of the acidic segment of the VP3 C-terminal region, whose importance was previously established (29, 37), with the pVP2 amphipathic $\alpha$-helix as an initial event in the adoption of different conformational states. In this context it is easily envisioned how the D431N mutation is not only unable to cleavage the Ala-441—Pro-442 scissile bond but also might preclude or alter the interaction of VP3 with the helical region of VP2 at the inner basement of the VP2 S domain. Furthermore, we believe that the interaction of the C-terminal VP3 segment with the pVP2 amphipathic $\alpha$-helix might be necessary to temporally inhibit the last proteolytic event because, as reported previously, the pVP2 conformational state becomes irreversible (only able to assemble as pentamers) when its C-terminal region has been removed (21). Another fact that remains to be clarified in the sophisticated succession of interactions between VP3 and (p)VP2 refers to the high flexibility exhibited by the VP2 C-terminal end (21). It is likely that the conformational change originates from a rearrangement of some helical regions in the procapsid internal VP2 S domains as described for the Nudaurelia capensis $\omega$ virus conformational change (14, 17, 38).

Noda- and tetraviruses undergo a biphasic maturation process. During the first step, triggered by a reduction in pH, the procapsids undergo large scale structural rearrangements, thus quickly evolving to smaller, less porous, capsids; the second step is dependent on the first and consists of a relatively slow autoproteolytic cleavage of the precursor CP subunits. Maturation of IPNV, a closely related birnavirus, also occurs by pVP2 processing to VP2 in which spherical provirions evolve to relatively smaller icosahedral virions (13). Our attempts to isolate IBDV-derived provirions using a wide variety of approaches have failed at present. This could be due to several factors: (i) a comparatively faster pVP2 → VP2 conversion rate for the IBDV capsid than that of its IPNV counterpart; or (ii) a weaker interaction between the IBDV pVP2 with the scaffolding protein VP3, thus leading to the assembly of more labile provirions.

In addition to the structural similarities between their CP polypeptides described above, birna-, noda-, and tetravirus share many other features at multiple levels (39). These viruses possess bipartite genomes with a similar overall organization (one segment coding for the RNA polymerase, and the other one encoding the capsid precursor protein). Interestingly, birna-, noda-, and tetravirus mRNA lack 3′-terminal poly(A) tails (15, 40). Their RNA-dependent RNA polymerases exhibit a non-canonical organization exclusive of this three-virus group containing a specific sequence permutation of the catalytic palm subdomain (41–43). An additional similarity between birnaviruses and positive-sense ssRNA viruses is the protein priming of RNA synthesis, described for IPNV (44) and originally discovered in picornaviruses (45). A further parallel among noda-, tetra-, and birnaviruses refers to the presence of active capsid-associated $\alpha$-helical peptides generated during the proteolytic processing of the CP precursor C-terminal region. These peptides form hydrophilic channels that permeabilize biological membranes, allowing genome translocation during the virus entry process (11, 46). Finally, the multifunc-

tional IBDV VP3 protein (involved in virus assembly as an scaffolding protein and RNA synthesis as an RNA-dependent RNA polymerase activator) is mostly found associated to the dsRNA segments forming ribonucleoprotein complexes (47). In this sense, nodavirus also expresses a dsRNA-binding protein that acts as a potent suppressor, inhibiting host RNA silencing (48, 49). Our finding that the IBDV CP precursor is self-cleaved in a *cis*-processing event mediated by an aspartic acid residue adds further experimental evidence reinforcing the structural and functional relationships among icosahedral ssRNA and dsRNA viruses.

Viral CPs ensure the successful propagation of viral genomes by sheltering them from a hostile environment and guiding them through the interaction with specific cell receptors in their journey to reach an appropriate milieu for a successful replication process. Nevertheless, there is increasing evidence that CPs play other important roles. In addition to the Asp- or Glu-based proteolytic activities associated to birna-, noda-, and tetravirus, other CPs such that of Semliki Forest virus, an enveloped plus strand RNA virus, exhibits a self-cleaving serine protease activity (50). Enzymatic activities associated to CP in most known examples found in fully assembled virus particles are not exclusively restricted to protease activities. The CP of *Leishmania* RNA virus, a dsRNA virus that persistently infects the parasitic protozoan *Leishmania*, possesses a site-specific RNA endoribonuclease activity that cleaves viral positive-sense RNA (51, 52). L-A virus, another dsRNA virus that infects the yeast *Saccharomyces cerevisiae*, has a CP that removes the $m^7$GMP caps from host cellular mRNAs and covalently attaches them to a His residue on the capsid outer surface (53, 54). Unfortunately, the lack of specific sequence consensus motifs complicates the search for CP-associated enzymatic activities. Finally, these studies might settle the basis for the future design of capsid-targeted antiviral compounds trapping IBDV virion particles at an intermediate maturation stage rather than interrupting the assembly of capsid subunits, *e.g.* binding to trimers.

*Acknowledgment—We thank J. L. Carrascosa (Consejo Superior de Investigaciones Científicas, Madrid) for stimulating discussions and other helpful input.*

## REFERENCES


1. Delmas, B., Kibenge, F. S. B., Leong, J. C., Mundt, E., Vakharia, V. N., and Wu, J. L. (2005) in *Virus Taxonomy* (Fauquet, C. M., Mayo, M. A., Maniloff, J., Desselberger, U., and Ball, L. A., eds) pp. 561–569, Elsevier Science Publishers B. V., Amsterdam
2. van den Berg, T. P., Eterradossi, N., Toquin, D., and Meulemans, G. (2000) *Rev. Sci. Tech.* **19,** 509–543
3. Caspar, D. L. D., and Klug, A. (1962) *Cold Spring Harbor Symp. Quant. Biol.* **27,** 1–24
4. Baker, T. S., Olson, N. H., and Fuller, S. D. (1999) *Microbiol. Mol. Biol. Rev.* **63,** 862–922
5. Coulibaly, F., Chevalier, C., Gutsche, I., Pous, J., Navaza, J., Bressanelli, S., Delmas, B., and Rey, F. A. (2005) *Cell* **120,** 761–772
6. Böttcher, B., Kiselev, N. A., Stel'Mashchuk, V. Y., Perevozchikova, N. A., Borisov, A. V., and Crowther, R. A. (1997) *J. Virol.* **71,** 325–330
7. Castón, J. R., Martínez-Torrecuadrada, J. L., Maraver, A., Lombardo, E., Rodríguez, J. F., Casal, J. I., and Carrascosa, J. L. (2001) *J. Virol.* **75,** 10815–10828
8. Sánchez, A. B., and Rodríguez, J. F. (1999) *Virology* **262,** 190–199
9. Chevalier, C., Lepault, J., Erk, I., Da Costa, B., and Delmas, B. (2002) *J. Virol.* **76,** 2384–2392
10. Da Costa, B., Chevalier, C., Henry, C., Huet, J. C., Petit, S., Lepault, J., Boot, H., and Delmas, B. (2002) *J. Virol.* **76,** 2393–2402
11. Galloux, M., Libersou, S., Morellet, N., Bouaziz, S., Da Costa, B., Ouldali, M., Lepault, J., and Delmas, B. (2007) *J. Biol. Chem.* **282,** 20774–20784
12. Dobos, P. (1996) *Annu. Rev. Fish Dis.* **5,** 25–54
13. Villanueva, R. A., Galaz, J. L., Valdes, J. A., Jashes, M. M., and Sandino, A. M. (2004) *J. Virol.* **78,** 13829–13838
14. Canady, M. A., Tihova, M., Hanzlik, T. N., Johnson, J. E., and Yeager, M. (2000) *J. Mol. Biol.* **299,** 573–584
15. Schneemann, A., Reddy, V., and Johnson, J. E. (1998) *Adv. Virus Res.* **50,** 381–446
16. Gallagher, T. M., and Rueckert, R. R. (1988) *J. Virol.* **62,** 3399–3406
17. Taylor, D. J., Krishna, N. K., Canady, M. A., Schneemann, A., and Johnson, J. E. (2002) *J. Virol.* **76,** 9972–9980
18. Zlotnick, A., Reddy, V. S., Dasgupta, R., Schneemann, A., Ray, W. J., Jr., Rueckert, R. R., and Johnson, J. E. (1994) *J. Biol. Chem.* **269,** 13680–13684
19. Saugar, I., Luque, D., Ona, A., Rodriguez, J. F., Carrascosa, J. L., Trus, B. L., and Caston, J. R. (2005) *Structure* **13,** 1007–1017
20. Oña, A., Luque, D., Abaitua, F., Maraver, A., Castón, J. R., and Rodríguez, J. F. (2004) *Virology* **322,** 135–142
21. Luque, D., Saugar, I., Rodriguez, J. F., Verdaguer, N., Garriga, D., Martin, C. S., Velazquez-Muriel, J. A., Trus, B. L., Carrascosa, J. L., and Caston, J. R. (2007) *J. Virol.* **81,** 6869–6878
22. Garriga, D., Querol-Audi, J., Abaitua, F., Saugar, I., Pous, J., Verdaguer, N., Castón, J. R., and Rodriguez, J. F. (2006) *J. Virol.* **80,** 6895–6905
23. Lee, C. C., Ko, T. P., Chou, C. C., Yoshimura, M., Doong, S. R., Wang, M. Y., and Wang, A. H. (2006) *J. Struct. Biol.* **155,** 74–86
24. Fernandez-Arias, A., Martinez, S., and Rodriguez, J. F. (1997) *J. Virol.* **71,** 8014–8018
25. Martinez-Torrecuadrada, J. L., Castón, J. R., Castro, M., Carrascosa, J. L., Rodriguez, J. F., and Casal, J. I. (2000) *Virology* **278,** 322–331
26. Lombardo, E., Maraver, A., Castón, J. R., Rivera, J., Fernandez-Arias, A., Serrano, A., Carrascosa, J. L., and Rodriguez, J. F. (1999) *J. Virol.* **73,** 6973–6983
27. Ward, G. A., Stover, C. K., Moss, B., and Fuerst, T. R. (1995) *Proc. Natl. Acad. Sci. U. S. A.* **92,** 6773–6777
28. Earl, P. L., and Moss, B. (1993) in *Current protocols in molecular biology* (Ausubel, F. M., Brent, R., Kingston, R. E., More, D. D., Seidman, J. G., Smith, J. A., and StruhI, K., eds) pp. 16.17.1–16.18.10, John Wiley & Sons, New York
29. Maraver, A., Oña, A., Abaitua, F., Gonzalez, D., Clemente, R., Ruiz-Díaz, J. A., Castón, J. R., Pazos, F., and Rodríguez, J. F. (2003) *J. Virol.* **77,** 6438–6449
30. Leslie, A. (1991) in *Crystallographic computing* (Moras, D., Podjarny, A., and Thiery, J., eds) pp. 27–38, Oxford University Press, Oxford
31. Evans, P. (1994) *Acta Crystallogr. D Biol. Crystallogr.* **50,** 760–763
32. Emsley, P., and Cowtan, K. (2004) *Acta Crystallogr. D Biol. Crystallogr.* **60,** 2126–2132
33. Brunger, A. T., Adams, P. D., Clore, G. M., DeLano, W. L., Gros, P., Grosse-Kunstleve, R. W., Jiang, J. S., Kuszewski, J., Nilges, M., Pannu, N. S., Read, R. J., Rice, L. M., Simonson, T., and Warren, G. L. (1998) *Acta Crystallogr. D Biol. Crystallogr.* **54,** 905–921
34. Castón, J. R., Rodríguez, J. F., and Casrrascosa, J. L. (2008) in *Segmented double-stranded RNA viruses: Structure and Molecular Biology* (Patton, J. T., ed) pp. 133–144, Caister Academic Press, Norfolk
35. Fernandez-Arias, A., Risco, C., Martinez, S., Albar, J. P., and Rodriguez, J. F. (1998) *J Gen. Virol.* **79,** 1047–1054
36. Taylor, D. J., and Johnson, J. E. (2005) *Protein Sci.* **14,** 401–408
37. Chevalier, C., Lepault, J., Da Costa, B., and Delmas, B. (2004) *J. Virol.* **78,** 3296–3303
38. Bothner, B., Taylor, D., Jun, B., Lee, K. K., Siuzdak, G., Schultz, C. P., and Johnson, J. E. (2005) *Virology* **334,** 17–27
39. Ahlquist, P. (2005) *Curr. Biol.* **15,** 465–467
40. Hanzlik, T. N., and Gordon, K. H. (1997) *Adv. Virus Res.* **48,** 101–168
41. Garriga, D., Navarro, A., Querol-Audi, J., Abaitua, F., Rodriguez, J. F., and Verdaguer, N. (2007) *Proc. Natl. Acad. Sci. U. S. A.* **104,**

20540–20545
42. Gorbalenya, A. E., Pringle, F. M., Zeddam, J. L., Luke, B. T., Cameron, C. E., Kalmakoff, J., Hanzlik, T. N., Gordon, K. H., and Ward, V. K. (2002) *J. Mol. Biol.* **324,** 47–62
43. Pan, J., Vakharia, V. N., and Tao, Y. J. (2007) *Proc. Natl. Acad. Sci. U. S. A.* **104,** 7385–7390
44. Xu, H. T., Si, W. D., and Dobos, P. (2004) *Virology* **322,** 199–210
45. Paul, A. V., van Boom, J. H., Filippov, D., and Wimmer, E. (1998) *Nature* **393,** 280–284
46. Cheng, R. H., Reddy, V. S., Olson, N. H., Fisher, A. J., Baker, T. S., and Johnson, J. E. (1994) *Structure* **2,** 271–282
47. Hjalmarsson, A., Carlemalm, E., and Everitt, E. (1999) *J. Virol.* **73,** 3484–3490
48. Chao, J. A., Lee, J. H., Chapados, B. R., Debler, E. W., Schneemann, A., and Williamson, J. R. (2005) *Nat. Struct. Mol. Biol.* **12,** 952–957
49. Chen, H. Y., Yang, J., Lin, C., and Yuan, Y. A. (2008) *EMBO Rep.* **9,** 754–760
50. Morillas, M., Eberl, H., Allain, F. H., Glockshuber, R., and Kuennemann, E. (2008) *J. Mol. Biol.* **376,** 721–735
51. MacBeth, K. J., and Patterson, J. L. (1995) *J. Virol.* **69,** 3458–3464
52. MacBeth, K. J., and Patterson, J. L. (1995) *Proc. Natl. Acad. Sci. U. S. A.* **92,** 8994–8998
53. Blanc, A., Ribas, J. C., Wickner, R. B., and Sonenberg, N. (1994) *Mol. Cell. Biol.* **14,** 2664–2674
54. Tang, J., Naitow, H., Gardner, N. A., Kolesar, A., Tang, L., Wickner, R. B., and Johnson, J. E. (2005) *J. Mol. Recognit.* **18,** 158–168